

Analyses of Earthquake Source, Path, and Site Factors From ANSS Data Along the Wasatch Front, Utah

FINAL TECHNICAL REPORT

Submitted to the

**U.S. Geological Survey
Under the National Earthquake Hazards Reduction Program
Program Element III Research on Earthquake Occurrence,
Physics, and Effects**



Award No. 05HQGR0010

Period of Performance: 1 December 2004 to 29 February 2008

By

Ivan G. Wong

Seismic Hazards Group, URS Corporation, 1333 Broadway, Suite 800, Oakland, CA 94612
Phone: (510) 874-3014, Fax: (510) 874-3268
E-mail: ivan_wong@urscorp.com

Walter J. Silva

Pacific Engineering & Analysis, 856 Seaview Drive, El Cerrito, CA 94530

James C. Pechmann

Department of Geology and Geophysics, University of Utah, 115 South 1460 East Rm 383 FASB,
Salt Lake City, UT 84112

Robert B. Darragh

Pacific Engineering & Analysis, 856 Seaview Drive, El Cerrito, CA 94530

Tian Yu

Institute of Engineering Mechanics, China Earthquake Administration, 29 Xuefu Road, Harbin, China

31 January 2011

ANALYSES OF EARTHQUAKE SOURCE, PATH, AND SITE FACTORS FROM ANSS DATA ALONG THE WASATCH FRONT, UTAH

Ivan G. Wong¹, Walter J. Silva², James Pechmann³, Robert Darragh², and Tian Yu⁴

To be submitted to the
Bulletin of the Seismological Society of America

31 January 2011

¹ URS Corporation, Seismic Hazards Group, 1333 Broadway, Suite 800, Oakland, CA 94612

² Pacific Engineering & Analysis, 856 Seaview Drive, El Cerrito, CA 94530

³ Department of Geology and Geophysics, University of Utah, 135 South 1460 East, Salt Lake City, UT 84112

⁴ Institute of Engineering Mechanics, China Earthquake Administration, 29 Xuefu Road, Harbin, China

ABSTRACT

The highly-populated Wasatch Front area in Utah, which includes the cities of Salt Lake City, Provo, Ogden, and Logan, is one of the most seismically hazardous regions in the Intermountain U.S. because of its proximity to the Wasatch fault zone and location within the southern Intermountain Seismic Belt. The ground-shaking hazard resulting from large (moment magnitude $[M] \geq 6.8$) earthquakes rupturing segments of the Wasatch fault has been estimated to be high because of the locations of the urban areas in the hanging wall of the fault, possible rupture directivity effects, shallow site response, and basin amplification. Predictions of ground motions are, however, highly uncertain. Clearly the best approach to estimating strong earthquake ground shaking is through the use of empirical data. However, the lack of strong motion data for large earthquakes in the Wasatch Front area and the Basin and Range Province hinders our ability to predict strong ground shaking.

In this study, we investigation earthquake stress drops, crustal attenuation, and near-surface attenuation (parameterized by kappa) in the Wasatch Front region in order to enable improved predictions of earthquake ground motions in this region. We inverted for model parameters characterizing these source, path, and site factors using a dataset of Advance National Seismic System (ANSS) strong motion and broadband records from stations located along the Wasatch Front. A Levenberg-Marquardt technique was used to perform the inversion on 409 records of 17 earthquakes of local magnitude (M_L) 2.6 to 4.2 recorded at epicentral distances of 14 to 368 km. The resulting stress drops ranged from 3 to 147 bars with a geometric mean value of 20 bars. The quality factor obtained from the inversions were 147 and 0.51, respectively, and the mean rock and soil kappas were 0.030 and 0.036 sec, respectively.

INTRODUCTION

The best approach to estimating strong earthquake ground shaking is through the use of empirical strong motion data. Because there is a lack of strong motion data for moderate and large earthquakes (moment magnitude $[M] > 5.0$) along Utah's Wasatch fault as well as in the adjacent Basin and Range Province, it is important that we understand the factors that control strong ground shaking. In this study, we evaluated three source, path, and site factors that affect the ground-shaking hazard along the central Wasatch Front of Utah: earthquake stress drop, frequency-

dependent crustal attenuation $Q(f) = Q_0 f^{\eta}$, and kappa (κ), the constant in the near-surface attenuation factor $e^{-\pi f \kappa}$. These parameters were determined through an inversion of Advanced National Seismic System (ANSS) strong motion and broadband recordings of earthquakes occurring within the Wasatch Front (Figure 1). From 2001 through 2007, 83 earthquakes of Richter local magnitude (M_L) 2.5 to 4.2 were recorded in the area shown on Figure 1 by the ANSS network operated by the University of Utah Seismograph Stations (UUSS) and the U.S. Geological Survey (USGS). Although this dataset does not include any moderate to large events, insights can be gained by looking into the source, path, and site effects that may not be magnitude or strain-dependent. The methodology employed in our study uses a nonlinear least-squares inversion of Fourier amplitude spectra for point-source model parameters based on the stochastic ground motion model. Assessments of the ranges of stress drops, $Q(f)$, and kappa will allow for a clearer understanding of the factors controlling the ground shaking hazard along the Wasatch Front and improve ground motion predictions for use in hazard maps and site-specific hazard evaluations.

Salt Lake City and the central Wasatch Front (Brigham City south to Nephi), Utah, are situated within the southern portion of the Intermountain Seismic Belt (ISB), one of the most seismically active regions in the western U.S. (Smith and Sbar, 1974; Smith and Arabasz, 1991). It extends from northern Arizona northward through central Utah and along the Idaho-Wyoming border to its termination in northwestern Montana. The deformational processes occurring within the ISB are principally in response to ongoing tectonic extension within the western portion of the North America plate (Zoback and Zoback, 1989). The ISB is characterized by late-Quaternary normal faulting, diffuse shallow seismicity, and episodic surface-faulting earthquakes (Richter magnitude [M_L] $6\frac{1}{2}$ to $7\frac{1}{2}$) (Smith and Arabasz, 1991).

Arabasz *et al.* (1992) characterized the ISB in Utah by: (1) a predominance of normal faulting with some contemporary strike-slip faulting also occurring, principally in south-central Utah; (2) moderate background seismicity; (3) diffuse seismicity that generally does not correlate with Quaternary faults and is typically at focal depths of less than 15 to 20 km; (4) relatively long and often variable recurrence intervals for surface faulting on individual fault segments (typically more than 1,000 years); (5) slip rates on late Quaternary faults of approximately 1 mm/yr or less; and (6) the historical absence of any surface-faulting earthquake in Utah larger than the 1934 surface wave

magnitude (M_S) 6.6 Hansel Valley earthquake, despite the presence of abundant late-Pleistocene and Holocene fault scarps.

Based on the historical earthquake record compiled by the UUSS since 1850, eight earthquakes have reached or exceeded M_L 5.5 in the Wasatch Front region. The largest historical earthquakes observed within the region have been the 1934 surface-wave magnitude (M_S) 6.6 Hansel Valley earthquake plus three events of approximate M_L 6 (measured or else estimated from maximum intensities) on 10 November 1884, 5 October 1909, and 27 March 1975 (Arabasz *et al.*, 1992). This historical record stands in sharp contrast to the geologic evidence for repeated late Quaternary M 6.8 and greater earthquakes occurring along the Wasatch fault and other fault zones (e.g., DuRoss, 2008).

In terms of ground shaking hazard to Salt Lake City and the Wasatch Front, the most significant fault is the Wasatch fault zone (Youngs *et al.*, 2000; Wong *et al.*, 2002a). The 343 km-long, westward-dipping Wasatch fault zone probably consists of 10 segments, each of which may be capable of generating a M 6.8 or larger earthquake (Machette *et al.*, 1991; 1992; DuRoss, 2008). The Salt Lake City, Weber and Provo segments are the most significant to Salt Lake City because of their proximity. Their estimated maximum magnitudes are approximately M 6.8 to 7.2 (DuRoss, 2008). Recurrence estimates for the Wasatch fault zone are based on numerous paleoseismic investigations (e.g., Swan *et al.*, 1980; Schwartz and Coppersmith, 1984; Machette *et al.*, 1991, 1992; Black *et al.*, 1996; Nelson *et al.*, 2006). For the five most active segments (Brigham City, Weber, Salt Lake City, Provo and Nephi), which are located in the central portion of the fault, average late Holocene recurrence intervals range from 900 to 1,300 years (DuRoss *et al.*, 2010). Paleoseismic evidence for the past 6,500 years indicates that a major surface-faulting event has occurred along these central segments about once every 360 years, although recurrence intervals along the Wasatch fault zone may not be uniform (DuRoss, 2008).

PREVIOUS STUDIES

Because modern research on the Wasatch fault's earthquake potential and hazards did not really begin until the early 1970's, studies into potential ground shaking along the Wasatch fault have been relatively few in number. The earliest studies of earthquake ground motions in the Salt Lake Valley involved the evaluations of site amplification due to basin sediments based on spectral ratios from

records of distant explosions (Wong, 1979; Hays and King, 1984; King *et al.*, 1987). Some later studies focused on analyzing two- and three-dimensional basin effects using finite-element or finite-difference approaches (Benz and Smith, 1988; Murphy, 1989, Hill *et al.*, 1990; Olsen *et al.*, 1995, 1996). Such effects may predominate at longer periods (greater than about 1.0 sec), which are critical for tall or long structures. A probabilistic analysis of earthquake ground shaking along the Wasatch Front was performed in the mid-1980's (Youngs *et al.*, 2000) and more recently a series of scenario and probabilistic ground shaking hazard maps were produced for the Salt Lake City metropolitan area (Wong *et al.*, 2002a) and the central Wasatch Front (Wong *et al.*, 2002b; Solomon *et al.*, 2004). Recent scenario ground motions for Wasatch fault earthquakes have been numerically simulated by Roten *et al.* (2009; 2010) and Liu and Archuleta (2009).

Research into the critical factors that control ground shaking hazard (stress drop, crustal attenuation, κ , and site amplification) in the Wasatch Front region has been limited. In large part, this is because predictions of ground motions have relied on the assumption that ground shaking behaves in the same manner as it does in California. This situation is a result of the lack of strong motion data not only along the Wasatch Front but in the Basin and Range Province. No large Basin and Range earthquake ($M \geq 6.5$) has been recorded at distances less than 80 km.

Studies by Stark *et al.* (1992), Wong *et al.* (1996), and Spudich *et al.* (1997; 1999), however, suggested that ground motions in extensional regimes such as the Basin and Range Province may be lower than in California for the same magnitude and distance. The inference was that this difference may be due to the lower stress drops of normal-faulting earthquakes compared to reverse-faulting events, as first suggested by McGarr (1984). In numerical ground motion modeling such as in the stochastic point-source model, the stress drop (or stress parameter) controls the level of high-frequency ground shaking. A similar argument has been made in Italy (Cocco and Rovelli, 1989). In contrast, Westaway and Smith (1989) argued that normal-faulting earthquakes produce ground motions no different than other types of earthquakes based on an evaluation of strong motion data.

In simulations of the dynamic rupture process of a normal fault, Shi *et al.* (2003) suggested that ground motions from normal-faulting earthquakes are lower than those from both strike-slip and reverse-faulting earthquakes. Oglesby *et al.* (1998) also observed this difference in numerical simulations. They indicated that the cause of this difference is due to the interaction between the

earthquake-generate stress field and the traction-free boundary condition of the free-surface that leads to variations in time-dependent normal stress on the fault that are opposite for reverse and normal slip.

In the Next Generation of Attenuation (NGA) Project, fault type was addressed by the model developers. Although the amount of strong motion from normal faulting earthquakes is quite limited, four of the five developer teams modeled ground motions from normal faults as being lower than strike-slip and reverse faults. For example, Chiou and Youngs (2008) predict 20% lower ground motions at some frequencies for a **M** 7.0 earthquake.

As part of the Yucca Mountain Project, Becker and Abrahamson (1997) analyzed the strong motion records compiled by Spudich *et al.* (1997) from extensional regimes worldwide. The dataset consisted of 9 earthquakes ranging from **M** 5.1 to 6.9. They computed Brune stress drops ranging from 16 to 93 bars with a median value of 29 bars using amplification factors from Silva *et al.* (1997).

The first two authors of this report evaluated Brune stress drops for several Basin and Range earthquakes including the 31 October M_L 6.0 and 28 November M_L 5.5 1935 Helena, Montana earthquakes, the 30 August 1962 M_L 5.6 Cache Valley, Utah earthquake, several aftershocks of the 1983 **M** 6.8 Borah Peak, Idaho, earthquake, small regional events ($< M_L$ 4.6) recorded by the Idaho National Laboratory seismic network as well as two other datasets of normal faulting aftershocks from California (1975 Oroville and 1980 Mammoth Lakes sequences) (Woodward-Clyde Federal Services, 1996). For the Basin and Range earthquakes, the mean stress drop was 40 bars (Woodward-Clyde Federal Services *et al.*, 1996).

No studies have been performed to evaluate the variability in kappa in the Wasatch Front region. Kappa can have a very significant effect on high-frequency ground motions, with lower values of kappa resulting in larger high-frequency ground motions (Silva and Darragh, 1993; Silva *et al.*, 1996). The average kappa for the western U.S. is 0.03 to 0.04 sec (Silva and Darragh, 1993). In their analysis, Becker and Abrahamson (1997) computed a median kappa of 0.047 sec.

Two studies to estimate $Q(f)$ for the Wasatch Front region have been performed (Brockman and Bollinger, 1992; Jeon and Herrmann, 2004). We have inverted for this parameter although its

importance to hazard is not as significant as in other regions in probabilistic terms since the nearby Wasatch fault is the controlling source. $Q(f)$ is important at long distances (> 100 km).

Site amplification at the individual recording sites may be the most significant factor that controls ground shaking at soil sites. Amplification factors for the Wasatch Front region were computed by Wong *et al.* (2002a) using the point-source stochastic ground motion model (Silva *et al.*, 1996). Pankow and Pechmann (2004) measured frequency-dependent low-strain site amplification factors using data from 18 earthquakes recorded on the ANSS stations. Their site amplification factors were determined for three site response units defined by Ashland (2001) using distance-corrected spectral ratios between horizontal component ground motion records from soil sites and reference rock sites.

In a study by Wong and Silva (1993), stochastic numerical ground motion modeling was performed to estimate the hazard at three representative sites in the Salt Lake City area. Because numerical modeling requires specified source, path, and site parameters, this study made the first critical examination of factors controlling ground motion hazard in the region. Key parameters included stress drop, $Q(f)$, κ , and site amplification. This evaluation was repeated by Wong *et al.* (2002a) in the development of scenario and probabilistic earthquake ground shaking maps for the Salt Lake City metropolitan area. They used magnitude-dependent stress drops of 60, 45, and 36 bars for M 5.5, 6.5, and 7.5, respectively, with a σ_{in} of 0.7. These stress drops, which are appropriate for extensional regime, were derived by the second and fourth authors in this study from an evaluation of static stress drops from the NGA strong motion database. A Q_0 of 400, η of 0.20, and κ of 0.04 sec were also used (Wong *et al.*, 2002a).

DATA PROCESSING

In this study, we analyzed strong motion and broadband data from ANSS and UUSS stations in the central Wasatch Front region. At the end of 2007, the ANSS network recorded by the UUSS in this region consisted of 81 strong motion stations, seven with co-located three-component broadband instruments, and five additional broadband stations (Figure 1). Most of these 86 stations are operated by UUSS with USGS and State of Utah funding, and ten are operated by the USGS. The study area consists primarily of the area from 39.35° to 42.0° N. and 111.0° to 113.0° W. where all of the earthquakes and all but one of the stations used in this study are

located (Figure 1). We selected 17 of the larger events from 2001 through 2007 in the ANSS dataset based on their distribution within the Wasatch Front and the number and distribution of recording sites (Figure 1; Table 1). The 17 earthquakes were recorded by a total of 74 stations resulting in 409 records (Table 2). Each station had been classified as a rock or soil site by UUSS.

In the first stage of the data processing, the acceleration response was removed from each record to obtain a time history of acceleration. S-wave arrival times were visually picked from the resulting acceleration records. Each record was visually examined to select an appropriate S-wave time window for analysis. The S-wave windows were generally satisfactory except for several recordings that were dominated by noise. These records were discarded and are not included in the analyses.

The subsequent processing steps included windowing the time series, mean removal, and 5% cosine tapering of the start and end of the windowed time series before transformation to the frequency domain using the fast Fourier transform. Window lengths are generally between 5 to 10 sec. Shorter time windows were used for impulsive S-wave arrivals. Longer windows were used for several records that contained emergent S-wave arrivals.

The Fourier amplitude spectra inverted in the analyses were computed from the windowed S-waves on the two horizontal components. The two horizontal spectra are combined to form the normal vector sum acceleration spectrum $A(f) = [(A_E^2(f) + A_N^2(f))/2]^{1/2}$ where $A_E(f)$ and $A_N(f)$ are the Fourier amplitudes of the horizontal-component accelerograms and f is frequency. These spectra are then smoothed over frequency intervals Δf chosen so that $\log \Delta f = 0.1$

INVERSION METHOD

The approach utilized in this study uses an inversion scheme developed by the second author (Silva *et al.*, 1997). In this inversion scheme, earthquake source, path and site parameters are obtained by using a nonlinear least-squares inversion of Fourier amplitude spectra for point-source model parameters. The point-source parameters are those that are incorporated into the stochastic ground motion model of Hanks and McGuire (1981), Boore (1983), and Silva *et al.* (1997; 1998). The ground motion model used in the inversion is

$$A(f) = M_0 C \frac{f^2}{1 + (f/f_c)^2} G(R) e^{-\pi \eta R / \beta_0 Q(f)} e^{-\pi f \kappa} S(f)$$

where M_0 is the seismic moment, C is a constant, f_c is the earthquake corner frequency, R is the hypocentral distance, $G(R)$ is the geometrical spreading factor, β_0 is the shear-wave velocity of the upper crust, $Q(f) = Q_0 f^\eta$ is a frequency-dependent quality factor, where Q_0 and η are model parameters, $e^{-\pi f \kappa}$ represents near-surface attenuation, parameterized by κ , and $S(f)$ is the near-surface site amplification. In the inversions performed in this study, \mathbf{M} is fixed to the M_L value assigned by UUSS.

The stress drop ($\Delta\sigma$) is calculated from the seismic moment and corner frequency using the relation:

$$f_c = \beta_0 \left(\frac{\Delta\sigma}{8.44 \cdot M_0} \right)^{\frac{1}{3}}$$

(Brune, 1970; 1971). In keeping with the model's simplicity, the point-source distance metric uses hypocentral depth for small earthquakes. The geometrical spreading factor is fixed in the inversions except for a distance, R_0 , at which it is assumed to change from a body wave rate to a surface wave rate. At distances less than R_0 , geometrical spreading is $1/R$ versus $1/R^{-1/2}$ at longer distances. Given these assumptions, the remaining parameters to be determined by the inversions are Q_0 , η , R_0 , κ , and the f_c for each earthquake or, effectively, the stress drop. Distinct kappa values are determined for each site and multiple stations (at varying distances) may be specified as belonging to a single site (or category).

The inversion procedure uses the Levenberg-Marquardt algorithm. The inversion scheme treats multiple earthquakes and sites simultaneously with the common crustal path damping parameter $Q(f)$. The parameter covariance matrix is examined to determine which parameters may be resolved for each data set. Asymptotic standard errors are computed at the final iteration. To reduce the non-uniqueness inherent in inversion schemes, a suite of starting models is employed. The final set of parameters is selected based upon a visual inspection of the model fits to the Fourier amplitude spectrum, the chi-square values, and the parameter covariance matrix.

The inversions were done on log amplitude spectra since strong ground motion data appear to be lognormally distributed. This approach is consistent with the model being represented as a product (rather than sum) of models. The low-frequency limit for the inversions was set at 0.5 Hz, based on consideration of signal-to-noise ratios. A high-frequency limit was set at 20 Hz to reduce the tendency toward high frequency weighting when using linear frequency spacing. Tests have been done using spectra smoothed over a constant log frequency window to provide exactly equal weighting. However, this procedure results in poorer fits (for fixed \mathbf{M}), possibly due to the models' tendency to overpredict low-frequency amplitudes at close distances.

A constraint that was encountered in performing the inversions of the Utah data was that crustal and soil profile amplification is typically accommodated by incorporating amplification factors appropriate for California generic rock and deep (> 150 m) soil. A preliminary round of inversions indicated that this assumption was not appropriate for the Wasatch Front based on large percentage of poor spectral fits. Hence the inversions were performed in four steps.

DEVELOPMENT OF ROCK V_S PROFILE

In the first step, only the rock site recordings were used in the inversion. A rock shear-wave velocity (V_S) and density (ρ) profile was required in order to account for near-surface site amplification at these sites. For this purpose, we developed what we consider to be a representative rock site velocity-density model using data for the site of station NOQ, which is located on Paleozoic limestone in the northern Oquirrh Mountains west of the Salt Lake Valley at 40° 39.17' N, 112° 07.13' W, elevation 1622 m (Table 2). We chose this site because it is one of the few rock sites in the Wasatch Front region for which there is reasonably reliable information available on the near-surface velocity structure. It is also an ANSS broadband and strong-motion recording site.

The uppermost 30 m of our rock site velocity model is from P- and S-wave refraction models for the NOQ site published by Stephenson *et al.* (2007) (Figure 2). The corresponding V_{s30} value is 660 m/sec. The model from 30 to 400 m depth is from a deep S-wave refraction profile by Stephenson *et al.* (2007) located about 150 m south of the NOQ site (Figure 2). We calculated the P-wave velocity (V_P) value from the V_S of 1675 m/sec assuming a V_P/V_S ratio of 1.896—the

ratio in the Wasatch Front Community Velocity Model (WFCVM; Magistrale *et al.*, 2009) in rock at 400 m depth.

The model from 400 to 19,000 m depth is from the WFCVM for the NOQ site (Figure 2). The WFCVM P-wave velocities above 4000 m depth are generalized from sonic log profiles from seven wells in bedrock in the Wasatch Front area (Pechmann *et al.*, 2010). The V_P below 5000 m depth in the WFCVM are from a tomographic inversion of P-wave arrival time data from the UUSS network by Lynch (1999). The V_P between 4000 and 5000 m are a weighted average of the velocities from these two sources. The V_S in the WFCVM are calculated from the V_P assuming a V_P/V_S of 2.0 at the surface and 1.74 at 1000 m depth, with a linear gradient in between.

From 19,000 m depth to the Moho at 42,000 m depth, we used a modified version of the Keller *et al.* (1975) refraction model (Bjarnason and Pechmann, 1989). We computed the densities for the rock site model below 19,000 m depth and above 400 m depth with the density- V_P relation used in the WFCVM:

$$\rho = 1865 + 0.1579 V_P$$

where ρ is in kg/m^3 and V_P is in m/sec. Frequency-dependent rock amplification factors (Figure 3) were computed from the rock profile (Figure 2) for the case of vertically-propagating S-waves.

INVERSIONS

Step 1. In this step, inversions were performed with the rock amplification factors using just the rock recordings to estimate Q_0 , η , R_0 , κ , and the stress drop, $\Delta\sigma$, for each of the 17 earthquakes. The rock inversions were done for a single value of κ to help stabilize them. The resulting values are

$$\begin{aligned} Q_0 &= 123.3 \\ \eta &= 0.67 \\ R_0 &= 51.2 \text{ km} \\ \bar{\Delta\sigma} &= 31.4 \text{ bars} \\ \bar{\kappa} (\text{rock}) &= 0.054 \text{ sec} \end{aligned}$$

Step 2. In this step, the results from Step 1 are used to invert the soil recordings to obtain an average set of site amplification factors for the soil sites. Q_0 , η , R_0 , κ , and the 16 values of $\Delta\sigma$ from Step 1 (event #1 does not have any useable recordings on soil sites) fixed to the values obtained in Step 1 to calculate predicted Fourier acceleration spectra. The mean residual over all the soil sites, the “bias” was then used to adjust the rock amplification factors to get the soil amplification factors shown in Figure 3. The soil amplification factors are higher than the rock amplification factors at all frequencies, with the differences decreasing with increasing frequency up to 5 Hz where the difference is constant.

Step 3. In this step, the rock and soil amplification factors are used to invert both the rock and soil records, again with a single κ value to stabilize the inversions. The resulting values are:

$$\begin{aligned} Q_0 &= 137.1 \\ \eta &= 0.56 \\ R_0 &= 59.9 \text{ km} \\ \overline{\Delta\sigma} &= 22.5 \text{ bars} \\ \overline{\kappa} &= 0.039 \text{ sec (for all sites)} \end{aligned}$$

Step 4. In the final step, Q_0 , η , and R_0 were fixed to the values obtained in Step 3 and the rock and soil amplification factors were used in the inversions to obtain a κ value for each station (Table 3) and a stress drop for each event (Table 1).

The final inversions are shown on Figures 4 to 20. In general, the comparisons between the recorded Fournier amplitude spectra (data) and the predicted spectra (final model) are good. For a few stations, the data appeared to be contaminated by noise or have other issues and so they were deleted from the final inversions (blank boxes in Figures 4 to 20). The final model bias for the soil, rock, and the combined rock and soil are shown on Figures 21 to 23, respectively. The bias for the rock sites and the combined sites are near zero. For the rock sites, the bias drops between 10 and 20 Hz. For the soil sites, the bias is high between 6 and 15 Hz and then it too drops at 20 Hz.

The final stress drops for the earthquakes range from 3 to 147 bars with a final geometric mean $\Delta\sigma$ of 20.1 bars (Tables 1 and 4). The one standard deviation range around the geometric mean stress drop is 7 to 60 bars. Silva *et al.* (1997) using the same inversion technique used in this

study calculated a mean stress drop of 59 bars for 9 California earthquakes ranging from M 5.7 to 7.3 including the 1994 M 6.7 Northridge and 1992 M 7.3 Landers earthquakes. Table 4 shows the final mean kappa values for all sites, rock sites, and soil sites. These kappas are within the range of typical values for the western U.S. (Silva and Darragh, 1993).

Jeon and Herrmann (2004) obtained somewhat higher Q_0 and η values of 160 and 0.75, respectively, although their computed $\Delta\sigma$ was an unusual 300 bars. Brockman and Bollinger (1992) obtained a Q_0 of 97, which is lower than our value, and an η of 0.80, which is higher than our value.

CONCLUSIONS

We inverted ANSS recordings of 17 earthquakes of M_L 2.6 to 4.2 located in the Wasatch Front area for source, path, and site factors. The results provide a suitable set of input parameters for stochastic ground-motion modeling in the Wasatch Front region. They also provide a reliable model for distance corrections of Fourier acceleration spectra, which can be used in more detailed future analyses of site amplification factors.

An important result is the estimation of stress drops for these admittedly small earthquakes. Previous studies suggested that stress drops for normal-faulting earthquakes in the adjacent Basin and Range Province are smaller than for typical California earthquakes. The results of these analyses suggest that is the case for the Wasatch Front area. The implication of smaller stress drops in the Wasatch Front and adjacent Basin and Range Province is that ground motions may be lower as compared to compressional regimes such as California. However, if stress drops are magnitude-dependent, then extrapolation to larger earthquakes ($M > 5.0$) of most engineering relevance is not possible at this time. Analyses of future larger earthquakes will be required to resolve this issue.

ACKNOWLEDGMENTS

This study was supported by the U.S. Geological Survey, Department of Interior, under NEHRP Award 05HQGR0010. Our thanks to Fabia Terra for her help with the compilation of the data set and to Melinda Lee and Danielle Lowenthal-Savy for their assistance in the preparation of this paper. The views and conclusions contained in this document are those of the authors and

should not be interpreted as necessarily representing the official policies, either expressed or implied of the U.S. Government.

REFERENCES

- Arabasz, W. J., Pechmann, J. C., and Brown, E.D., 1992, Observational seismology and the evaluation of earthquake hazards and risk in the Wasatch Front area, Utah, in P.L. Gori and W.W. Hays (eds.), *Assessment of Regional Earthquake Hazards and Risk Along the Wasatch Front, Utah*, U.S. Geological Survey Professional Paper 1500-A-J, p. D1-D36.
- Ashland, F.X., 2001, Site-response characterization for implementing SHAKEMAP in northern Utah, Utah Geological Survey Report of Investigation, v. 248, 10 p., 2 pl.
- Becker, A.M. and Abrahamson, N.A., 1997, Stress drops in normal faulting earthquakes (abs.), *Seismological Research Letters*, v. 68, p. 322.
- Benz, H. and Smith, R.B., 1988, Elastic-wave propagation and site amplification in the Salt Lake Valley, Utah, *Bulletin of the Seismological Society of America*, v. 73, p. 1865-1884.
- Bjarnason, I.T. and Pechmann, J.C., 1989, Contemporary tectonics of the Wasatch Front region, Utah, from earthquake focal mechanisms, *Bulletin of the Seismological Society of America*, v. 79, p. 731-755.
- Black, B.D., Lund, W.R., Schwartz, D.P., Gill, H.E., and Mayes, B.H., 1996, Paleoseismic investigation of the Salt Lake City segment of the Wasatch fault zone at the South Fork Dry Creek and Dry Gulch sites, Salt Lake County, Utah, Utah Geological Survey Special Study 92, 22 p.
- Boore, D.M., 1983, Stochastic simulation of high-frequency ground motions based on seismological models of the radiated spectra, *Bulletin of the Seismological Society of America*, v. 73, p. 1865-1884.
- Brockman, S.R. and Bollinger, G.A., 1992, Q estimates along the Wasatch Front in Utah derived from Sg and Lg wave amplitudes, *Bulletin of the Seismological Society of America*, v. 82, p. 135-147.
- Brune, J.N., 1970, Tectonic stress and the spectra of seismic shear waves from earthquakes, *Journal of Geophysical Research*, v. 75, p. 4997-5009.
- Brune, J.N., 1971, Correction, *Journal of Geophysical Research*, v. 76, p. 5002.

- Cocco, M. and Rovelli, A., 1989, Evidence for the variation of stress drop between normal and thrust faulting earthquakes in Italy, *Journal of Geophysical Research*, v. 94, p. 9399-9416.
- DuRoss, C.B., 2008, Holocene vertical displacement on the central segments of the Wasatch fault zone, Utah, *Bulletin of the Seismological Society of America*, v. 98, p. 2918-2933.
- DuRoss, C.B., Personius, S.F., Crone, A.J., Olig, S.S., and Lund, W.R., 2010, Revised earthquake timing, recurrence, and strawman rupture models for the central Wasatch fault, presentation to the Working Group on Utah Earthquake Probabilities.
- Hanks, T.C. and McGuire, R.K., 1981, The character of high-frequency strong ground motion, *Bulletin of the Seismological Society of America*, v. 71, p. 2071-2095.
- Hays, W.W. and King, K.W., 1984, The ground-shaking hazard along the Wasatch fault zone, Utah, *in* W.W. Hays and P.L. Gori (eds.), *Proceedings of Workshop XXVI on Evaluation of Regional and Urban Earthquake Hazards and Risk in Utah*, U.S. Geological Survey Open-File Report 84-763, p. 133-147.
- Hill, J., Benz, H., Murphy, M., and Schuster, G., 1990, Propagation and resonance of SH waves in the Salt Lake Valley, Utah, *Bulletin of the Seismological Society of America*, v. 80, p. 23-42.
- Jeon, Y. and Herrman, R.B., 2004, High-frequency earthquake ground motion scaling in Utah and Yellowstone, *Bulletin of the Seismological Society of America*, v. 94, p. 1644-1657.
- King, J.J., Doyle, T.E., and Jackson, S.M., 1987, Seismicity of the eastern Snake River Plain region, Idaho, prior to the Borah Peak, Idaho, earthquake: October 1972-October 1983, *Bulletin of the Seismological Society of America*, v. 77, p. 809-818.
- Liu, Q., and Archuleta, R.J., 2009, Earthquake ground motion for the Salt Lake City segment of the Wasatch fault, *Eos Trans. AGU*, v. 90, no. 52, Fall Meeting Supplement, Abstract S43A-1976.
- Lynch, D.P., 1999, Three-dimensional finite-difference tomography of the Basin and Range-Colorado Plateau-Rocky Mountain transition using earthquake and controlled source data, Master of Science Thesis, University of Utah, Salt Lake City, Utah, 155 pp.
- Machette, M.N., Personius, S. F., Nelson, A. R., Schwartz, D.P., and Lund, W. R., 1991, The Wasatch fault zone, Utah-segmentation and history of Holocene earthquakes: *Journal of Structural Geology*, v.13, p.137-149.

- Machette, M.N., Personius, S.F., and Nelson, A.R., 1992, Paleoseismology of the Wasatch fault zone: A summary of recent investigations, conclusions and interpretations, Chapter A, in Assessment of Regional Earthquake Hazards and Risk Along the Wasatch Front Area, Utah, U.S. Geological Survey Professional Paper 1500, p. A1-A71.
- Magistrale, H., Pechmann, J.C., and Olsen, K.B., 2009, The Wasatch Front, Utah, community seismic velocity model, Seismological Research Letters, v. 80, p. 368.
- McCalpin, J.P., 1994, Neotectonic deformation along the East Cache fault zone, Cache County, Utah: Utah Geological Survey Special Study 83, 37 p.
- McGarr, A., 1984, Scaling of ground motion parameters, state of stress, and focal depth, Journal of Geophysical Research, v. 89, p. 6969-6979.
- Murphy, M., 1989, Finite-difference simulation of seismic P- and SV-wave amplification in Salt Lake Valley, Utah, Master of Science Thesis, University of Utah, Salt Lake City, Utah.
- Nelson, A.R., Lowe, M, Personius, S.F., Bradley, L.A., Forman, S.L., Klauk, R., and Garr, J., 2006,. Holocene earthquake history of the northern Weber segment of the Wasatch fault zone, Utah, in Paleoseismology of Utah, W.R. Lund (Editor), Vol. 13, Utah Geol. Surv. Misc. Pub. 05-8, 39 pp., 2 plates.
- Oglesby, D.D., Archuleta, R.J., and Nielsen, S.B., 1998, Earthquakes on dipping faults: the effects of broken symmetry, Science, v., 280, p. 1055-1059.
- Olsen, K.B., Pechmann, J.C., and Schuster, G.T., 1995, Simulation of 3D elastic wave propagation in the Salt Lake Basin, Bulletin of the Seismological Society of America, v. 85, p. 1688-1710.
- Olsen, K.B., Pechmann, J.C., and Schuster, G.T., 1996, An analysis of simulated and observed blast records in the Salt Lake Basin, Bulletin of the Seismological Society of America, v. 86, p. 1061-1076.
- Pankow, K.L. and Pechmann, J.C., 2004, Determination of low-strain site-amplification factors in the Salt Lake Valley, Utah, using ANSS data, Basin and Range Province Seismic Hazards Summit II, 15 p.
- Pechmann, J.C., Jensen, K.J., and Magistrale, H, 2010, Constraints on the near surface seismic velocity structure of the Wasatch Front region, Utah, from sonic log analyses, Seismological Research Letters, v. 81, p. 358.

- Roten, D., Olsen, K.B., Cruz-Atienza, V.M., Pechmann, J.C., and Magistrale, H., 2009, 3-D ground motion modeling for M 7 dynamic rupture earthquake scenarios on the Wasatch fault, Utah, *Eos Trans. AGU*, v. 90, no. 52, Fall Meeting Supplement, Abstract S42B-07.
- Roten, D., Olsen, K.B., Pechmann, J.C., Cruz-Atienza, V.M., and Magistrale, H., 2010, Ground motion predictions from 0-10 Hz for M 7 earthquakes on the Salt Lake City segment of the Wasatch fault, Utah, *Seismological Research Letters*, v. 81, 320.
- Schwartz, D.P. and Coppersmith, K.J., 1984, Fault behavior and characteristic earthquakes—examples from the Wasatch and San Andreas fault zones: *Journal of Geophysical Research*, v. 89, p. 5681-5698.
- Shi, B., Brune, J.N., Zheng, Y., and Anooshehpour, A., 2003, Dynamics of earthquake normal faulting: two-dimensional lattice particle model, *Bulletin of the Seismological Society of America*, v. 93, p. 1179-1197.
- Silva, W.J., Abrahamson, N., Toro, G., and Costantino, C., 1997, Description and validation of the stochastic ground motion model: unpublished report submitted to Brookhaven National Laboratory, Associated University, Inc. Upton, New York.
- Silva, W.J. and Darragh, R.B., 1993, Engineering characterization of strong ground motion recorded at rock sites: unpublished report submitted to Electric Power Research Institute Research Project RP 2556-48.
- Silva, W.J., Wong, I.G., and Darragh, R.B., 1998. Engineering characterization of earthquakes strong ground motions in the Pacific Northwest, *in* A.M. Rogers, T.J. Walsh, W.J. Kockelman, and G.R. Priest (eds.), *Assessing Earthquake Hazards and Reducing Risk in the Pacific Northwest: U.S. Geological Survey Professional Paper 1560, 2*, 313-324.
- Smith, R.B., and Arabasz, W.J., 1991, Seismicity of the Intermountain seismic belt in D.B. Slemmons, E.R. Engdahl, M.D. Zoback, M. L. Zoback, and D. Blackwell (eds.), *Neotectonics of North America*, Geological Society of North America, SMV V-1, p. 185-228.
- Smith, R.B., and Sbar, M.L., 1974, Contemporary tectonics of the interior of the western United States with the emphasis of the Intermountain Seismic Belt: *Geological Society of America Bulletin*, v. 85, p. 1205-1218.

- Solomon, B.J., Storey, N., Wong, I., Silva, W., Gregor, N., Wright, D., and McDonald, G., 2004, Earthquake-hazards scenario for a M 7 earthquake along the Salt Lake City segment of the Wasatch fault zone, Utah, Utah Geological Survey Special Study (in press).
- Spudich, P., Fletcher, J.B., Hellweg, M., Boatwright, J., Sullivan, C., Joyner, W.B., Hanks, T.C., Boore, D.M., McGarr, A., Baker, L.M., and Lindh, A.G., 1997, SEA96- A new predictive relation for earthquake ground motions in extensional tectonic regimes: *Seismological Research Letters*, v. 68, p. 190-198.
- Spudich, P., Joyner, W.B., Lindh, A.G., Boore, D.M., Margaris, B.M., and Fletcher, J.B., 1999, SEA99 – A revised ground motion prediction relation for use in extensional tectonic regimes: *Bulletin of the Seismological Society of America*, v. 89, p. 1156-1170.
- Stark, C.L., Silva, W.J., Wong, I.G., and Jackson, S.M., 1992, Assessment of stress drops of normal faulting earthquakes in the Basin and Range province (abs.), *Seismological Research Letters*, v. 63, p. 39.
- Stephenson, W.J., Williams, R.A., Odum, J.K., and Worley, D.M., 2007, Miscellaneous high-resolution seismic imaging investigations in Salt Lake and Utah Valleys for earthquake hazards, U.S. Geological Survey Open-File Report 2007-1152, 29 pp.
- Swan, F.H. III, Schwartz, D.P., and Cluff, L.S., 1980, Recurrence of moderate to large magnitude earthquakes produced by surface faulting on the Wasatch fault zone, Utah: *Bulletin of the Seismological Society of America*, v. 70, p. 1431-1562.
- Westaway, R. and Smith, R.B., 1989, Strong ground motion in normal-faulting earthquakes, *Geophysical Journal*, v. 95, p. 529-559.
- Wong, I.G., 1979, Site amplification of seismic shear waves in Salt Lake Valley, Utah, *in* *Earthquake Studies in Utah, 1850 to 1978*, W.J. Arabasz, R.B. Smith and W.D. Richins (eds.), University of Utah Seismographic Stations, p. 321-337.
- Wong, I.G. and Silva, W.J., 1993, Site-specific strong ground motion estimates for the Salt Lake Valley, Utah, Utah Geological Survey Miscellaneous Publication 93-9, 34 p.
- Wong, I., Silva, W., Gregor, N., Wright, D., Ashland, F., McDonald, G., Olig, S., Christenson, G., and Solomon, B., 2002b, Earthquake scenario ground shaking maps for the central Wasatch Front, Utah, 7th U.S. National Conference on Earthquake Engineering Proceedings (CD ROM).

- Wong, I., Silva, W., Olig, S., Thomas, P., Wright, D., Ashland, F., Gregor, N., Pechmann, J., Dober, M., Christenson, G., and Gerth, R., 2002a, Earthquake scenario and probabilistic ground shaking maps for the Salt Lake City, Utah, metropolitan area, Utah Geological Survey Miscellaneous Publication MP-02-05, 50 p. with CD ROM.
- Wong, I.G., Silva, W.J., Youngs, R.R., and Stark, C.L., 1996, Numerical earthquake ground motion modeling and its use in microzonation, Proceedings, 11th World Conference on Earthquake Engineering, Pergamon (CD-ROM).
- Woodward-Clyde Federal Services, Geomatrix Consultants, and Pacific Engineering and Analysis, 1996, Site specific probabilistic seismic hazard analysis for the Idaho National Engineering Laboratory: Final Report prepared for Lockheed Martin Idaho Technologies and U.S. Department of Energy, INEL-95/0536, Volumes 1 and 2.
- Youngs, R.R., Swan, F.H., Power, M.S., Schwartz, D.P., and Green, R.K., 2000, Probabilistic analysis of earthquake ground shaking hazard along the Wasatch Front, Utah, in P.L. Gori and W.W. Hays (eds.), Assessment of Regional Earthquake Hazards and Risk Along the Wasatch Front, Utah: U.S. Geological Survey Professional Paper 1500-K-R, p. M1-M74.
- Zoback, M.D. and Zoback, M.L., 1989, Tectonic stress field of the continental United States, in Pakiser, L.C. and Mooney, W.D (eds.), Geophysical Framework of the Continental United States: Geological Society of America Memoir 172, p. 523-541.

Table 1. List of events analyzed in this study.

Event	Date	Event ID	Magnitude (M)	Latitude (degrees)	Longitude (degrees)	Depth (km)	$\Delta\sigma$ (bars)
1	20010524	10224024041	3.30	40.3777	-111.9307	5.9	10.62
2	20020728	20728193840	3.59	41.7445	-111.3802	9.3	5.84
3	20030103	30103050212	3.62	41.2745	-111.8020	11.70	22.52
4	20030201	30201203731	3.15	41.8288	-112.2120	0.22	12.38
5	20030417	30417010419	4.24	39.5095	-111.8962	0.08	2.83
6	20030712	30712015440	3.50	41.2855	-111.6148	8.97	38.98
7	20031227	31227003924	3.64	39.6480	-111.9430	0.88	15.43
8	20040225	40225004104	3.38	41.9977	-111.8182	1.68	44.00
9	20040313	40313130447	3.17	39.6572	-111.9377	1.77	13.19
10	20050518	50518192147	3.29	41.4245	-111.0898	1.56	11.43
11	20050723	50723053748	3.30	41.8835	-111.6325	11.07	147.27
12	20050905	50905093155	3.00	41.0222	-111.3568	7.41	27.26
13	20051120	51120102429	2.62	41.3672	-111.6910	2.77	132.13
14	20060611	60611100150	3.41	40.2468	-111.0733	10.37	15.11
15	20061220	61220181536	3.35	41.1270	-111.5745	7.94	89.78
16	20070901	70901183202	3.92	41.6423	-112.3185	5.61	6.07
17	20071105	71105214801	3.91	39.3458	-111.6475	5.50	16.81

Table 2. Wasatch Front Rock Site Velocity-Density Profile

Depth to Top (m)	V _S (m/sec)	V _P (m/sec)	Density (kg/m ³)
0	650.0	450.0	1967.6
4	970.0	450.0	2018.2
10	970.0	535.0	2018.2
12	2950.0	535.0	2330.8
17	2950.0	1290.0	2330.8
30	3175.8	1675.0	2366.5
400	3262.5	1744.7	2380.1
600	3419.1	1880.7	2404.9
800	3575.7	2024.7	2429.6
1000	3810.6	2190.0	2466.7
1400	4071.6	2340.0	2507.9
1800	4172.0	2397.7	2523.8
2200	4272.5	2455.5	2539.6
2600	4372.9	2513.2	2555.5
3000	4606.3	2647.3	2592.3
3400	4868.9	2798.2	2633.8
3800	5131.5	2949.2	2675.3
4200	5278.5	3033.6	2698.5
4600	5317.1	3055.8	2704.6
5000	5524.8	3175.1	2737.4
7000	5782.1	3323.0	2778.0
9000	5903.1	3392.6	2797.1
11000	5974.5	3433.6	2808.4
13000	6062.0	3483.9	2822.2
15000	6188.2	3556.5	2842.1
17000	6317.3	3630.6	2862.5
19000	6400.0	3680.0	2875.6
28000	7500.0	4310.0	3049.3
42000	7900.0	4540.0	3112.4

Table 3. Kappa and Rock/Soil Classification for the 74 Wasatch Front Recording Stations

NO	STA CODE	KAPPA (sec)	SITE TYPE
1	2272	0.043	SOIL
2	7228	0.039	SOIL
3	7229	0.047	SOIL
4	AHID	0.019	ROCK?
5	ALP	0.036	SOIL
6	ALT	0.065	ROCK
7	AVE	0.038	SOIL
8	BCS	0.047	SOIL
9	BCU	0.049	ROCK
10	BCW	0.038	ROCK
11	BES	0.050	SOIL
12	BGU	0.041	ROCK
13	BYU	0.022	SOIL
14	CFS	0.032	SOIL
15	CHS	0.058	SOIL
16	COY	0.015	ROCK
17	CTU	0.034	ROCK
18	CWR	0.049	ROCK
19	DOT	0.026	SOIL
20	DUG	0.070	ROCK
21	ELE	0.022	SOIL
22	EMF	0.038	SOIL
23	ETW	0.030	SOIL
24	FTT	0.028	SOIL
25	GAS	0.038	SOIL
26	GMV	0.025	ROCK
27	HCO	0.048	SOIL
28	HER	0.029	SOIL
29	HES	0.033	SOIL
30	HON	0.019	ROCK
31	HRU	0.026	ROCK
32	HVU	0.024	ROCK
33	HWUT	0.064	ROCK
34	ICF	0.030	SOIL
35	JLU	0.056	ROCK
36	JRP	0.022	SOIL
37	JVW	0.032	SOIL
38	LGC	0.049	SOIL
39	LKC	0.017	SOIL
40	LMU	0.037	ROCK
41	LRG	0.054	SOIL
42	LSU	0.046	SOIL
43	MAB	0.013	SOIL
44	MID	0.004	ROCK
45	MOR	0.042	ROCK
46	MPU	0.041	ROCK
47	NAI	0.023	ROCK
48	NLU	0.069	ROCK
49	NOQ	0.018	ROCK
50	OCP	0.064	SOIL

NO	STA CODE	KAPPA (sec)	SITE TYPE
51	OF2	0.048	SOIL
52	OPS	0.043	SOIL
53	OSS	0.026	SOIL
54	PCL	0.026	SOIL
55	PCR	0.053	SOIL
56	PGC	0.013	ROCK
57	RIV	0.041	SOIL
58	SCC	0.034	SOIL
59	SCS	0.038	SOIL
60	SCY	0.043	SOIL
61	SJF	0.040	SOIL
62	SPR	0.048	SOIL
63	SPS	0.030	SOIL
64	SPU	0.029	ROCK
65	WHS	0.047	SOIL
66	TMU	0.029	ROCK
67	TPU	0.050	SOIL
68	TRS	0.054	SOIL
69	UHP	0.032	SOIL
70	UTH	0.032	SOIL
71	VEC	0.042	SOIL
72	VES	0.031	SOIL
73	WBC	0.000	ROCK
74	WCF	0.051	SOIL

Table 4. Results of the Final Inversions

Q_0	137.05
η	0.56
$\bar{\Delta\sigma}$ (bars)	20.1
$\bar{\kappa}$ (sec)	0.034
$\bar{\kappa}$ for rock sites (sec)	0.030
$\bar{\kappa}$ for soil sites (sec)	0.036
R0 (km)	59.88

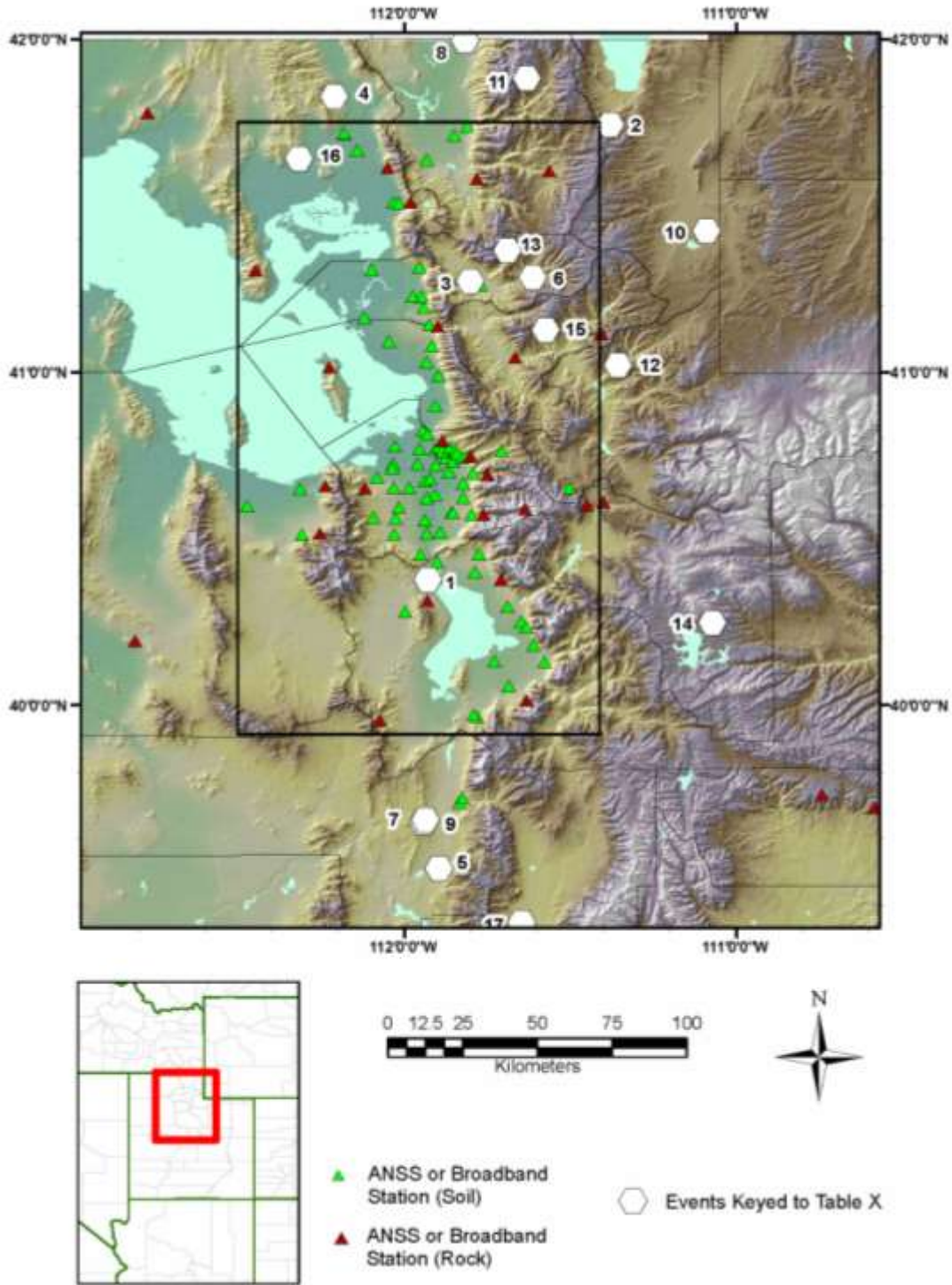
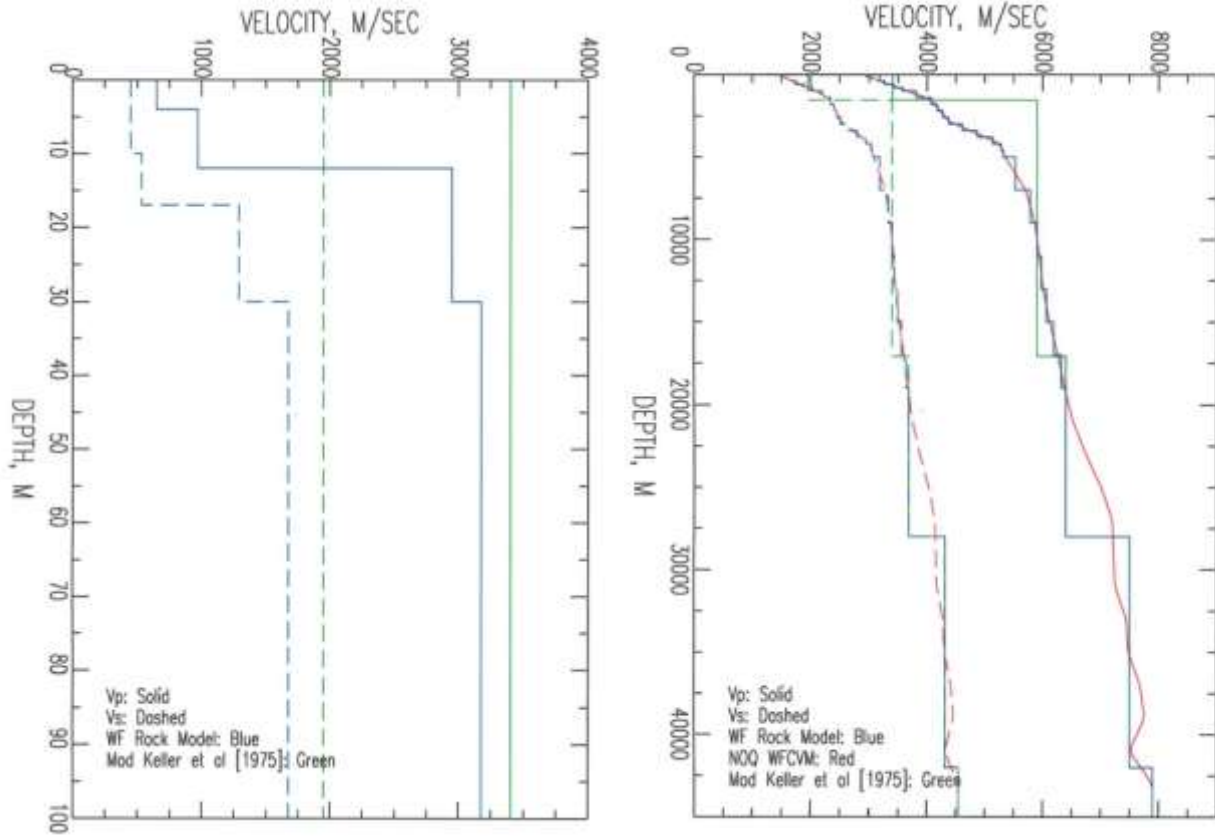


Figure 1. Map of ANSS broadband and strong-motion stations and 17 earthquakes analyzed in this study.



(a)

(b)

Figure 2. Hard rock V_S and V_P profiles developed for this study: (a) top 100 m and (b) full 40 km. Also shown is the model of Bjarnason and Pechmann (1989)

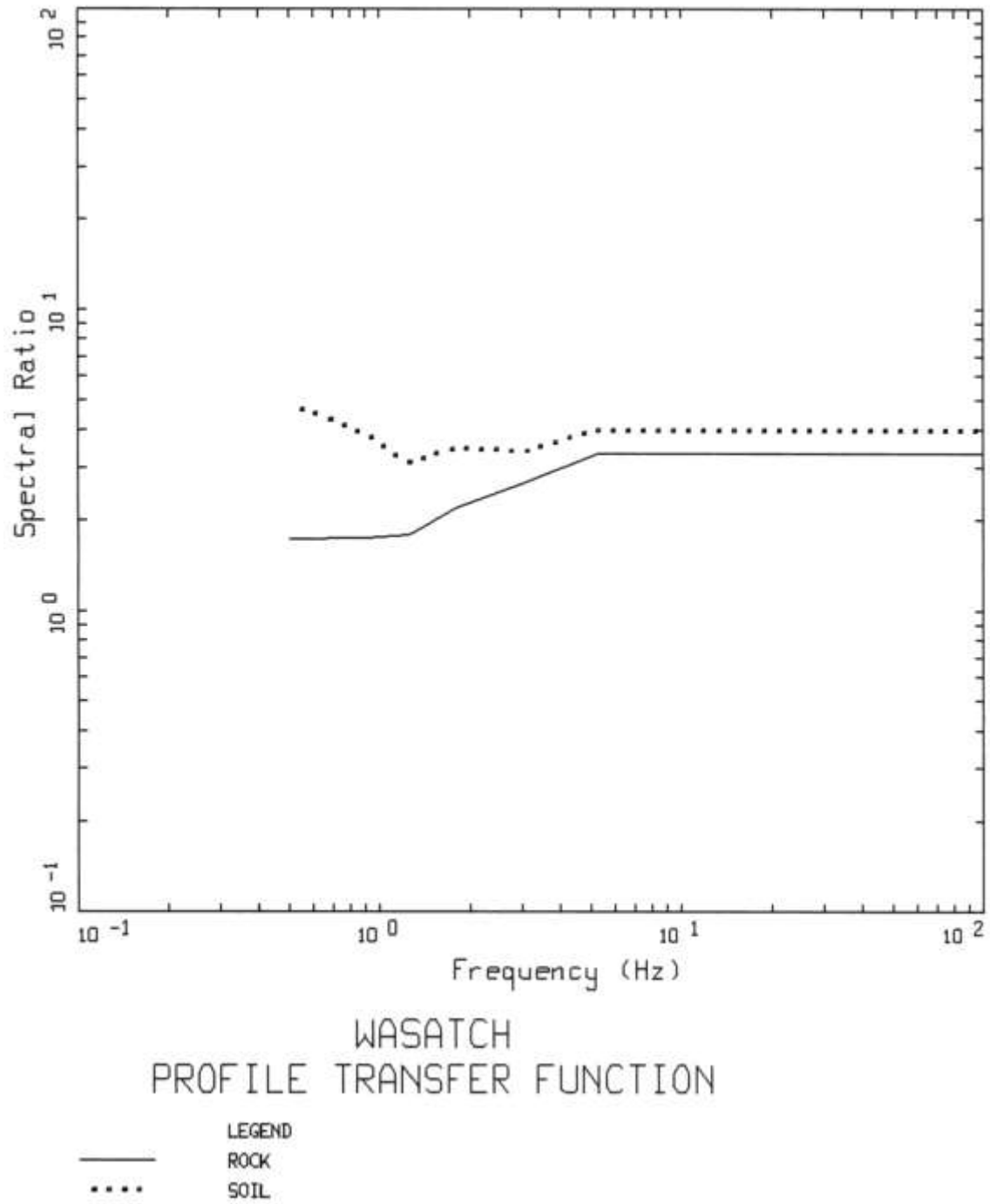
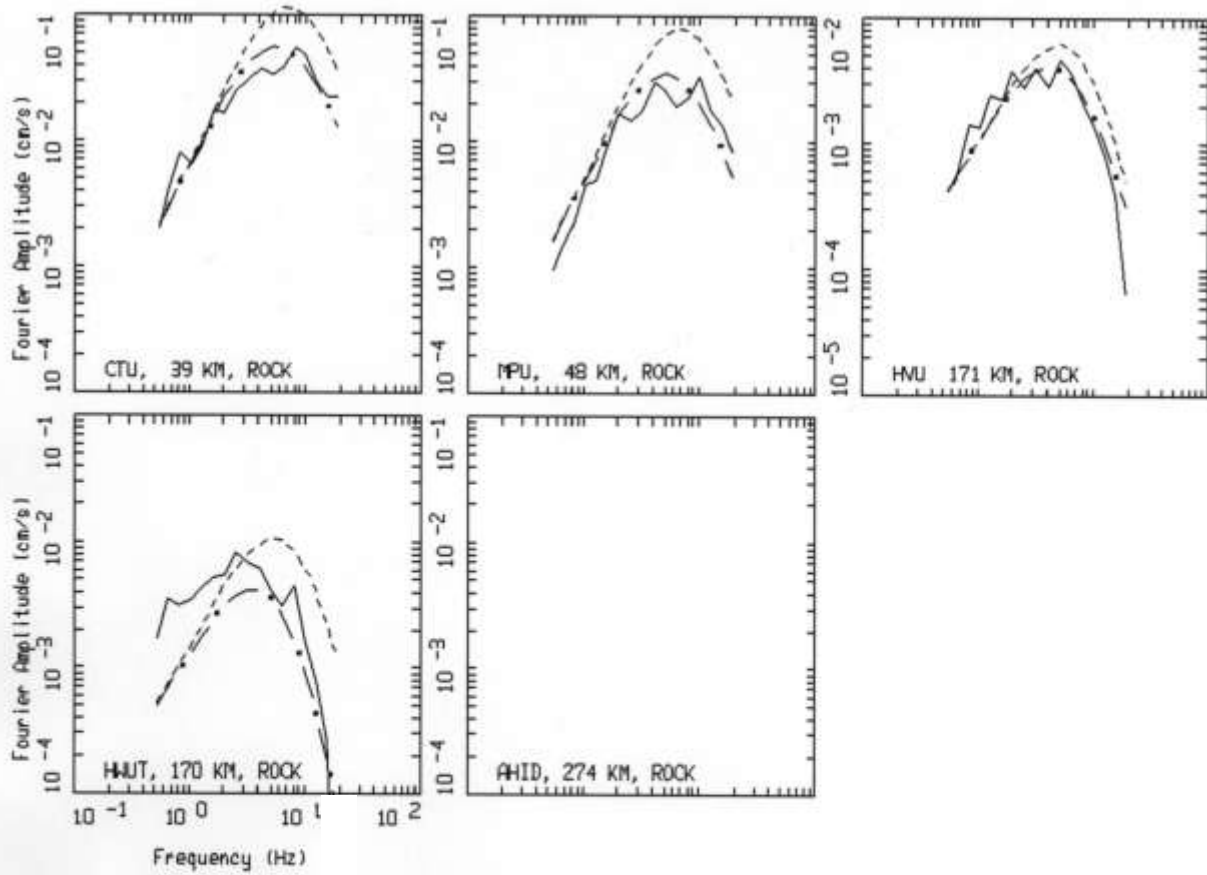


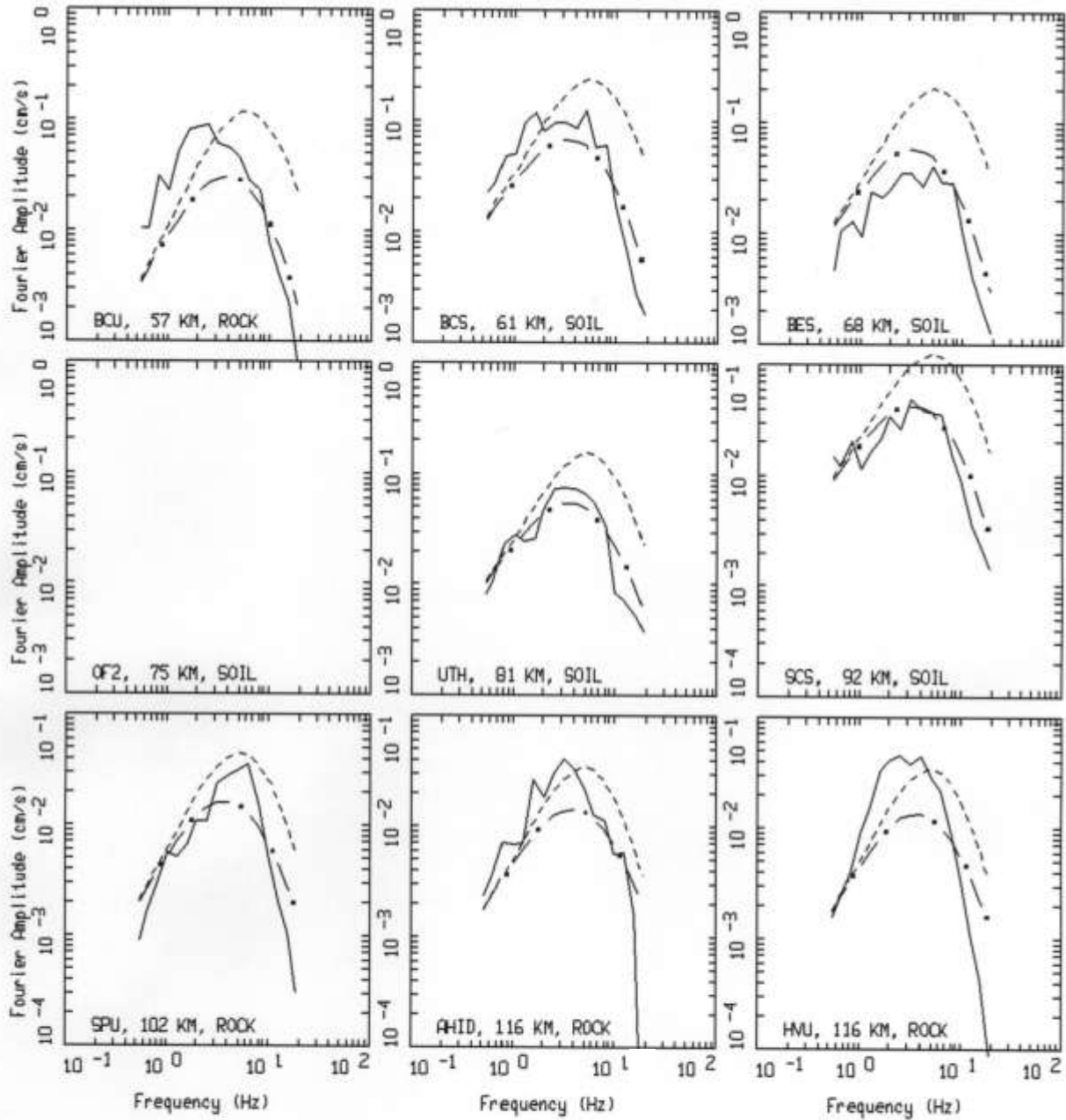
Figure 3. Wasatch Front frequency-dependent amplification factors for rock (Step 1) and soil (Step 2).



WASATCH EARTHQUAKES, EARTHQUAKE 1, PAGE 1 OF 1.
M = 3.30, 4 SITES (4 ROCK)

LEGEND
— DATA
- - - INITIAL MODEL
- . - FINAL MODEL

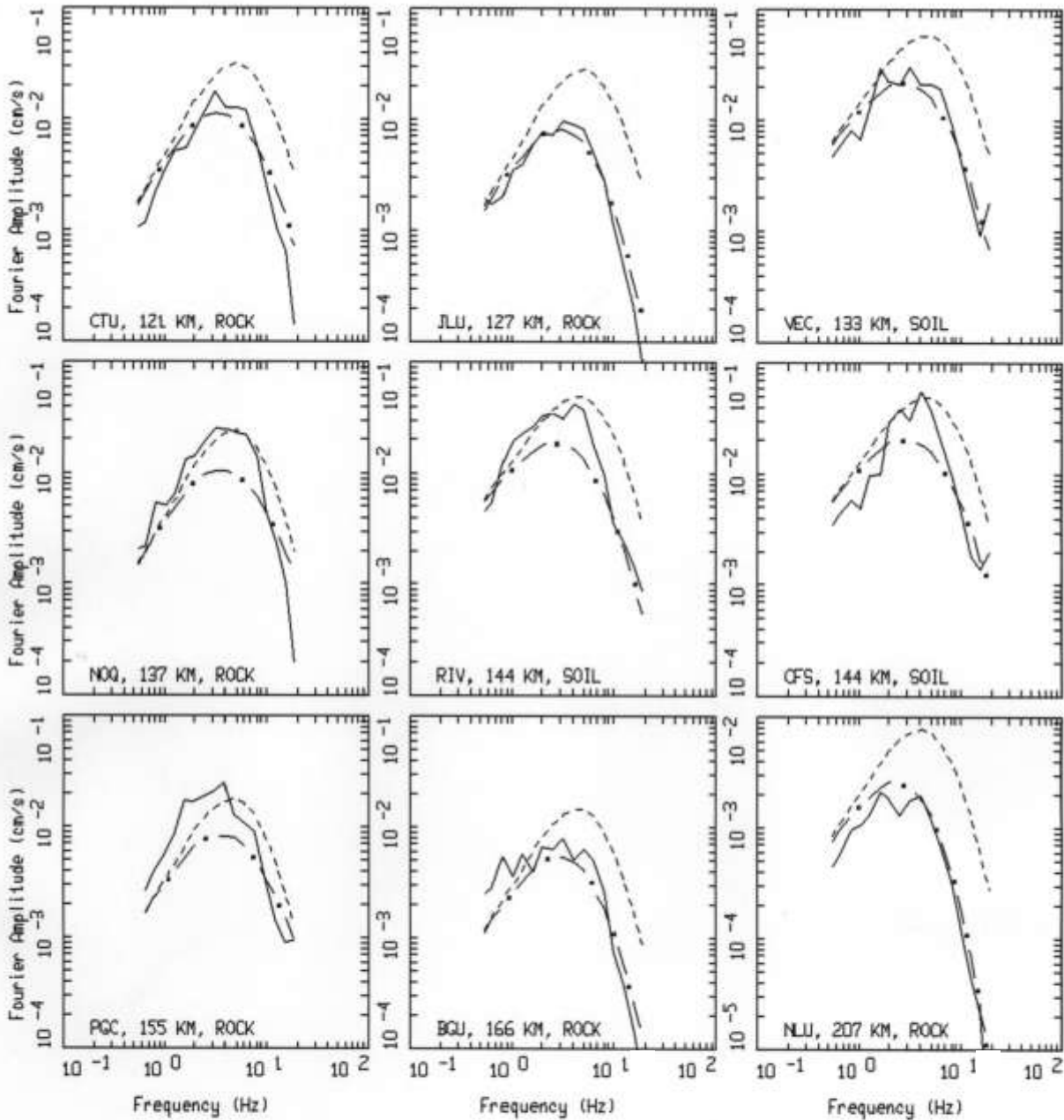
Figure 4. Spectral inversion results for Event #1.



WASATCH EARTHQUAKES, EARTHQUAKE 2, PAGE 1 OF 3.
 M = 3.59, 19 SITES (12 ROCK, 7 SOIL)

LEGEND
 — DATA
 - - - - INITIAL MODEL
 - • - FINAL MODEL

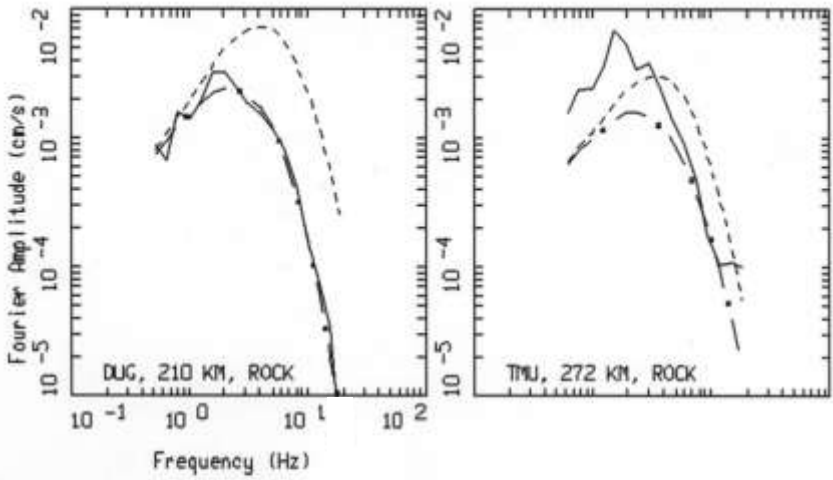
Figure 5. Spectral inversion results for Event #2.



WASATCH EARTHQUAKES, EARTHQUAKE 2, PAGE 2 OF 3.
 M = 3.59, 19 SITES (12 ROCK, 7 SOIL)

LEGEND
 — DATA
 - - - INITIAL MODEL
 - . - FINAL MODEL

Figure 5 (continued). Spectral inversion results for Event #2.



WASATCH EARTHQUAKES, EARTHQUAKE 2, PAGE 3 OF 3.
 M = 3.59, 19 SITES (12 ROCK, 7 SOIL)

LEGEND
 — DATA
 - - - - INITIAL MODEL
 - · - FINAL MODEL

Figure 5 (continued). Spectral inversion results for Event #2.

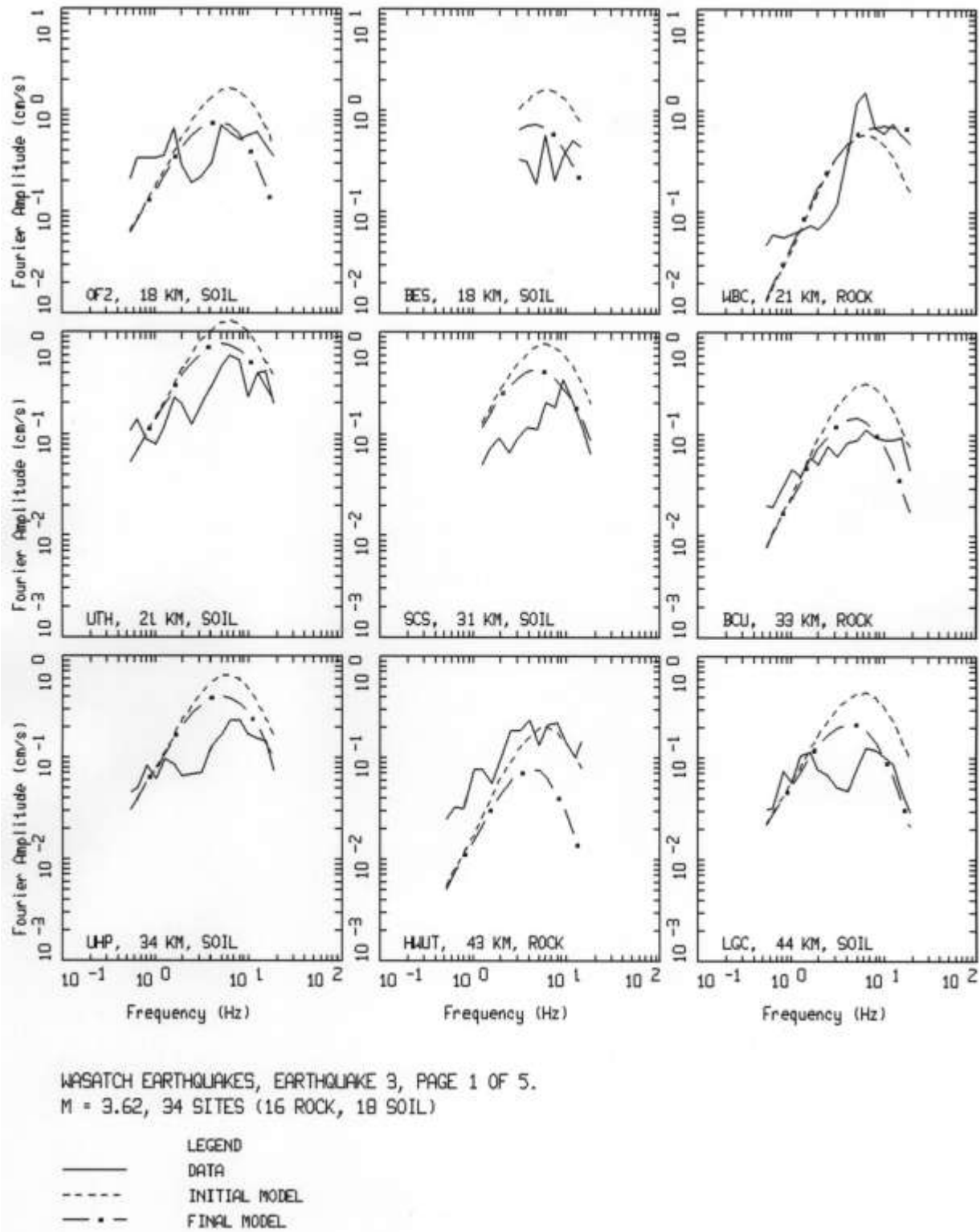


Figure 6. Spectral inversion results for Event #3.

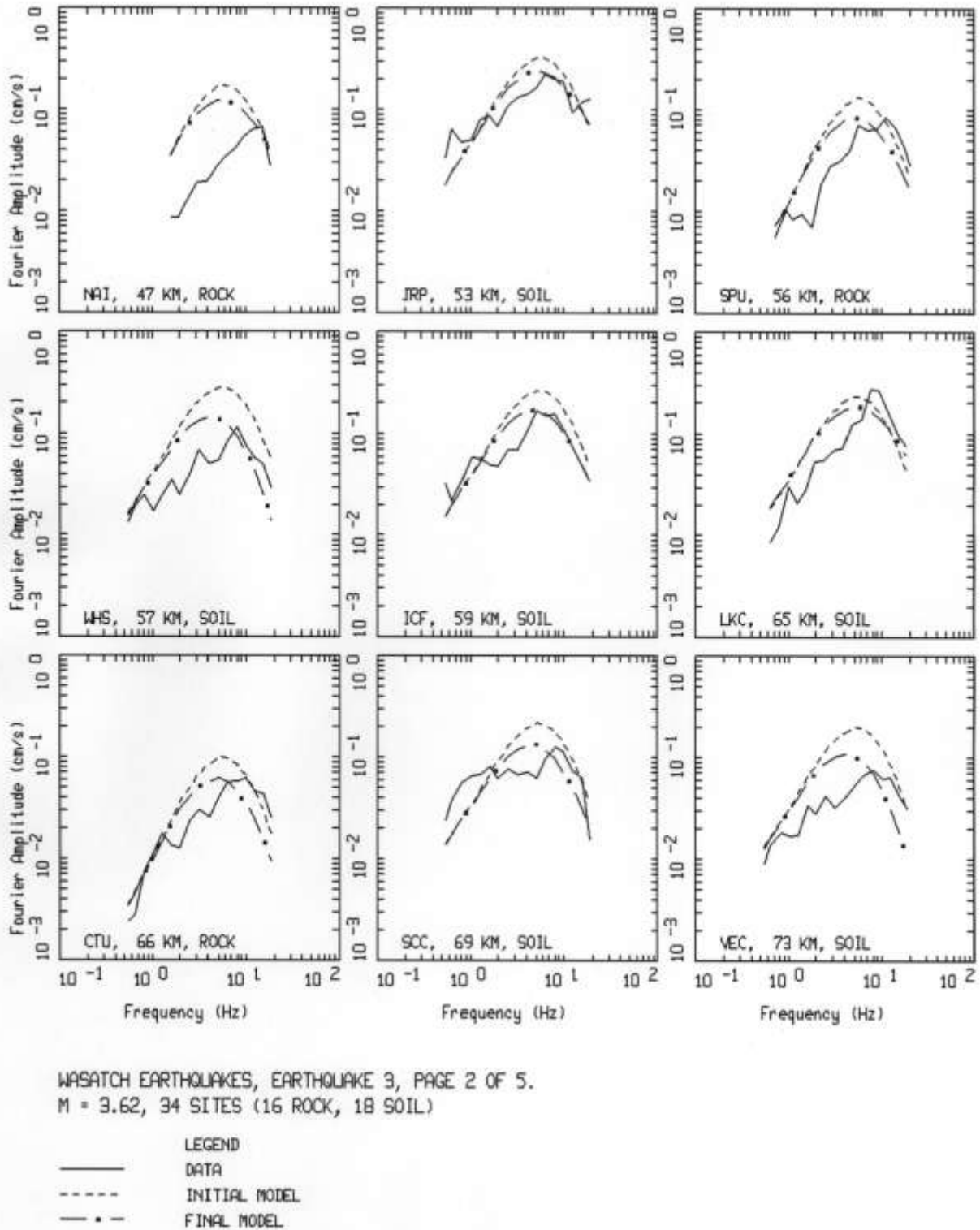
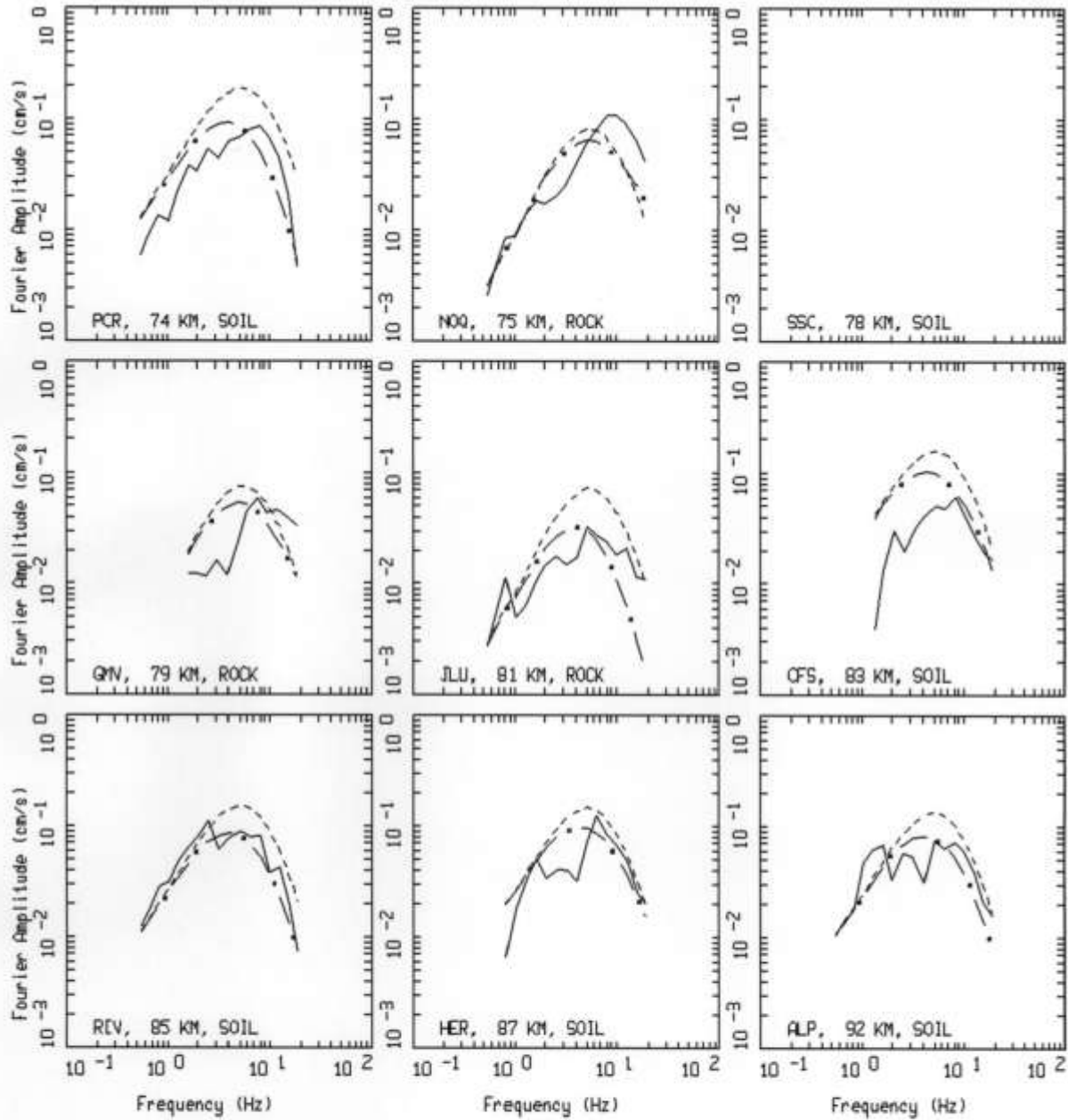


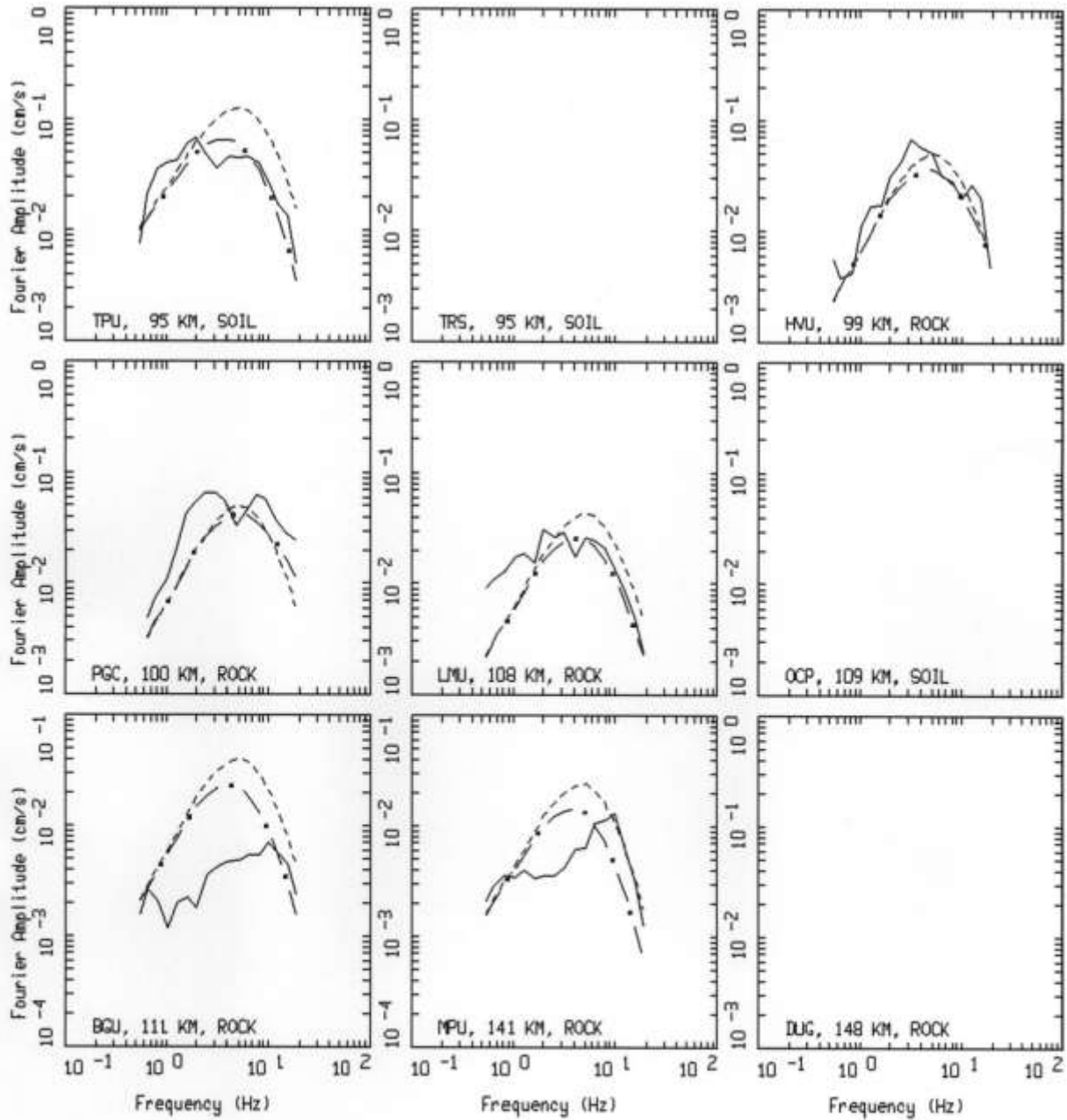
Figure 6 (continued). Spectral inversion results for Event #3.



WASATCH EARTHQUAKES, EARTHQUAKE 3, PAGE 3 OF 5.
 M = 3.62, 34 SITES (16 ROCK, 18 SOIL)

LEGEND
 — DATA
 - - - INITIAL MODEL
 - · - FINAL MODEL

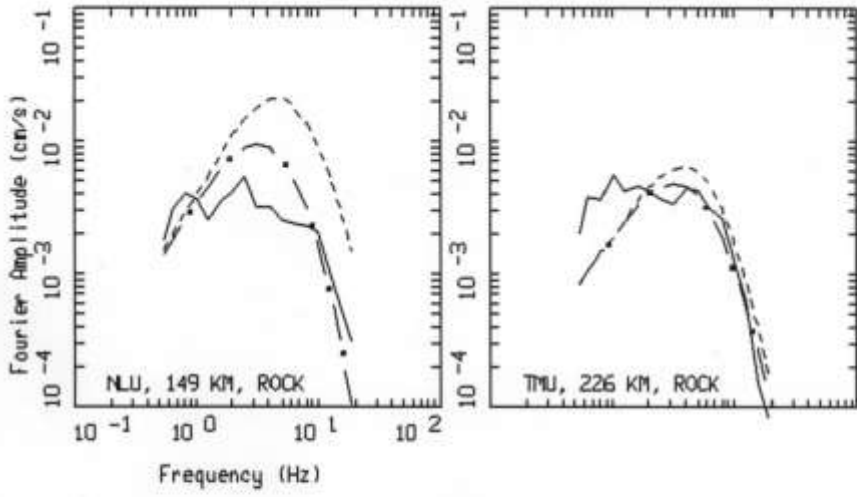
Figure 6 (continued). Spectral inversion results for Event #3.



WASATCH EARTHQUAKES, EARTHQUAKE 3, PAGE 4 OF 5.
M = 3.62, 34 SITES (16 ROCK, 18 SOIL)

LEGEND
— DATA
--- INITIAL MODEL
- · - FINAL MODEL

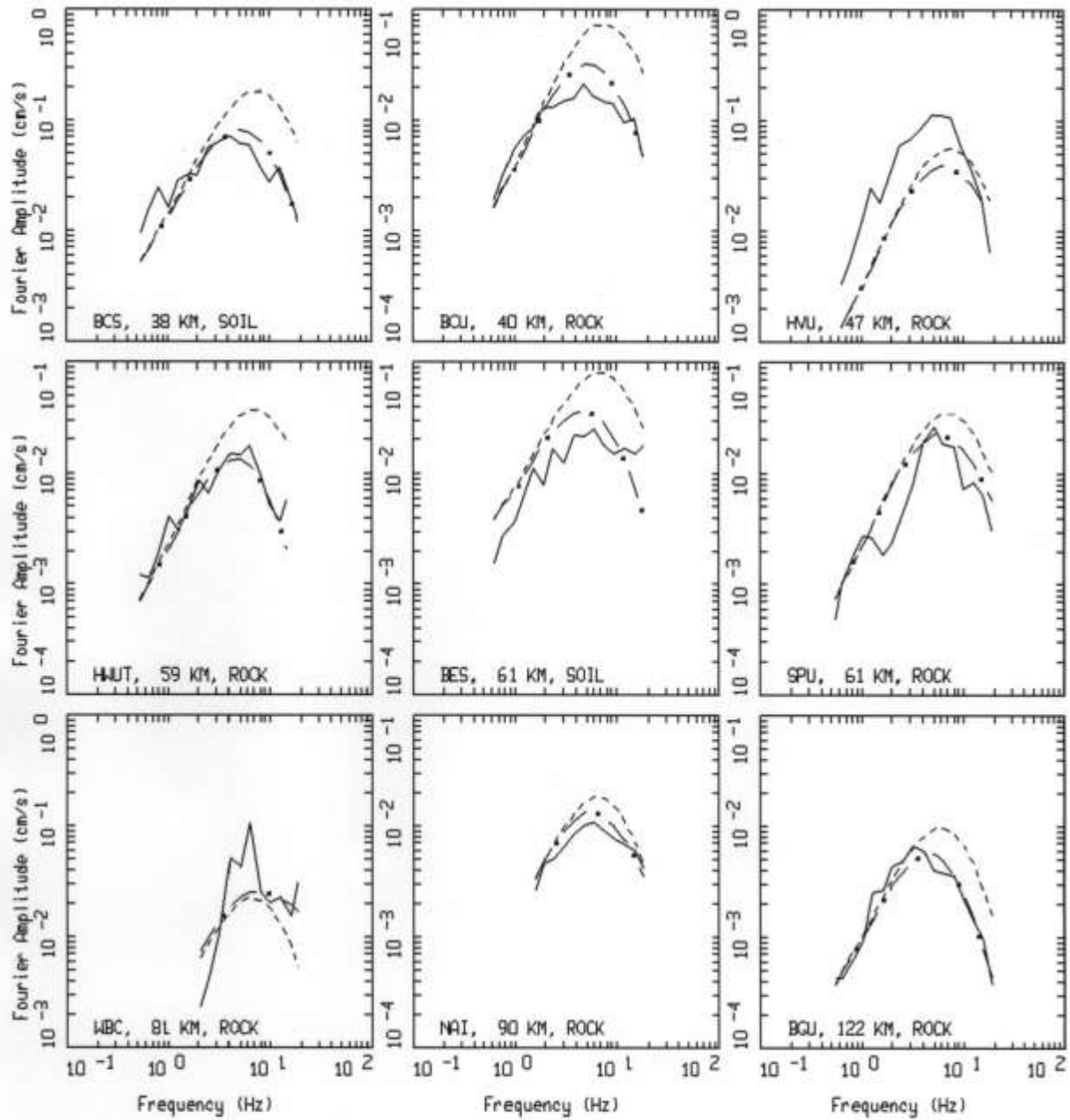
Figure 6 (continued). Spectral inversion results for Event #3.



WASATCH EARTHQUAKES, EARTHQUAKE 3, PAGE 5 OF 5.
 M = 3.62, 34 SITES (16 ROCK, 18 SOIL)

LEGEND
 — DATA
 - - - INITIAL MODEL
 - * - FINAL MODEL

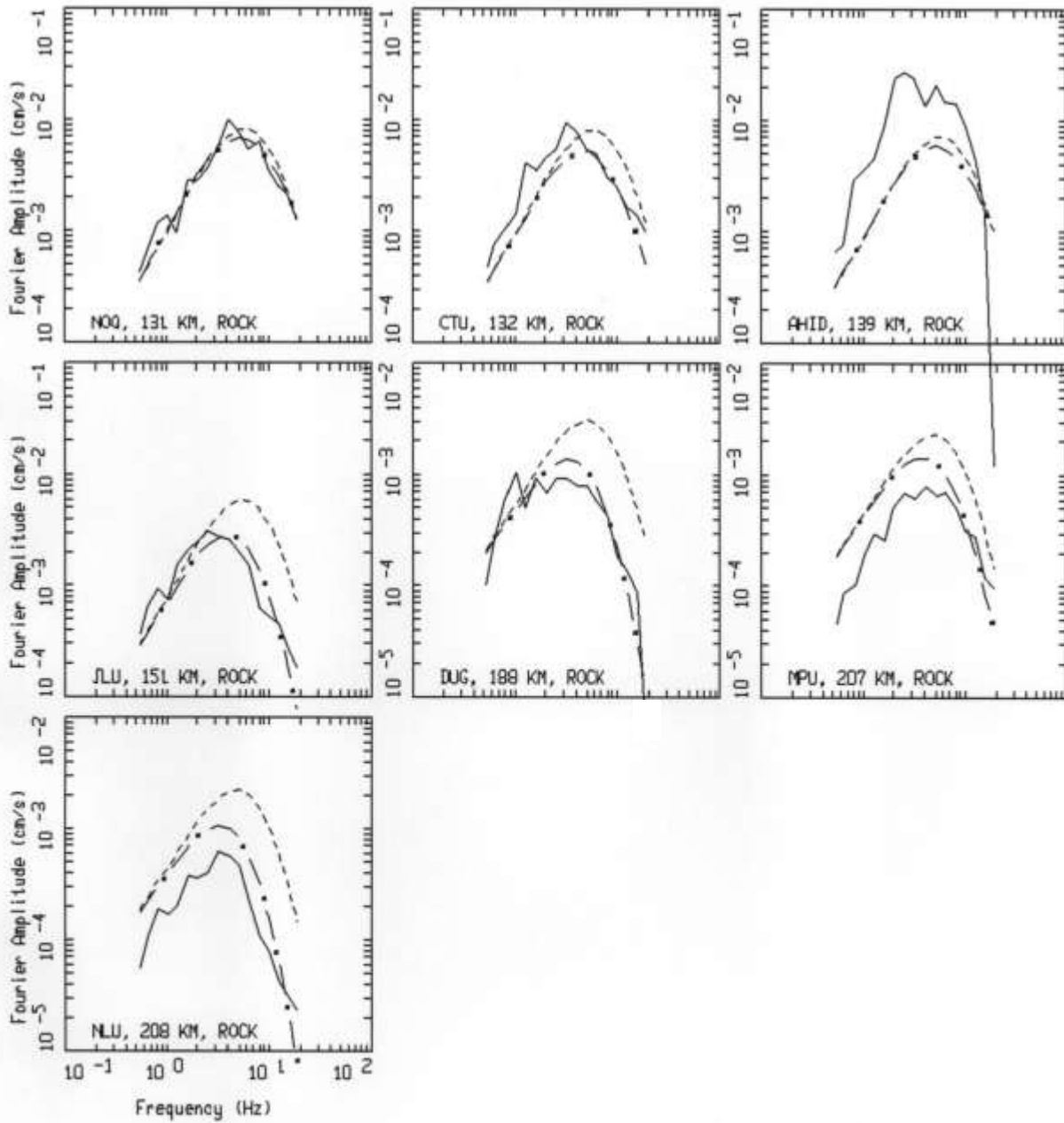
Figure 6 (continued). Spectral inversion results for Event #3.



WASATCH EARTHQUAKES, EARTHQUAKE 4, PAGE 1 OF 2.
 M = 3.15, 16 SITES (14 ROCK, 2 SOIL)

LEGEND
 — DATA
 - - - INITIAL MODEL
 - . - FINAL MODEL

Figure 7. Spectral inversion results for Event #4.



WASATCH EARTHQUAKES, EARTHQUAKE 4, PAGE 2 OF 2.
 M = 3.15, 16 SITES (14 ROCK, 2 SOIL)

LEGEND
 — DATA
 - - - INITIAL MODEL
 - * - FINAL MODEL

Figure 7 (continued). Spectral inversion results for Event #4.

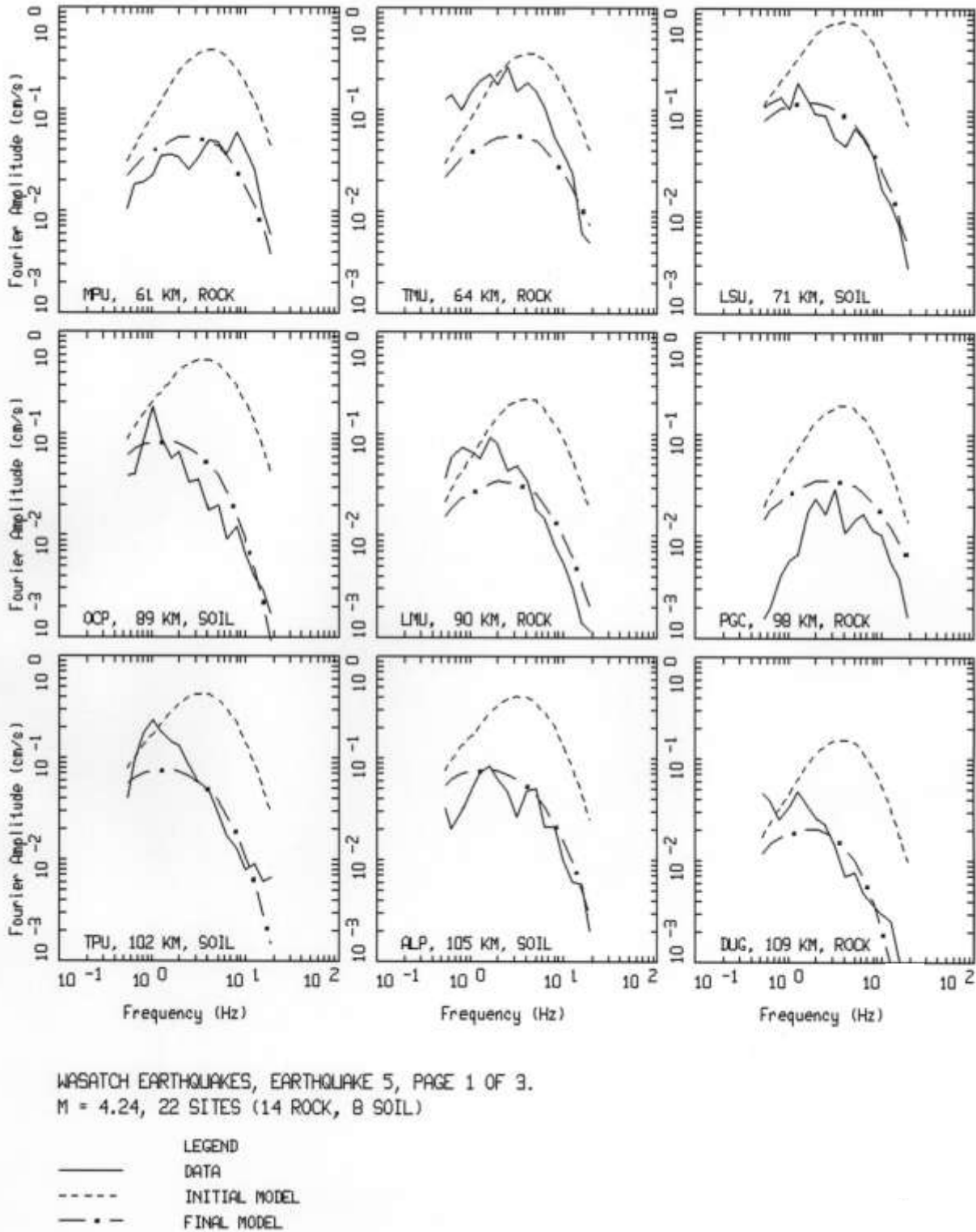
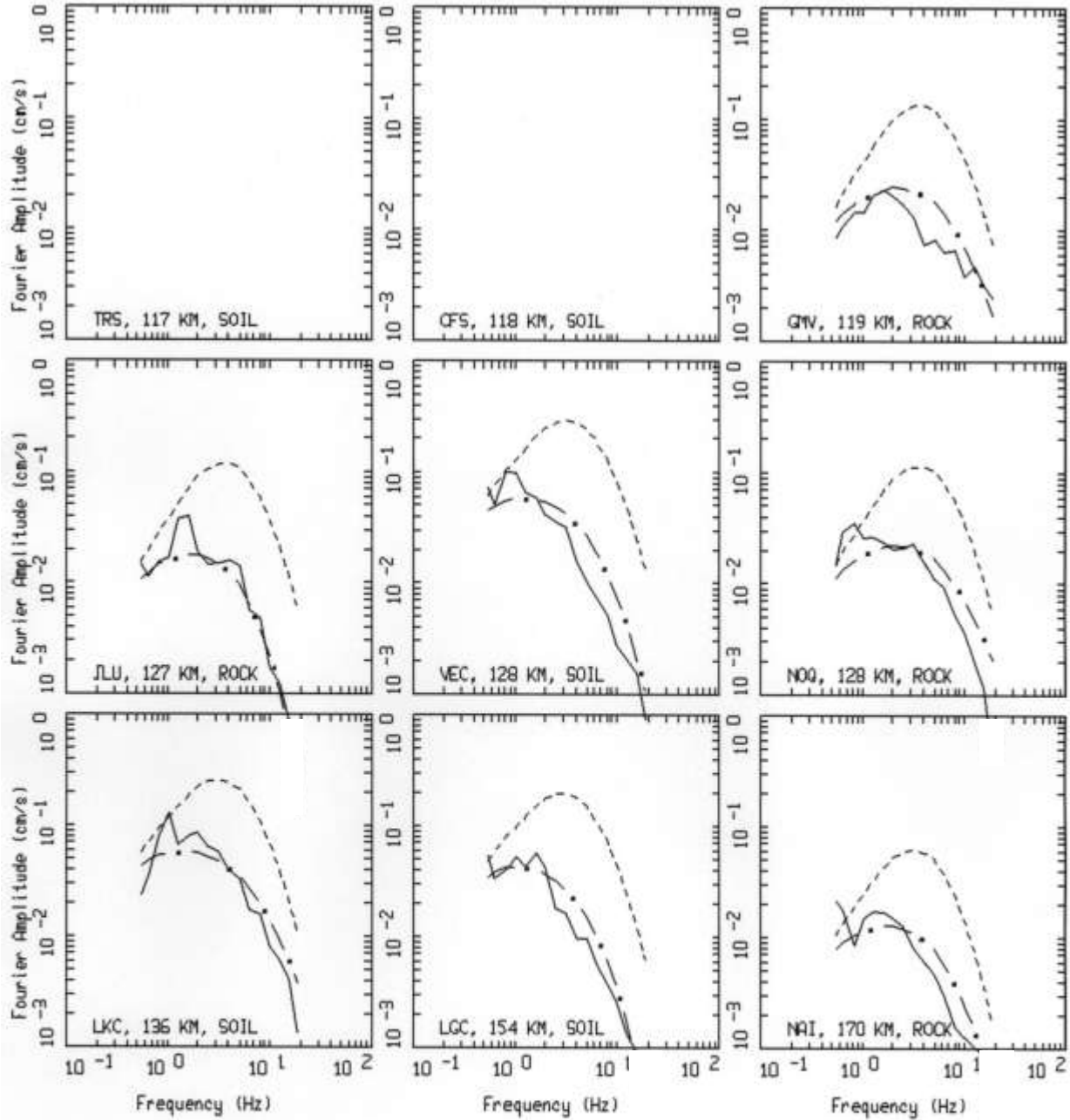


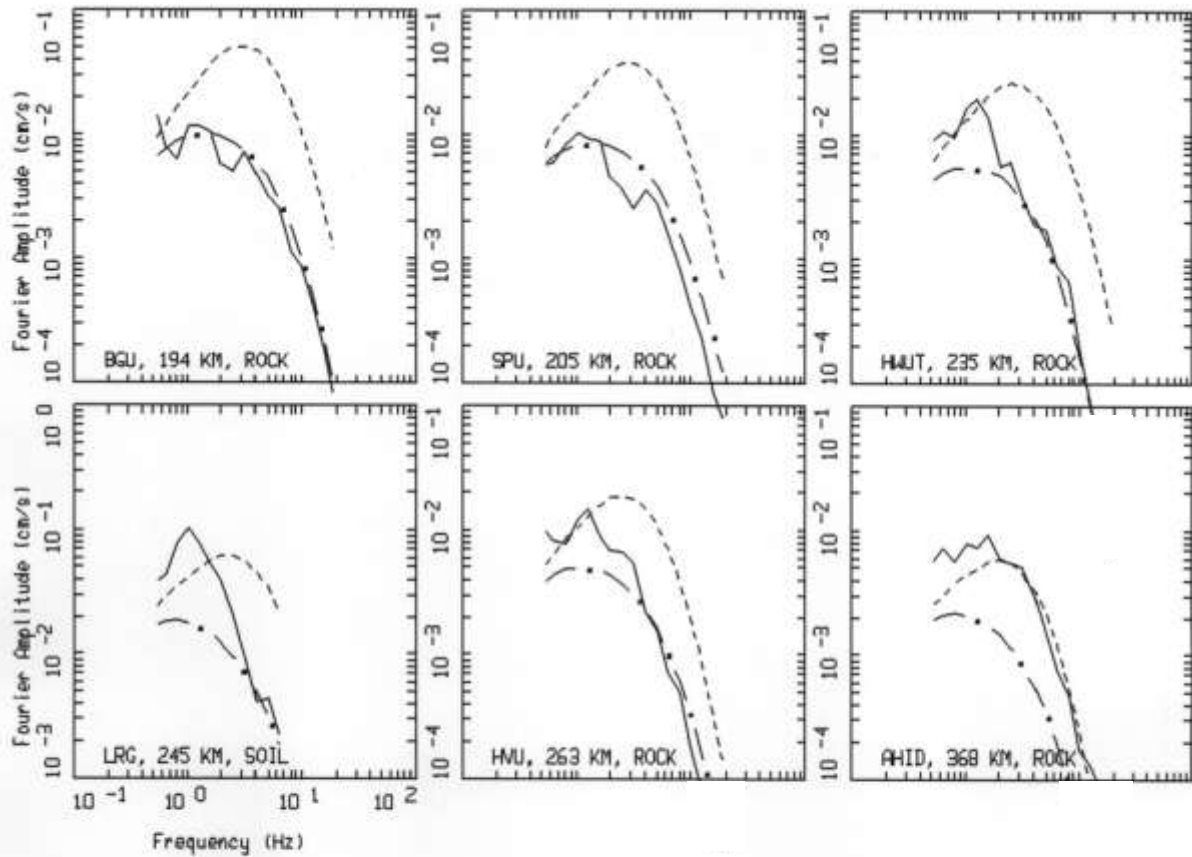
Figure 8. Spectral inversion results for Event #5.



WASATCH EARTHQUAKES, EARTHQUAKE 5, PAGE 2 OF 3.
M = 4.24, 22 SITES (14 ROCK, 8 SOIL)

LEGEND
— DATA
--- INITIAL MODEL
- . - FINAL MODEL

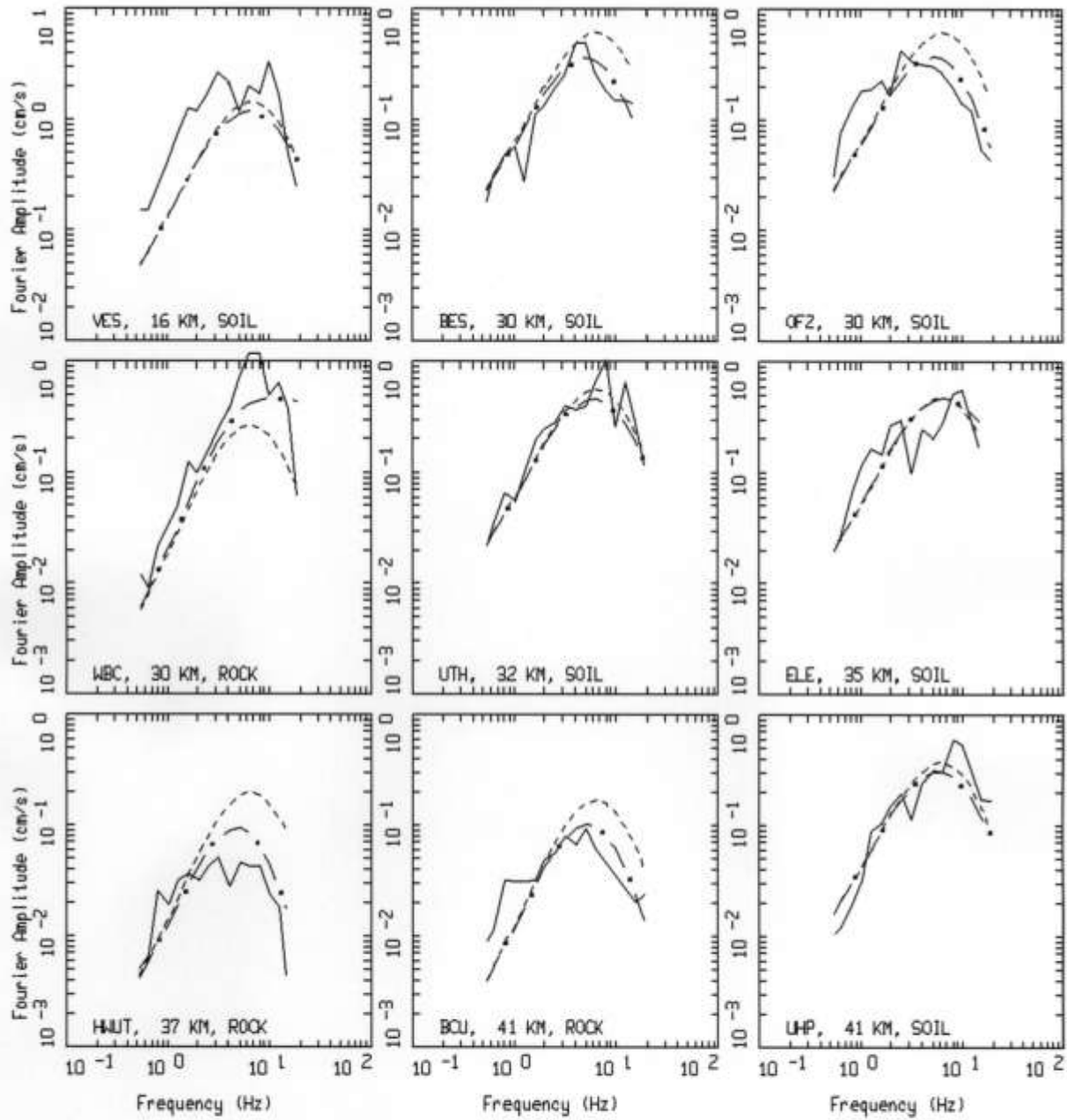
Figure 8 (continued). Spectral inversion results for Event #5.



WASATCH EARTHQUAKES, EARTHQUAKE 5, PAGE 3 OF 3.
M = 4.24, 22 SITES (14 ROCK, 8 SOIL)

LEGEND
— DATA
--- INITIAL MODEL
- · - FINAL MODEL

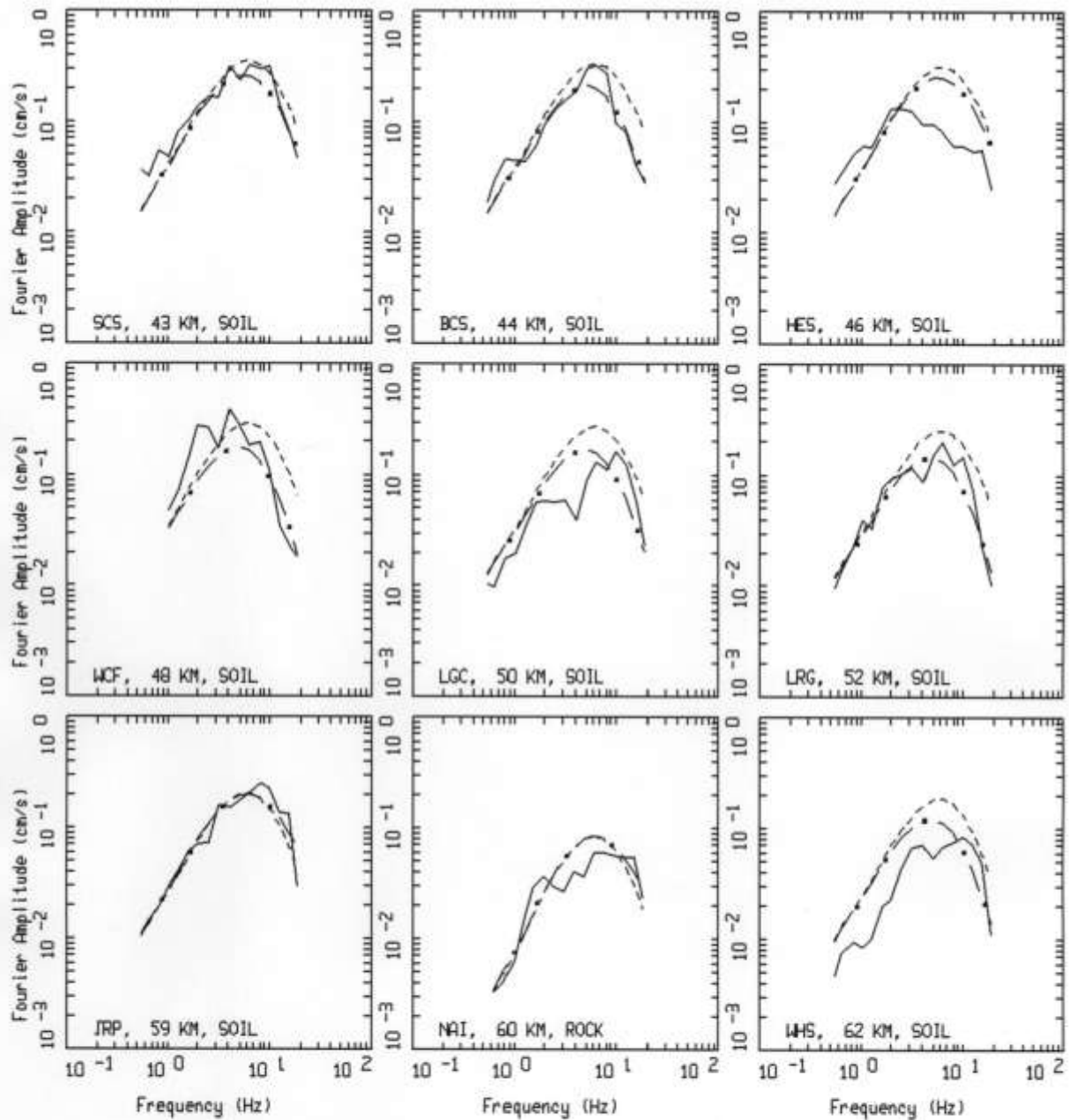
Figure 8 (continued). Spectral inversion results for Event #5.



WASATCH EARTHQUAKES, EARTHQUAKE 6, PAGE 1 OF 5.
 M = 4.24, 42 SITES (15 ROCK, 27 SOIL)

LEGEND
 — DATA
 - - - INITIAL MODEL
 - . - FINAL MODEL

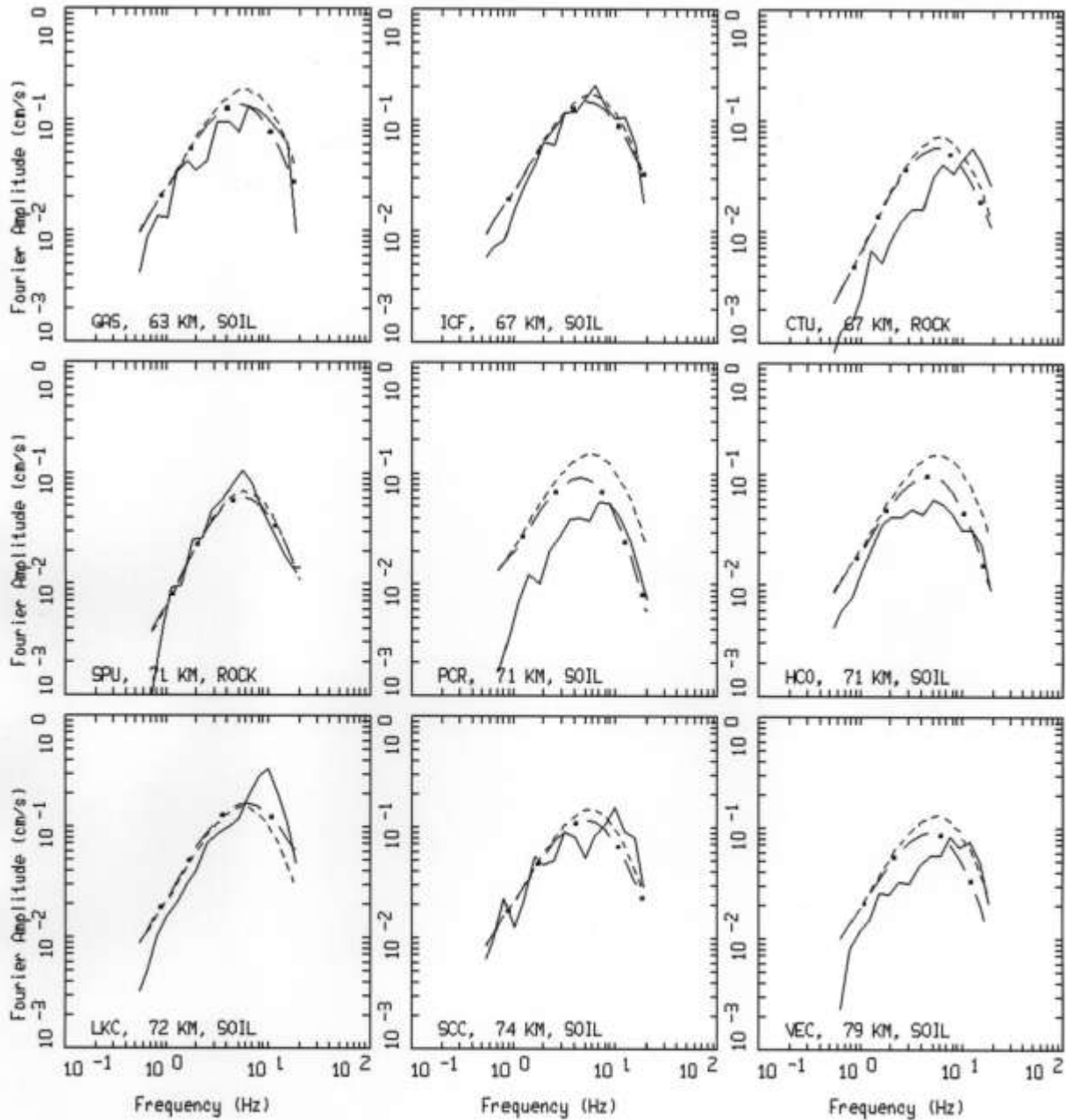
Figure 9. Spectral inversion results for Event #6.



WASATCH EARTHQUAKES, EARTHQUAKE 6, PAGE 2 OF 5.
 M = 4.24, 42 SITES (15 ROCK, 27 SOIL)

LEGEND
 — DATA
 - - - INITIAL MODEL
 - * - FINAL MODEL

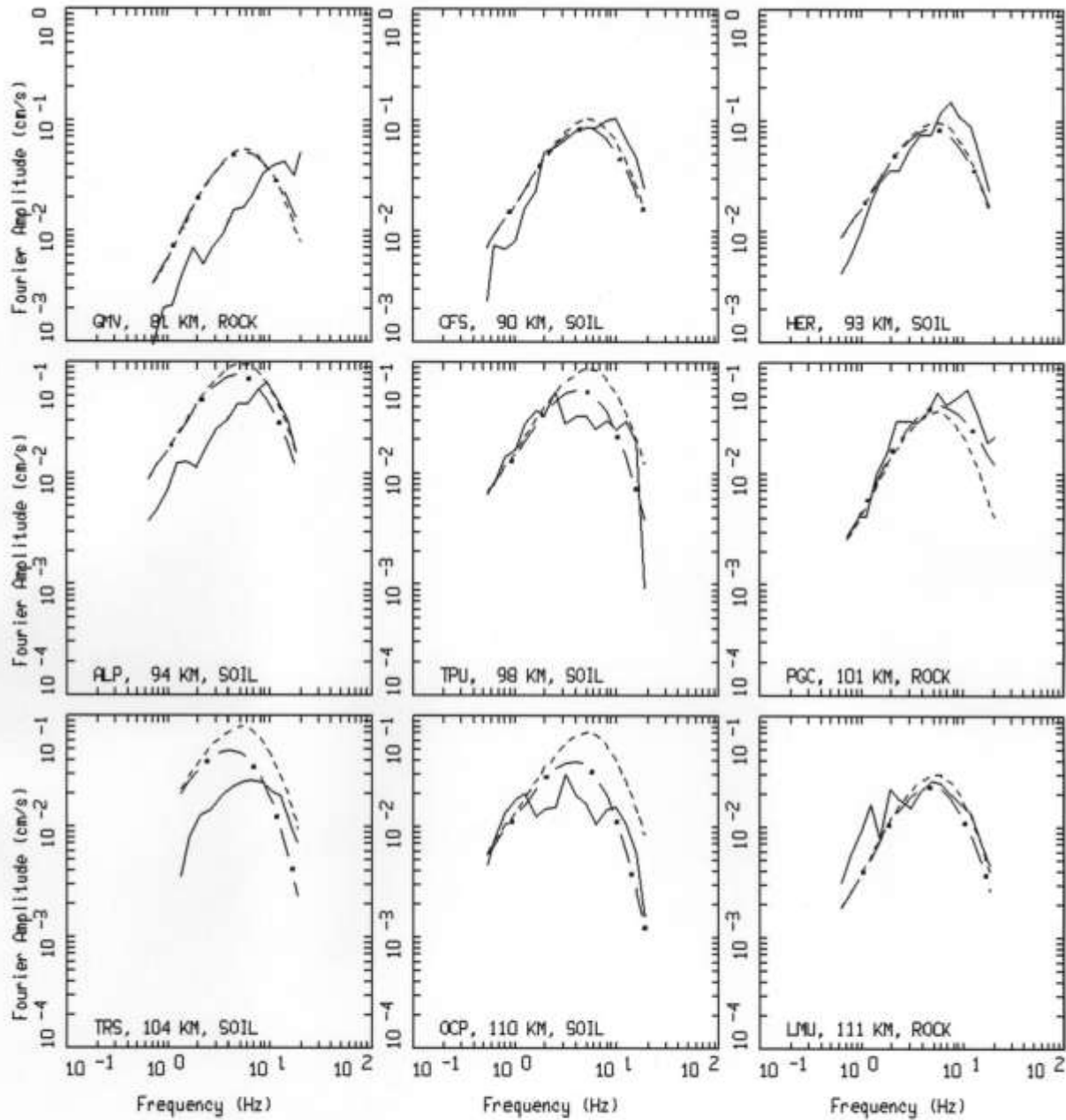
Figure 9 (continued). Spectral inversion results for Event #6.



WASATCH EARTHQUAKES, EARTHQUAKE 6, PAGE 3 OF 5.
 M = 4.24, 42 SITES (15 ROCK, 27 SOIL)

LEGEND
 — DATA
 - - - INITIAL MODEL
 - . - FINAL MODEL

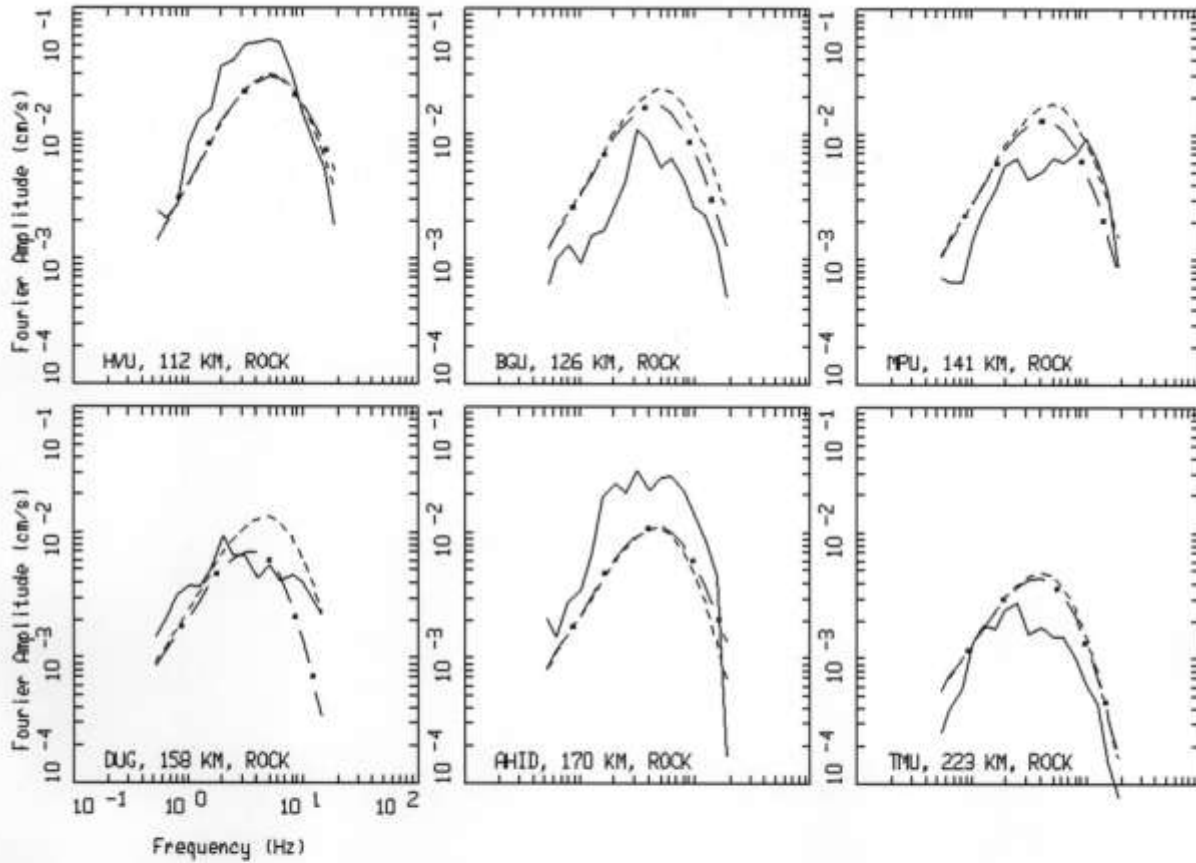
Figure 9 (continued). Spectral inversion results for Event #6.



WASATCH EARTHQUAKES, EARTHQUAKE 6, PAGE 4 OF 5.
 M = 4.24, 42 SITES (15 ROCK, 27 SOIL)

LEGEND
 — DATA
 - - - INITIAL MODEL
 - . - FINAL MODEL

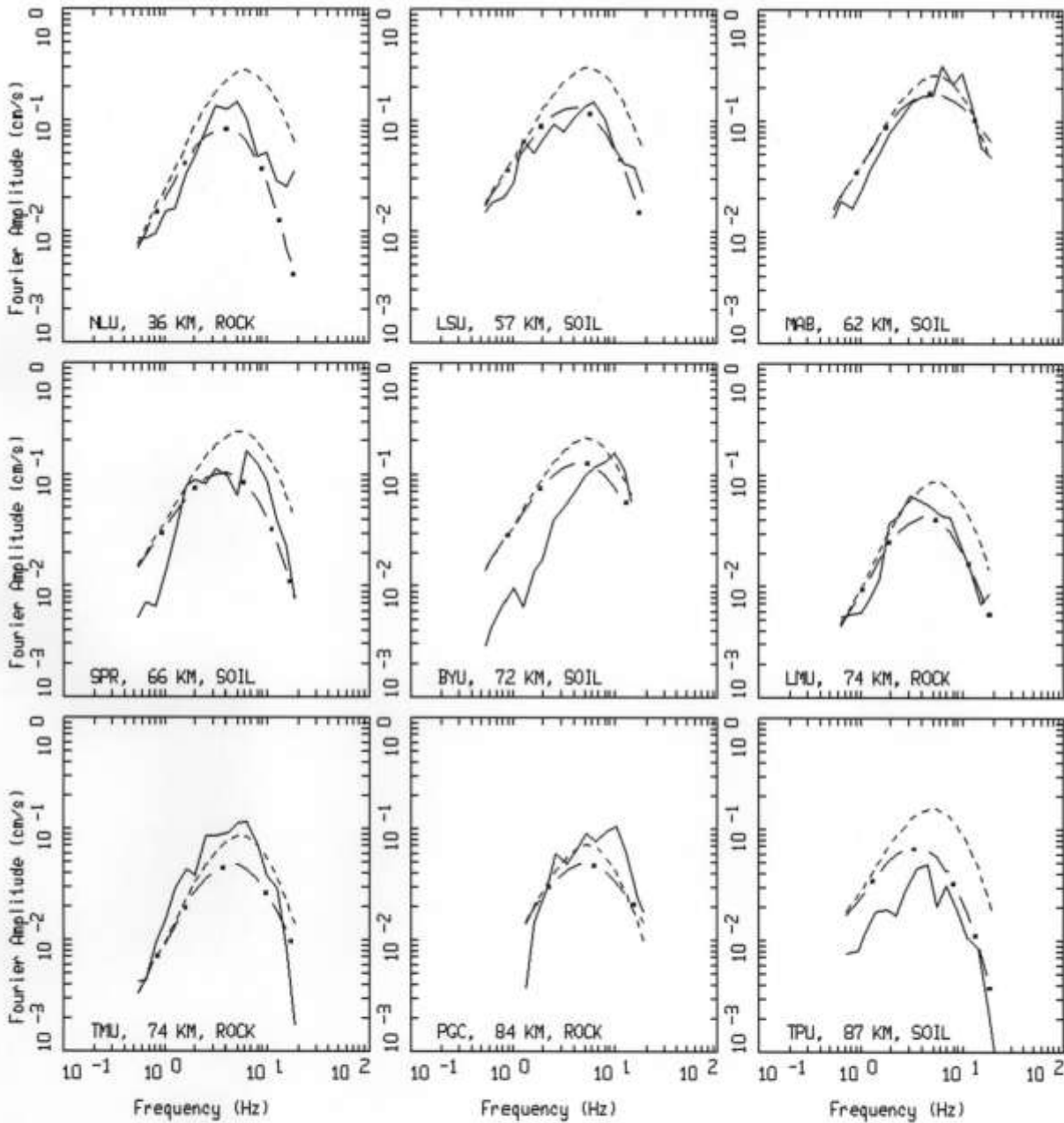
Figure 9 (continued). Spectral inversion results for Event #6.



WASATCH EARTHQUAKES, EARTHQUAKE 6, PAGE 5 OF 5.
M = 4.24, 42 SITES (15 ROCK, 27 SOIL)

LEGEND
— DATA
--- INITIAL MODEL
- · - FINAL MODEL

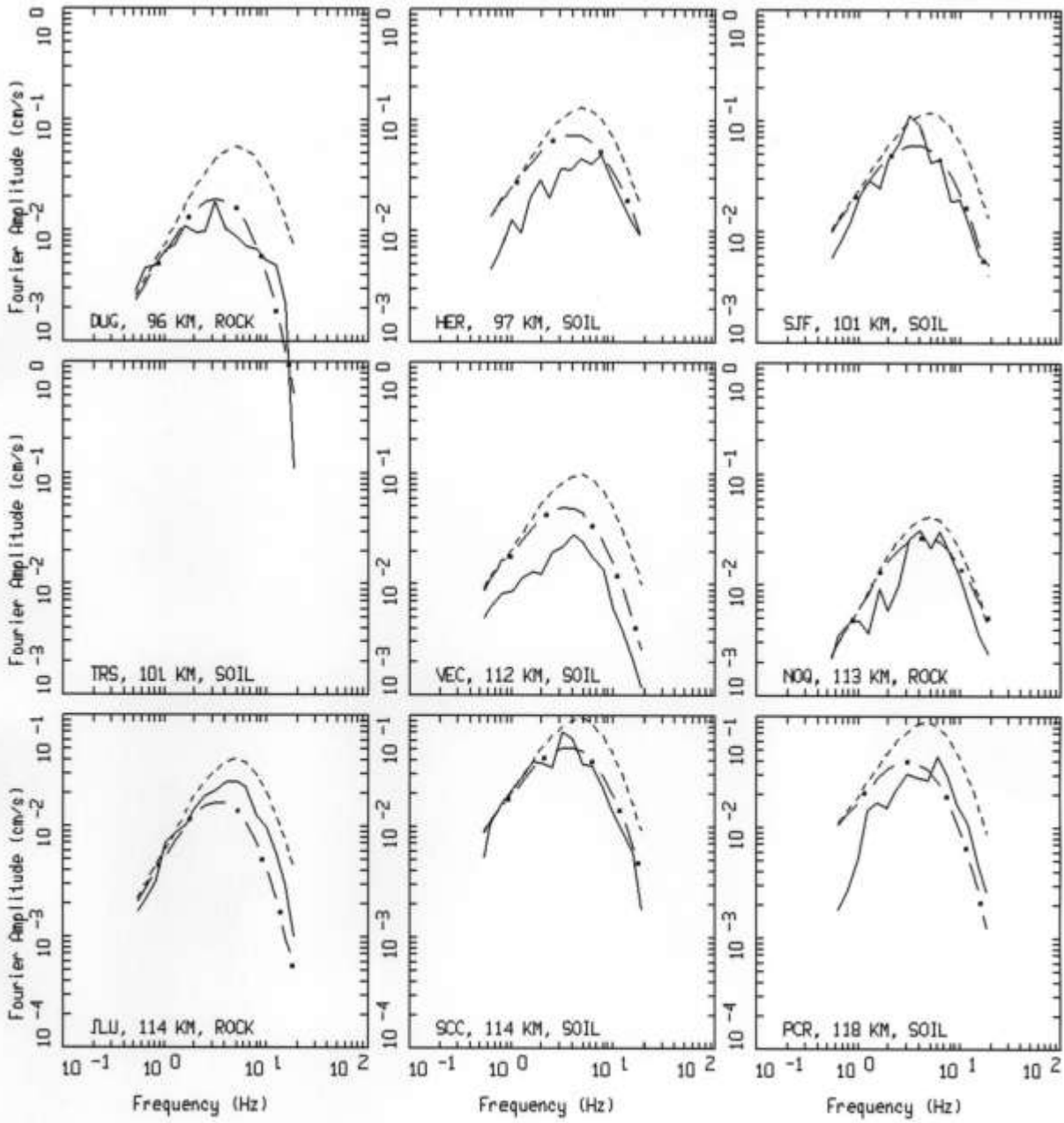
Figure 9 (continued). Spectral inversion results for Event #6.



WASATCH EARTHQUAKES, EARTHQUAKE 7, PAGE 1 OF 3.
M = 3.64, 23 SITES (12 ROCK, 11 SOIL)

LEGEND
— DATA
--- INITIAL MODEL
- · - FINAL MODEL

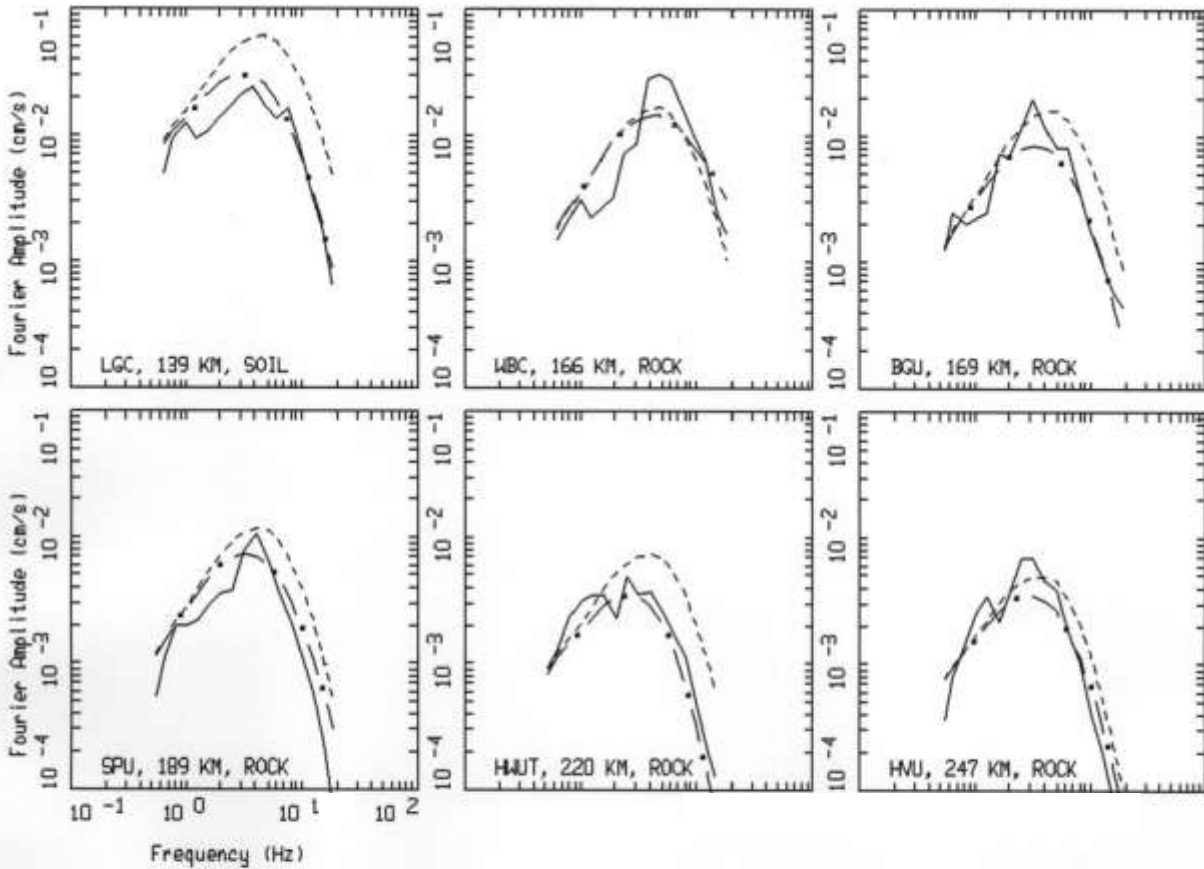
Figure 10. Spectral inversion results for Event #7.



WASATCH EARTHQUAKES, EARTHQUAKE 7, PAGE 2 OF 3.
M = 3.64, 23 SITES (12 ROCK, 11 SOIL)

LEGEND
— DATA
- - - - INITIAL MODEL
- • - FINAL MODEL

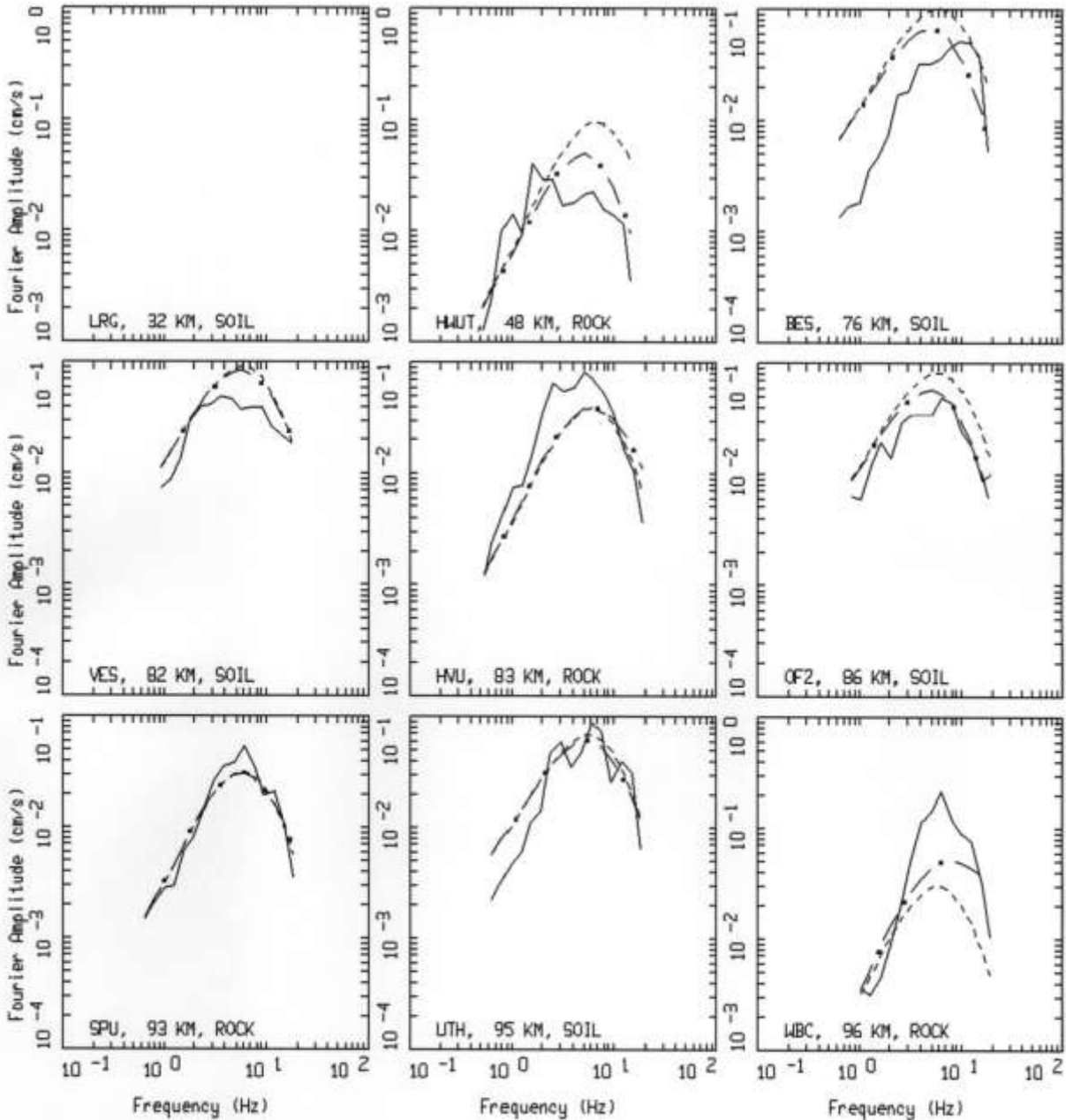
Figure 10 (continued). Spectral inversion results for Event #7.



WASATCH EARTHQUAKES, EARTHQUAKE 7, PAGE 3 OF 3.
 M = 3.64, 23 SITES (12 ROCK, 11 SOIL)

LEGEND
 — DATA
 - - - INITIAL MODEL
 - · - FINAL MODEL

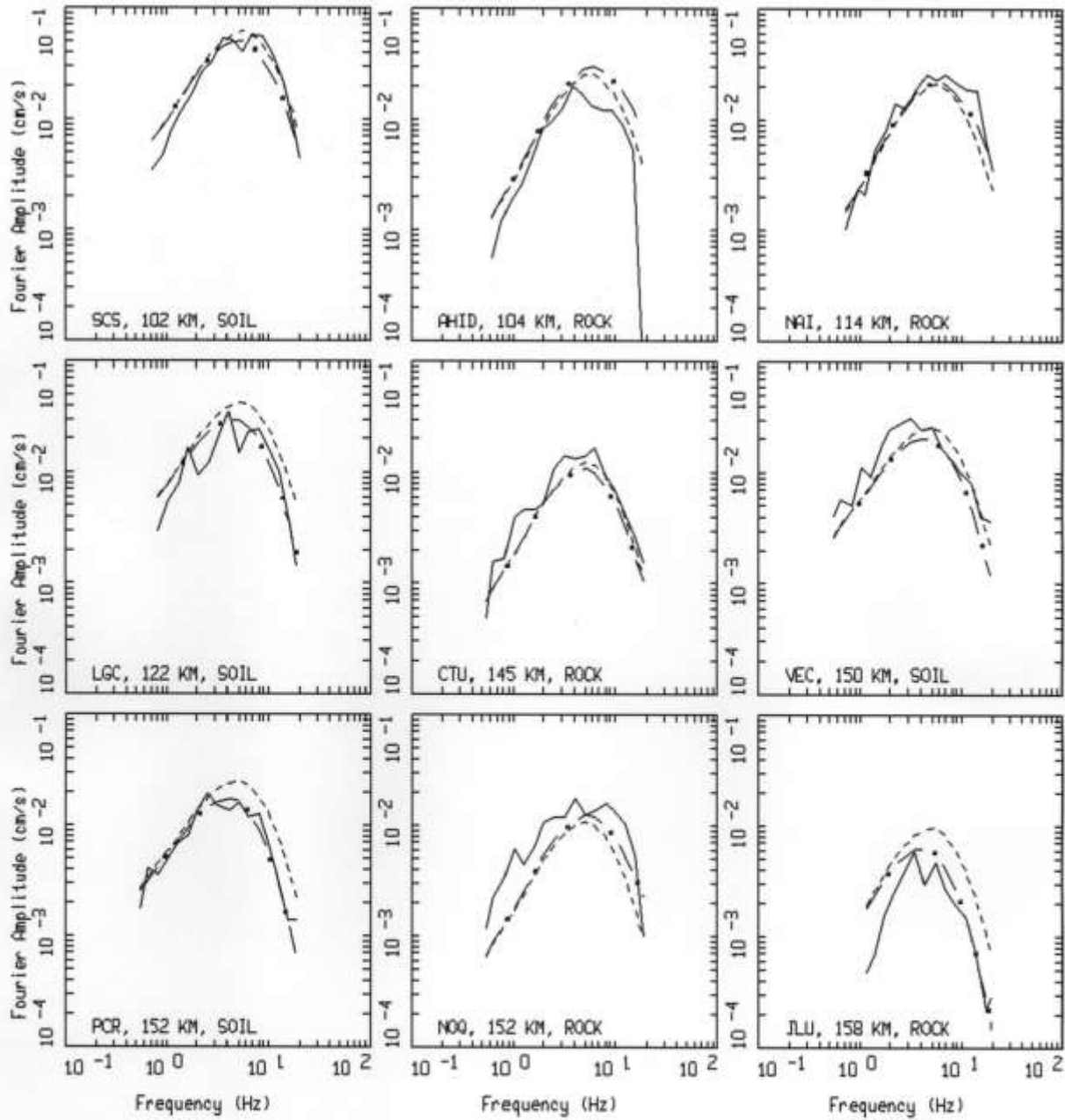
Figure 10 (continued). Spectral inversion results for Event #7.



WASATCH EARTHQUAKES, EARTHQUAKE 8, PAGE 1 OF 3.
M = 3.38, 21 SITES (13 ROCK, 8 SOIL)

LEGEND
— DATA
--- INITIAL MODEL
- · - FINAL MODEL

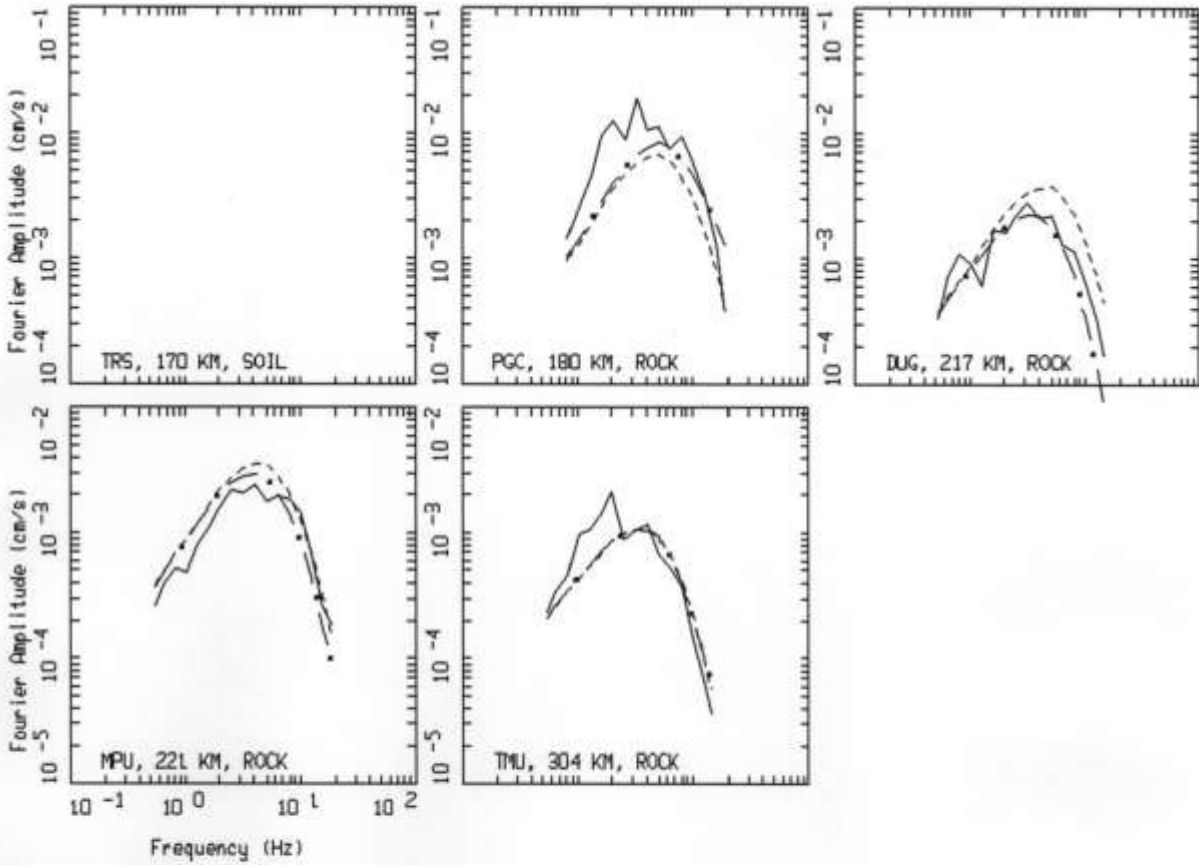
Figure 11. Spectral inversion results for Event #8.



WASATCH EARTHQUAKES, EARTHQUAKE 8, PAGE 2 OF 3.
 M = 3.98, 21 SITES (13 ROCK, 8 SOIL)

LEGEND
 — DATA
 - - - INITIAL MODEL
 - . - FINAL MODEL

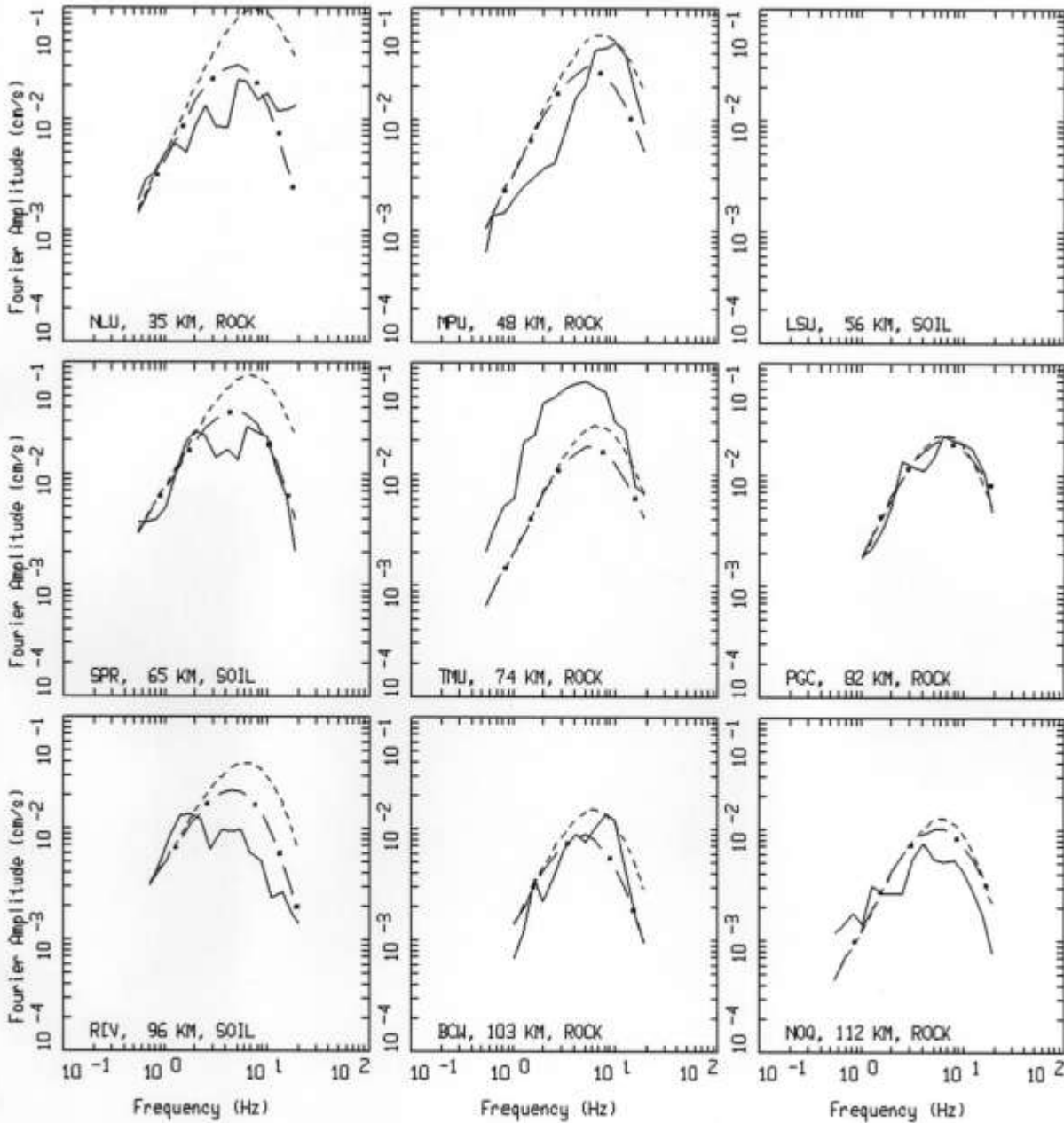
Figure 11 (continued). Spectral inversion results for Event #8.



WASATCH EARTHQUAKES, EARTHQUAKE B, PAGE 3 OF 3.
M = 3.38, 21 SITES (13 ROCK, 8 SOIL)

LEGEND
— DATA
- - - INITIAL MODEL
- . - FINAL MODEL

Figure 11 (continued). Spectral inversion results for Event #8.



WASATCH EARTHQUAKES, EARTHQUAKE 9, PAGE 1 OF 2.
M = 3.17, 12 SITES (10 ROCK, 2 SOIL)

LEGEND
— DATA
--- INITIAL MODEL
- · - FINAL MODEL

Figure 12. Spectral inversion results for Event #9.

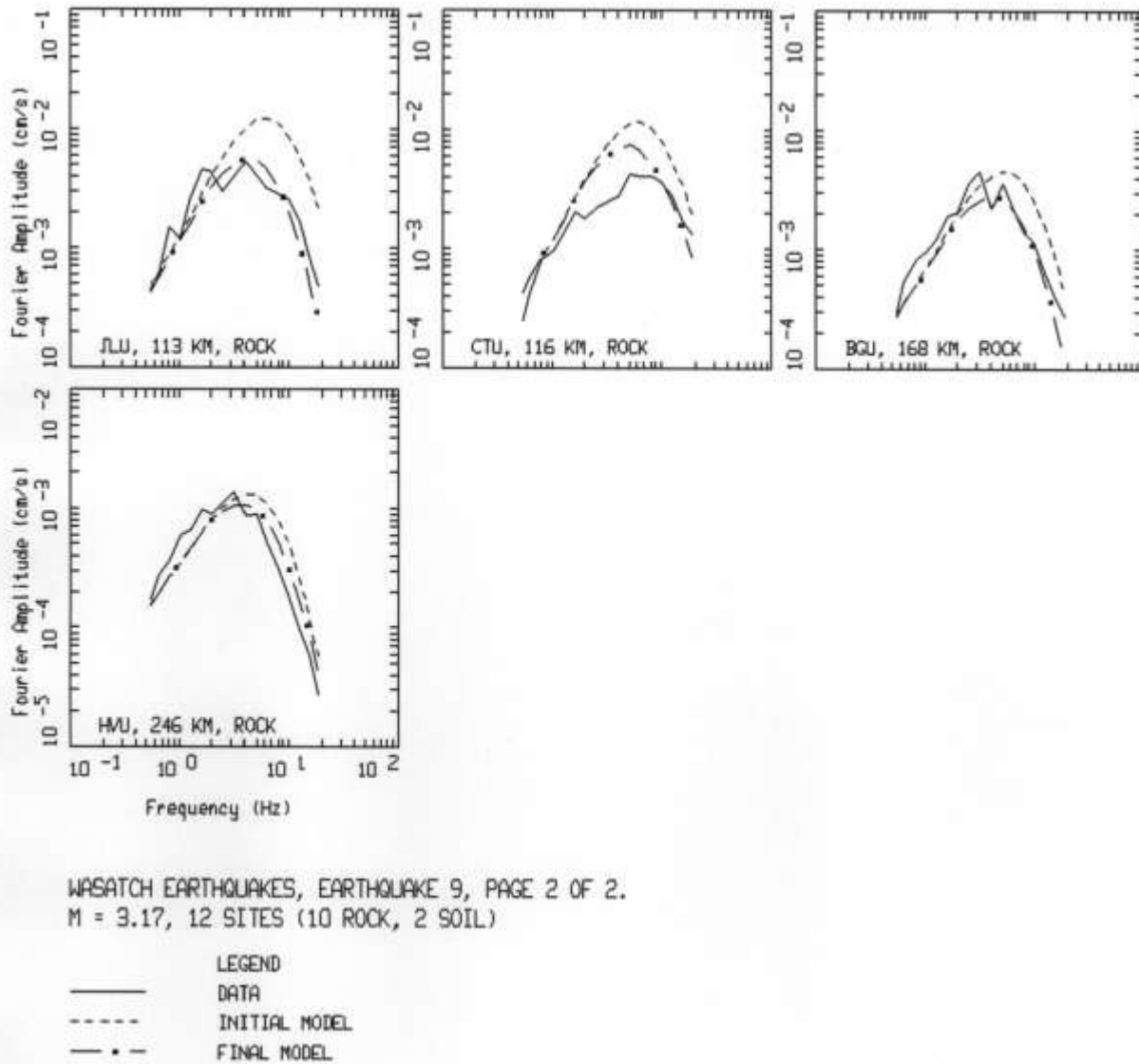
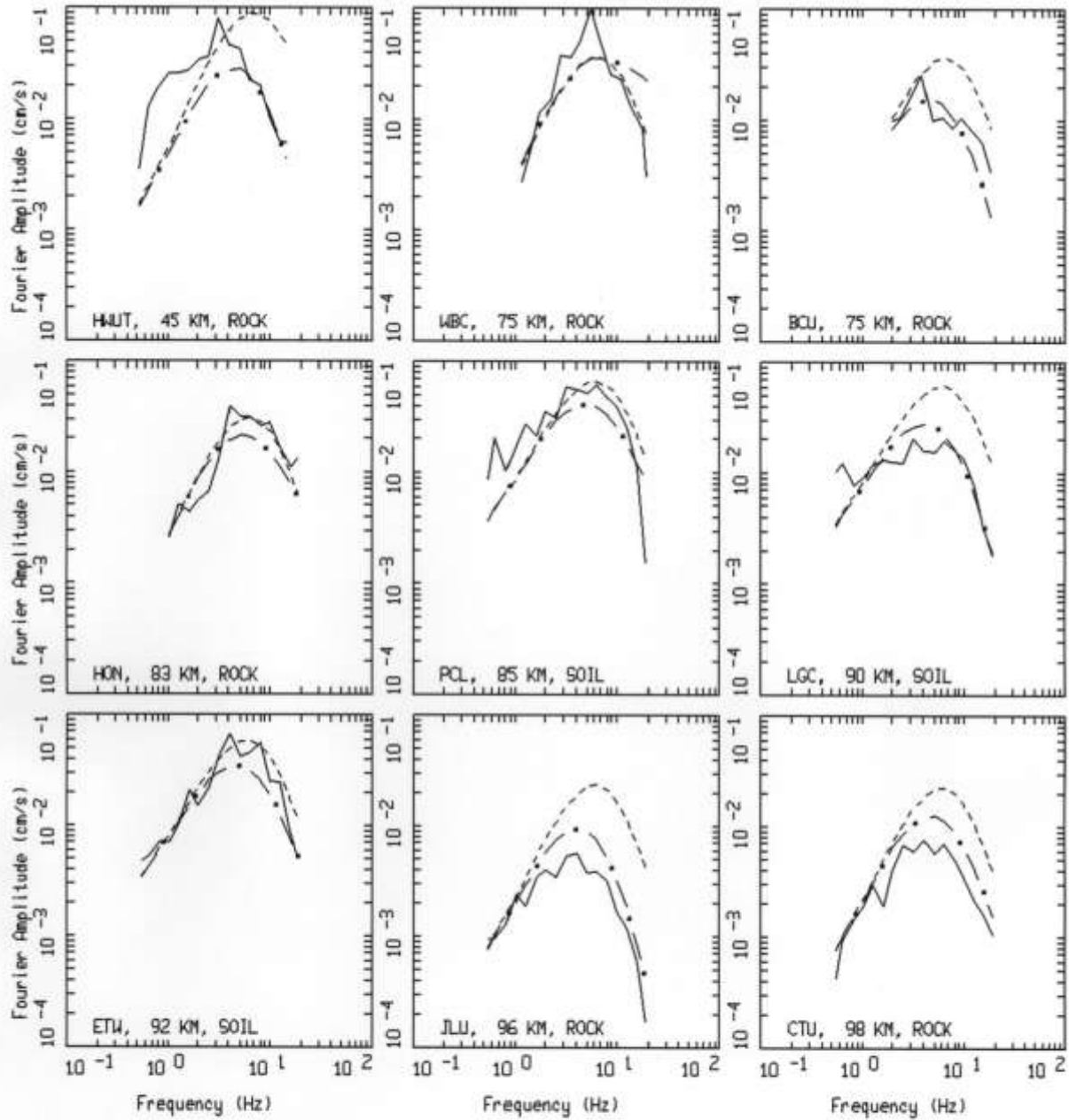


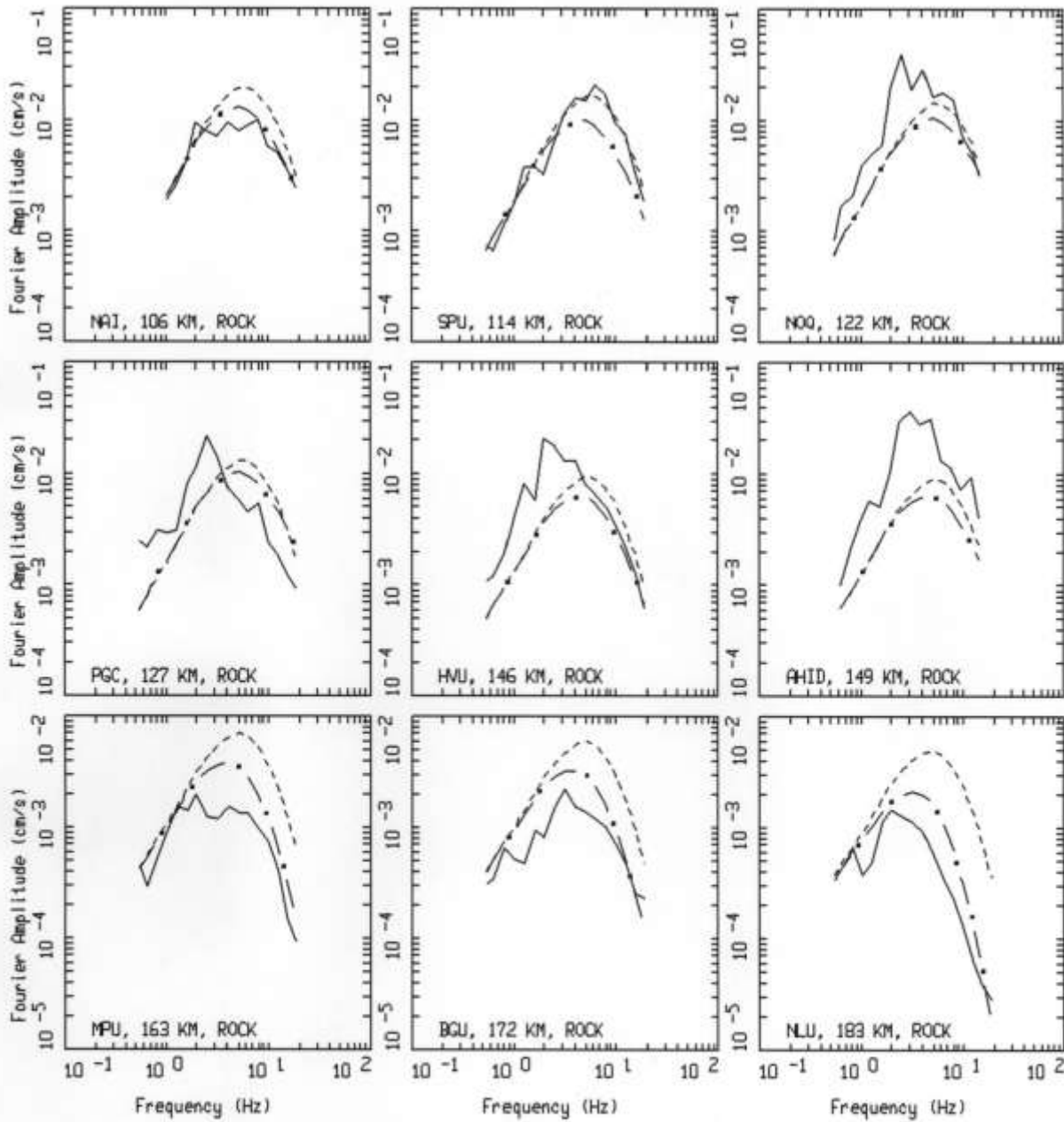
Figure 12 (continued). Spectral inversion results for Event #9.



WASATCH EARTHQUAKES, EARTHQUAKE 10, PAGE 1 OF 3.
M = 3.29, 19 SITES (16 ROCK, 3 SOIL)

LEGEND
— DATA
--- INITIAL MODEL
- · - FINAL MODEL

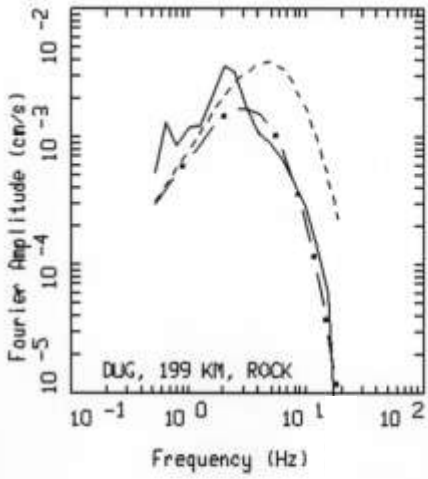
Figure 13. Spectral inversion results for Event #10.



WASATCH EARTHQUAKES, EARTHQUAKE 10, PAGE 2 OF 3.
 M = 3.29, 19 SITES (16 ROCK, 3 SOIL)

LEGEND
 — DATA
 - - - INITIAL MODEL
 - . - FINAL MODEL

Figure 13 (continued). Spectral inversion results for Event #10.



WASATCH EARTHQUAKES, EARTHQUAKE 10, PAGE 3 OF 3.
 M = 3.29, 19 SITES (16 ROCK, 3 SOIL)

LEGEND
 — DATA
 - - - INITIAL MODEL
 - * - FINAL MODEL

Figure 13 (continued). Spectral inversion results for Event #10.

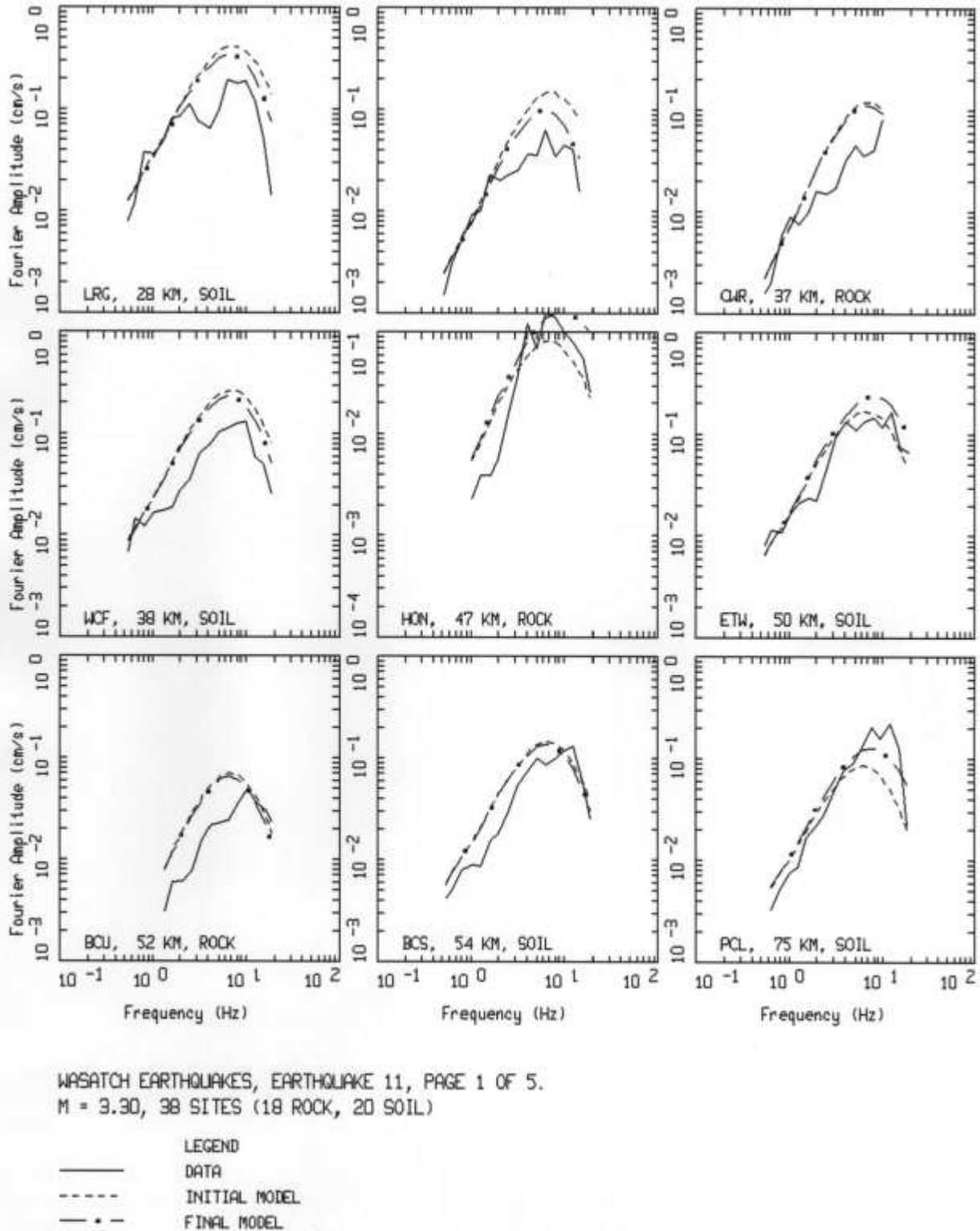


Figure 14. Spectral inversion results for Event #11.

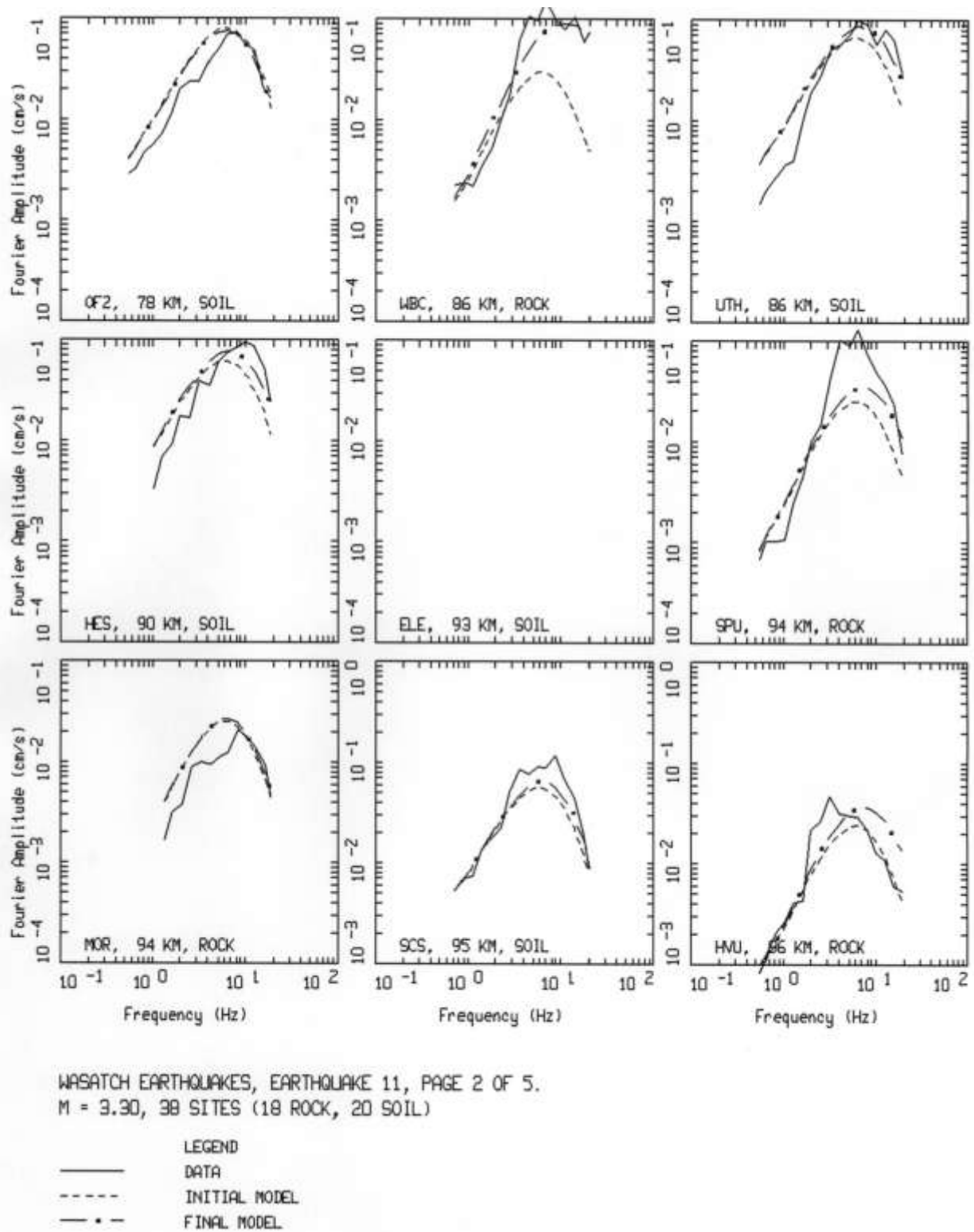
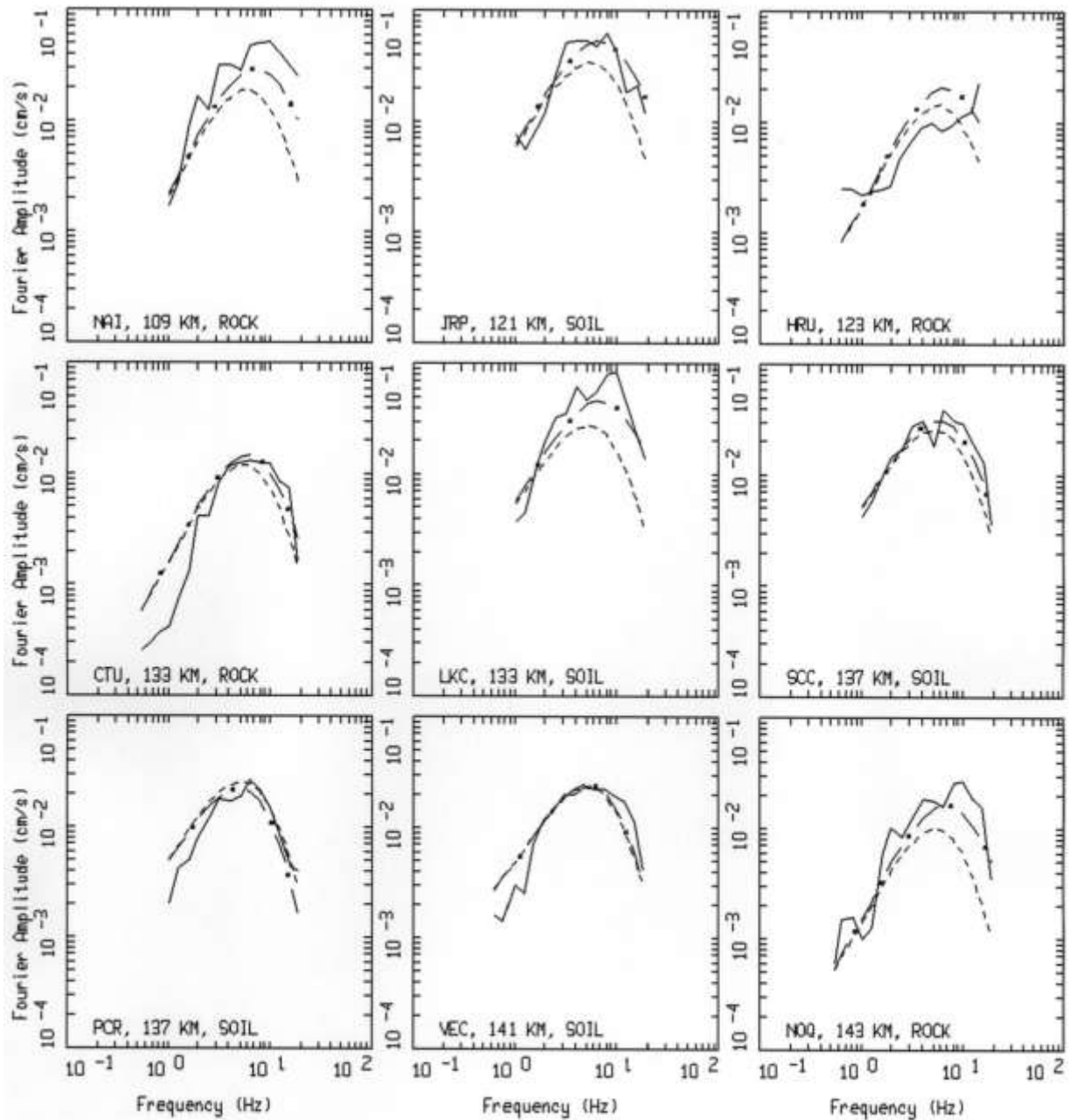


Figure 14 (continued). Spectral inversion results for Event #11.



WASATCH EARTHQUAKES, EARTHQUAKE 11, PAGE 3 OF 5.
 M = 3.30, 38 SITES (18 ROCK, 20 SOIL)

LEGEND
 — DATA
 - - - INITIAL MODEL
 - . - FINAL MODEL

Figure 14 (continued). Spectral inversion results for Event #11.

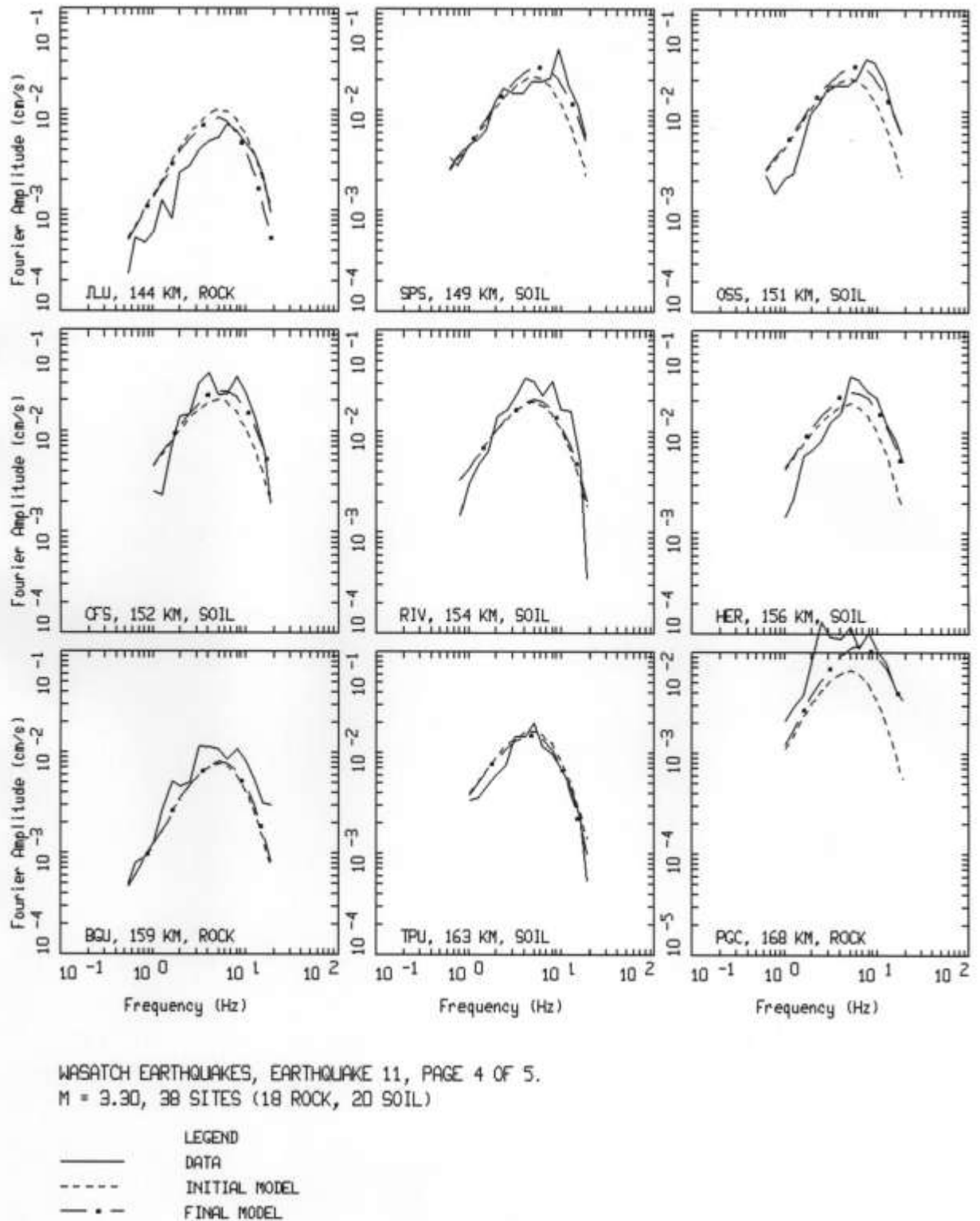
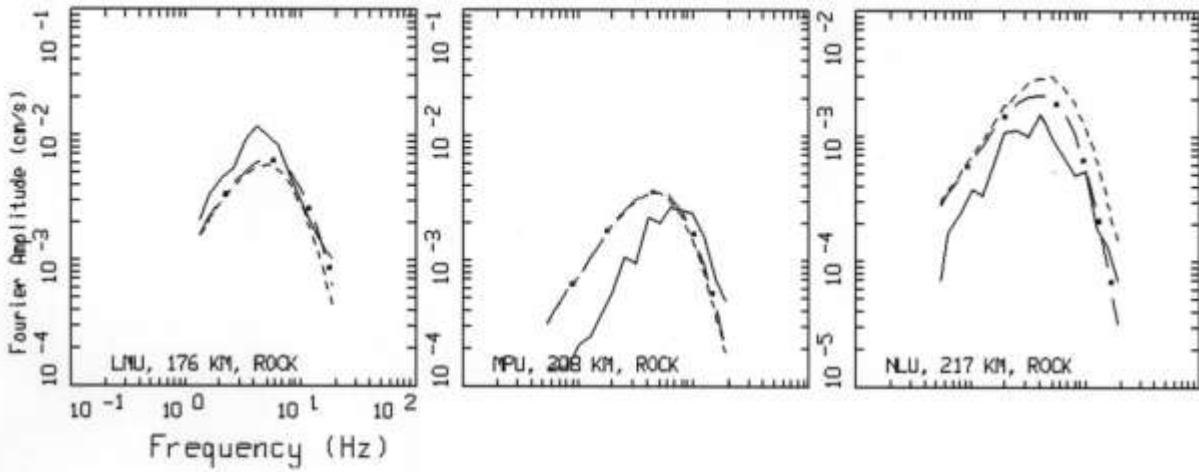


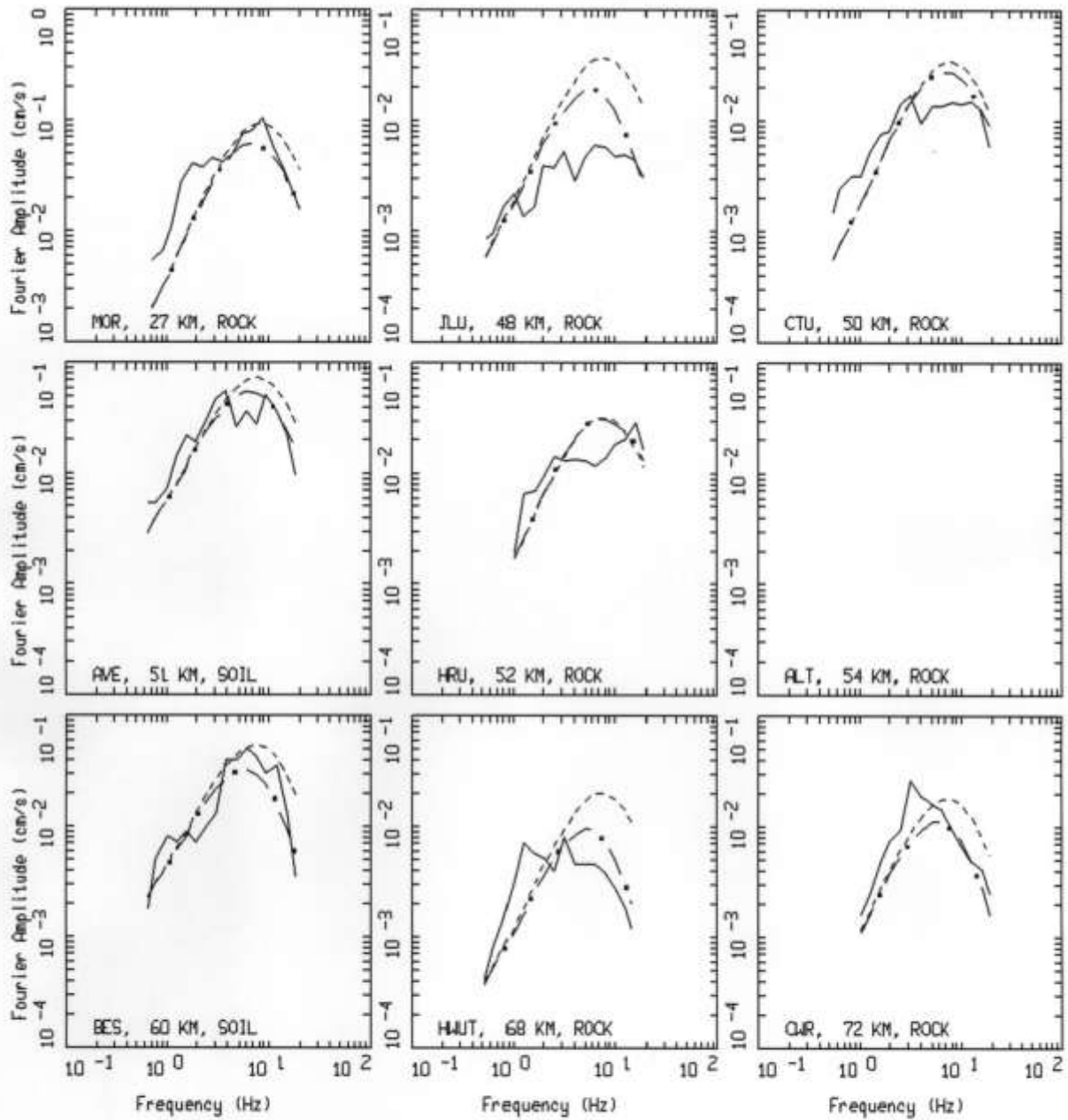
Figure 14 (continued). Spectral inversion results for Event #11.



WASATCH EARTHQUAKES, EARTHQUAKE 11, PAGE 5 OF 5.
 M = 3.30, 38 SITES (18 ROCK, 20 SOIL)

LEGEND
 — DATA
 - - - INITIAL MODEL
 - * - FINAL MODEL

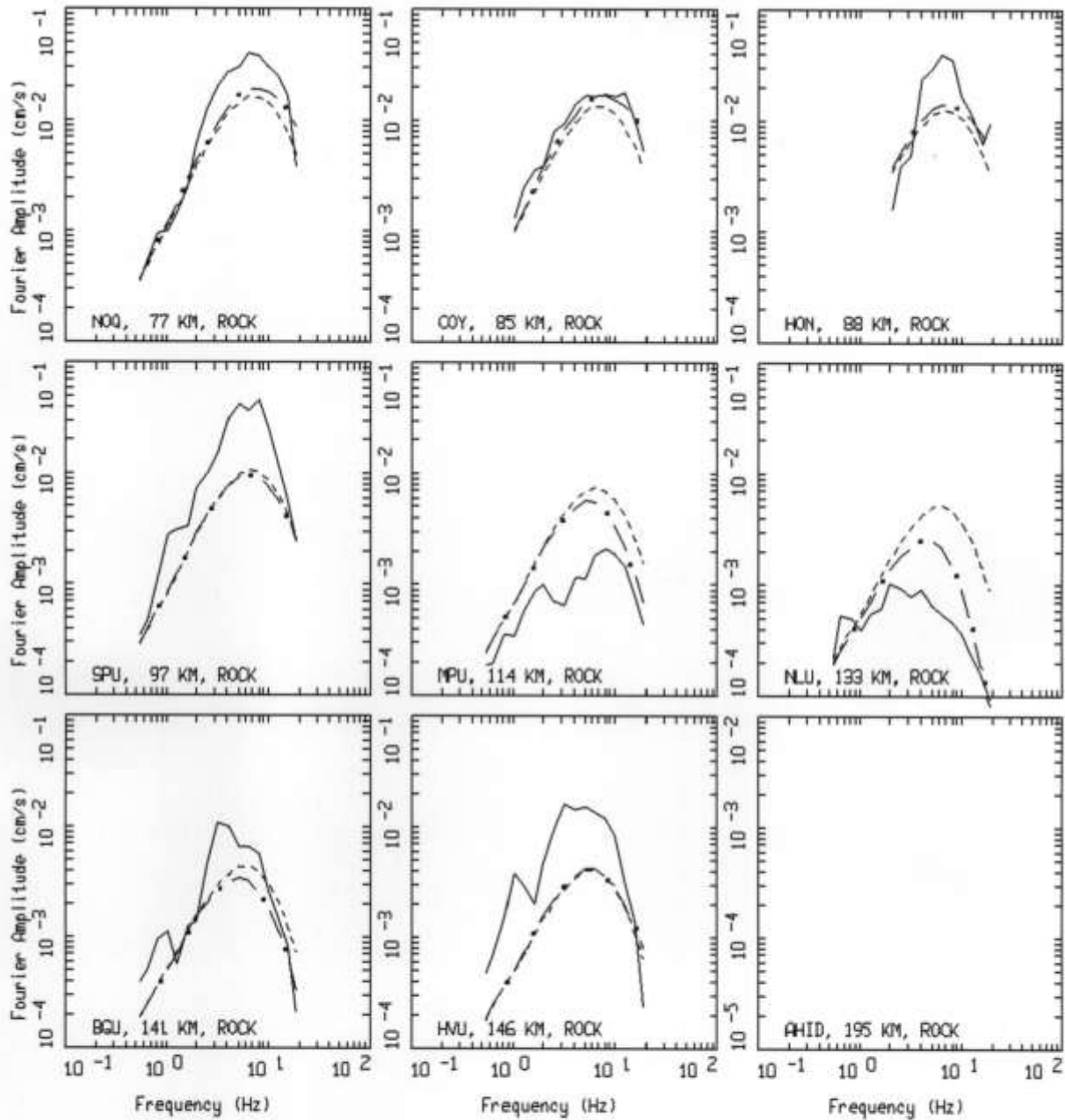
Figure 14 (continued). Spectral inversion results for Event #11.



WASATCH EARTHQUAKES, EARTHQUAKE 12, PAGE 1 OF 2.
M = 3.00, 16 SITES (15 ROCK, 1 SOIL)

LEGEND
— DATA
--- INITIAL MODEL
-•- FINAL MODEL

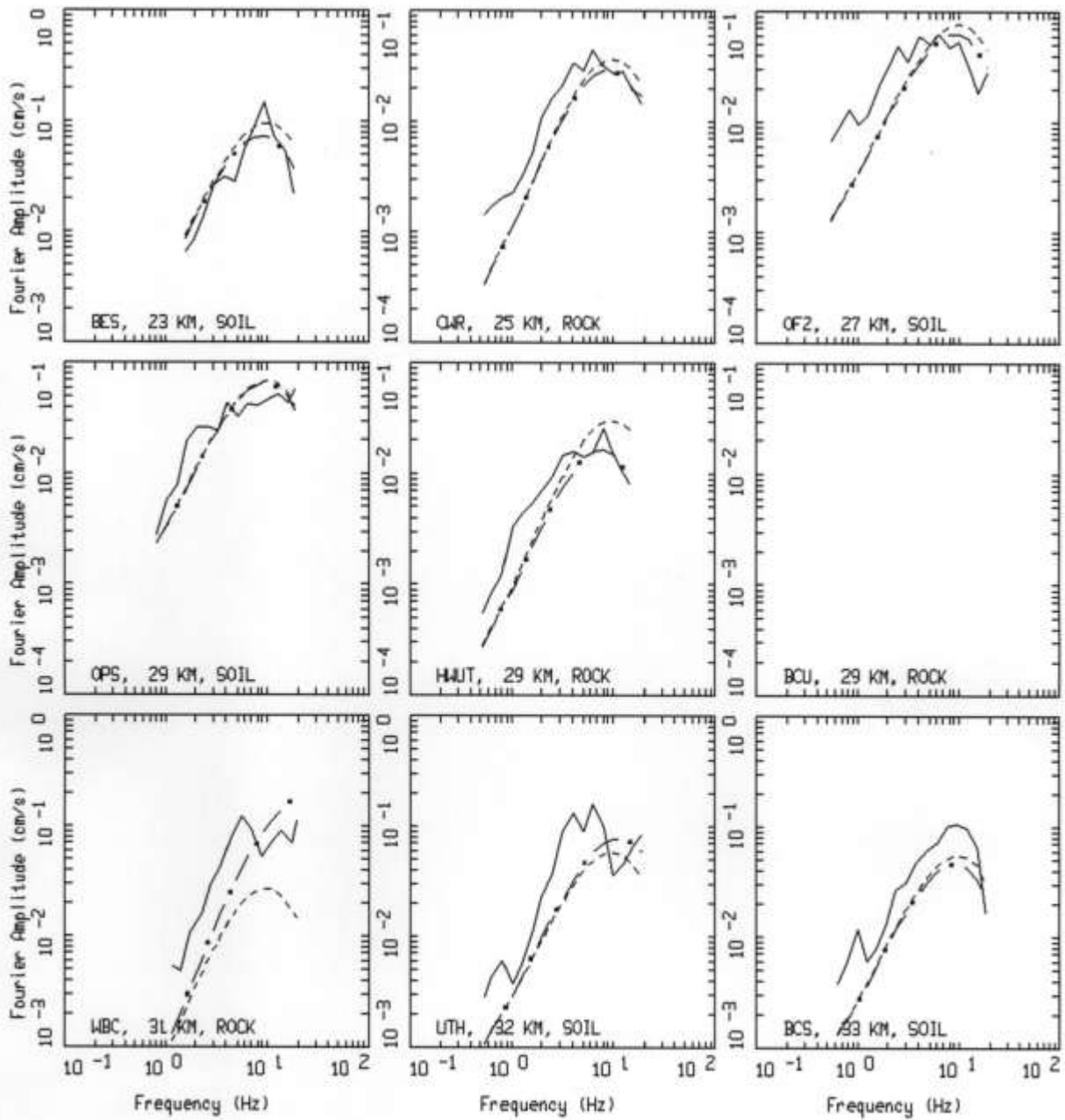
Figure 15. Spectral inversion results for Event #12.



WASATCH EARTHQUAKES, EARTHQUAKE 12, PAGE 2 OF 2.
 M = 3.00, 16 SITES (15 ROCK, 1 SOIL)

LEGEND
 — DATA
 - - - INITIAL MODEL
 - . - FINAL MODEL

Figure 15 (continued). Spectral inversion results for Event #12.



WASATCH EARTHQUAKES, EARTHQUAKE 13, PAGE 1 OF 3.
M = 2.62, 24 SITES (10 ROCK, 14 SOIL)

LEGEND
— DATA
--- INITIAL MODEL
- · - FINAL MODEL

Figure 16. Spectral inversion results for Event #13.

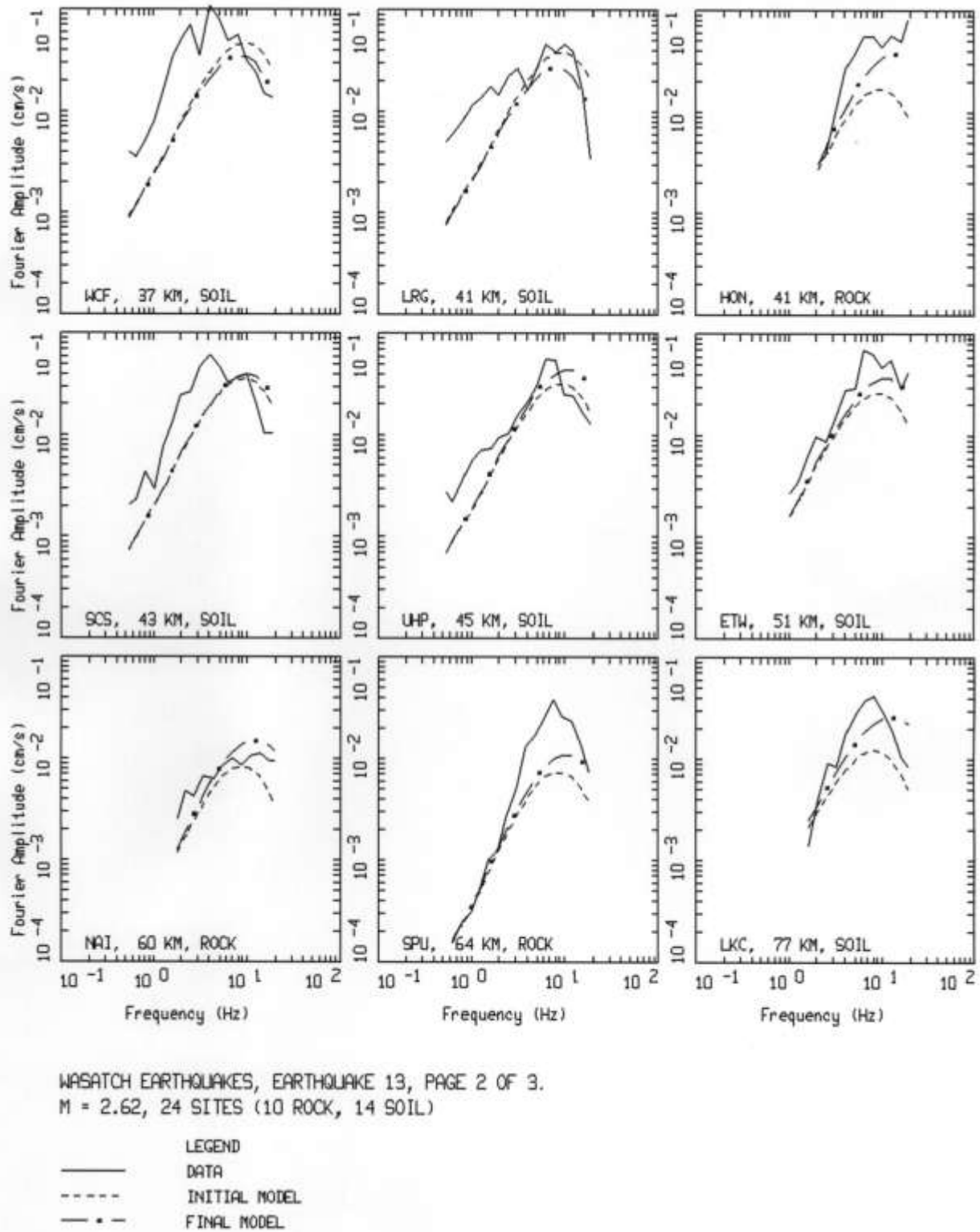
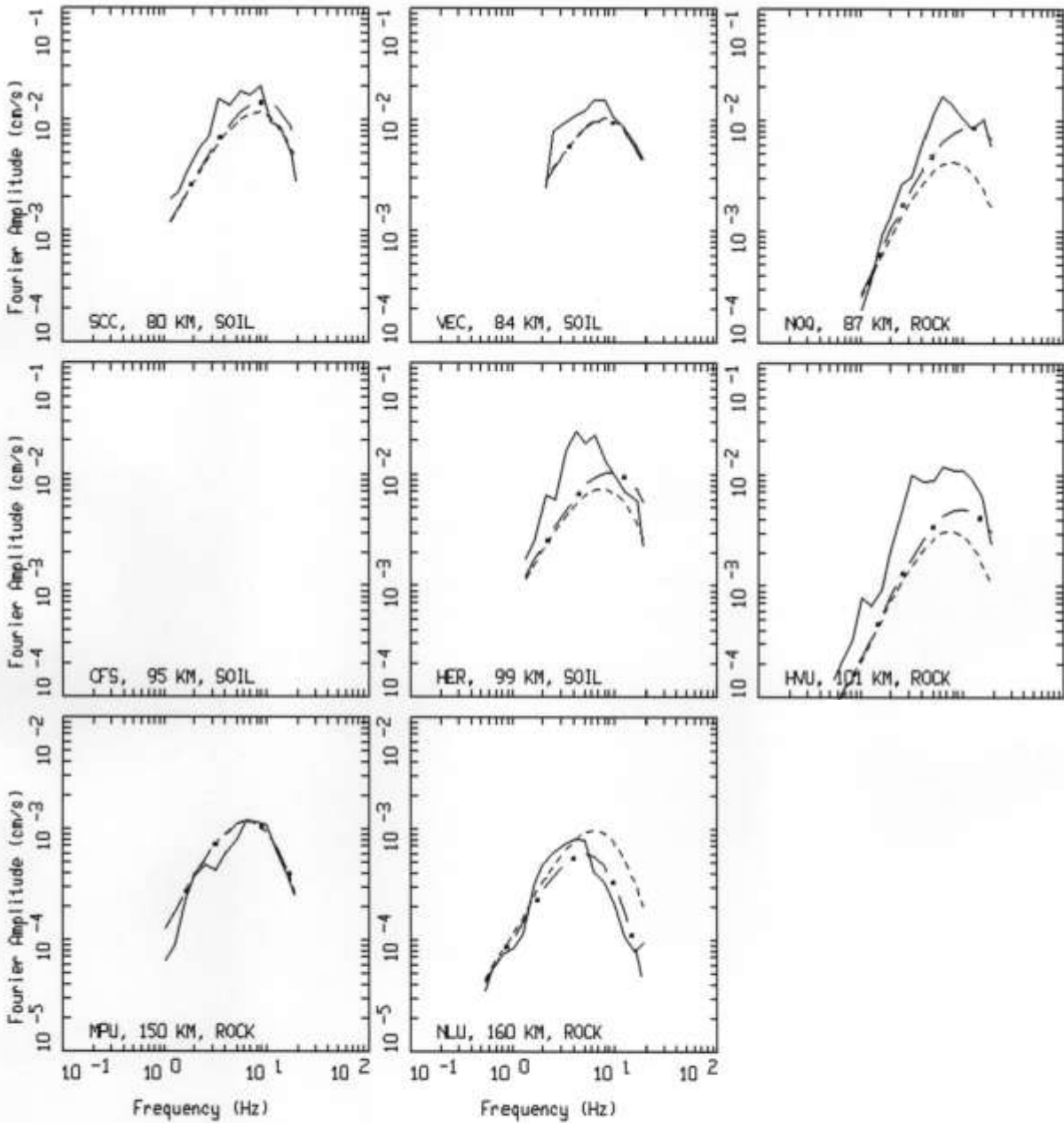


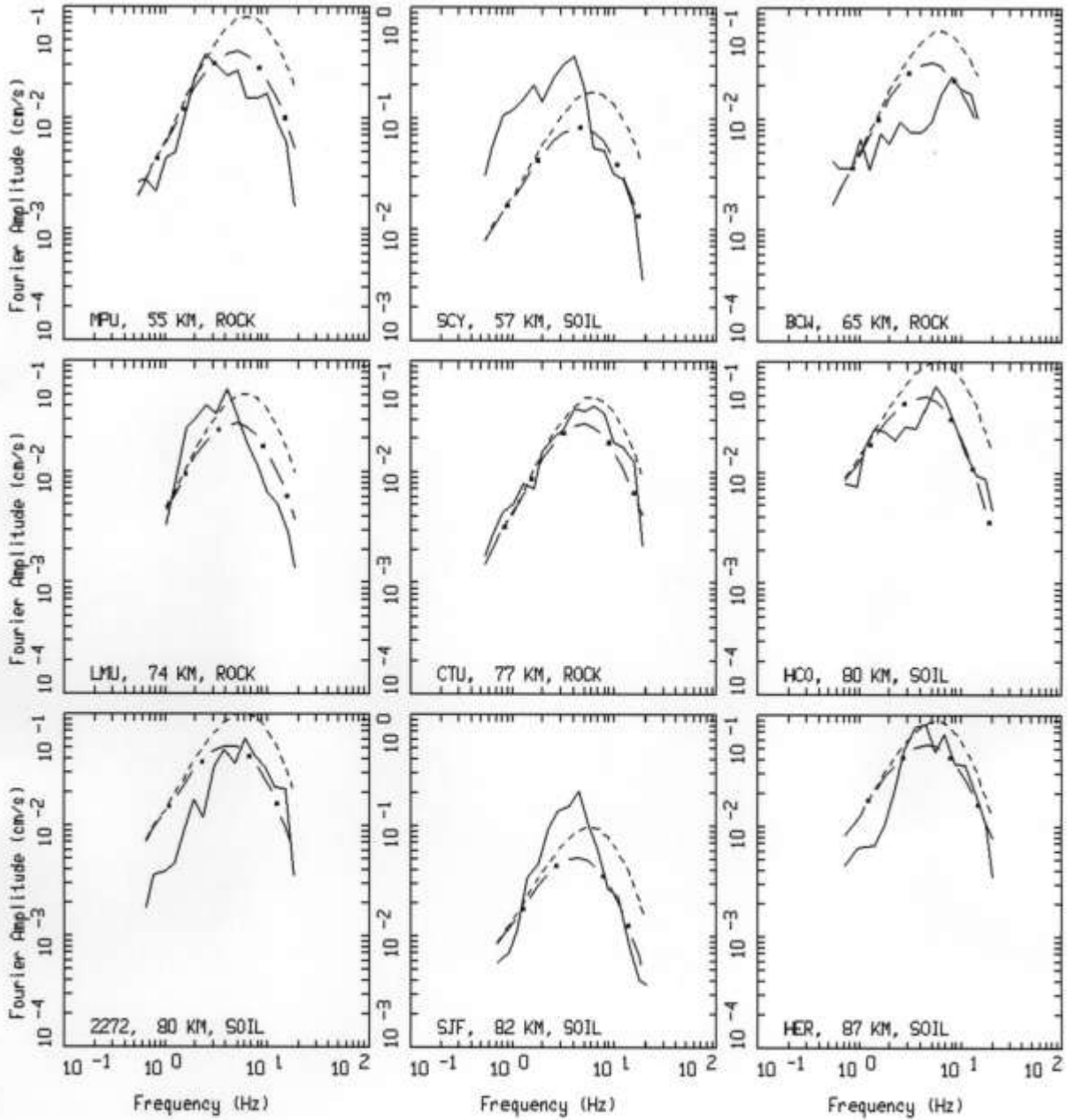
Figure 16 (continued). Spectral inversion results for Event #13.



WASATCH EARTHQUAKES, EARTHQUAKE 13, PAGE 3 OF 3.
 M = 2.62, 24 SITES (10 ROCK, 14 SOIL)

LEGEND
 — DATA
 - - - - INITIAL MODEL
 - * - FINAL MODEL

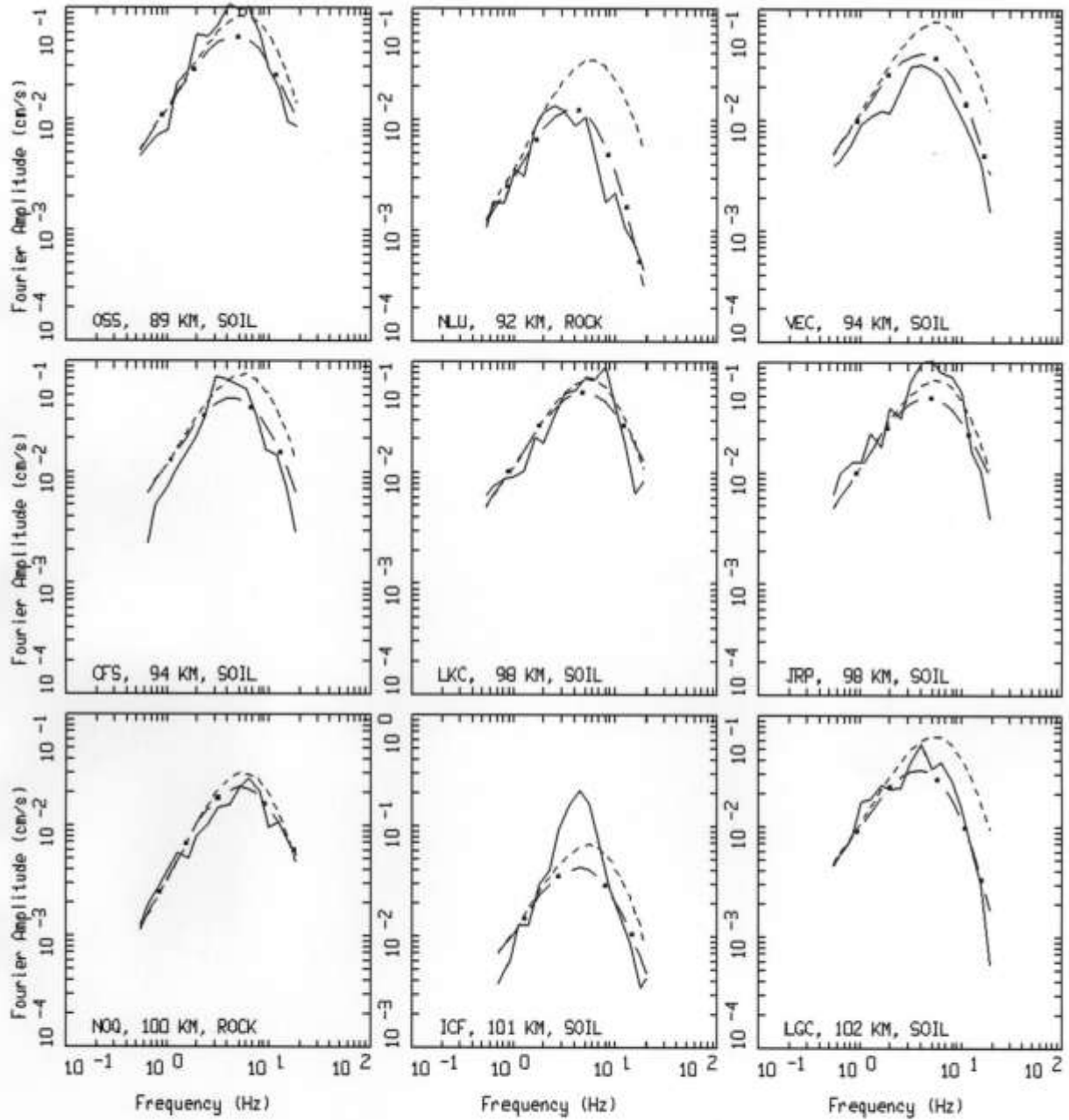
Figure 16 (continued). Spectral inversion results for Event #13.



WASATCH EARTHQUAKES, EARTHQUAKE 14, PAGE 1 OF 4.
M = 3.41, 30 SITES (12 ROCK, 18 SOIL)

LEGEND
— DATA
- - - INITIAL MODEL
- . - FINAL MODEL

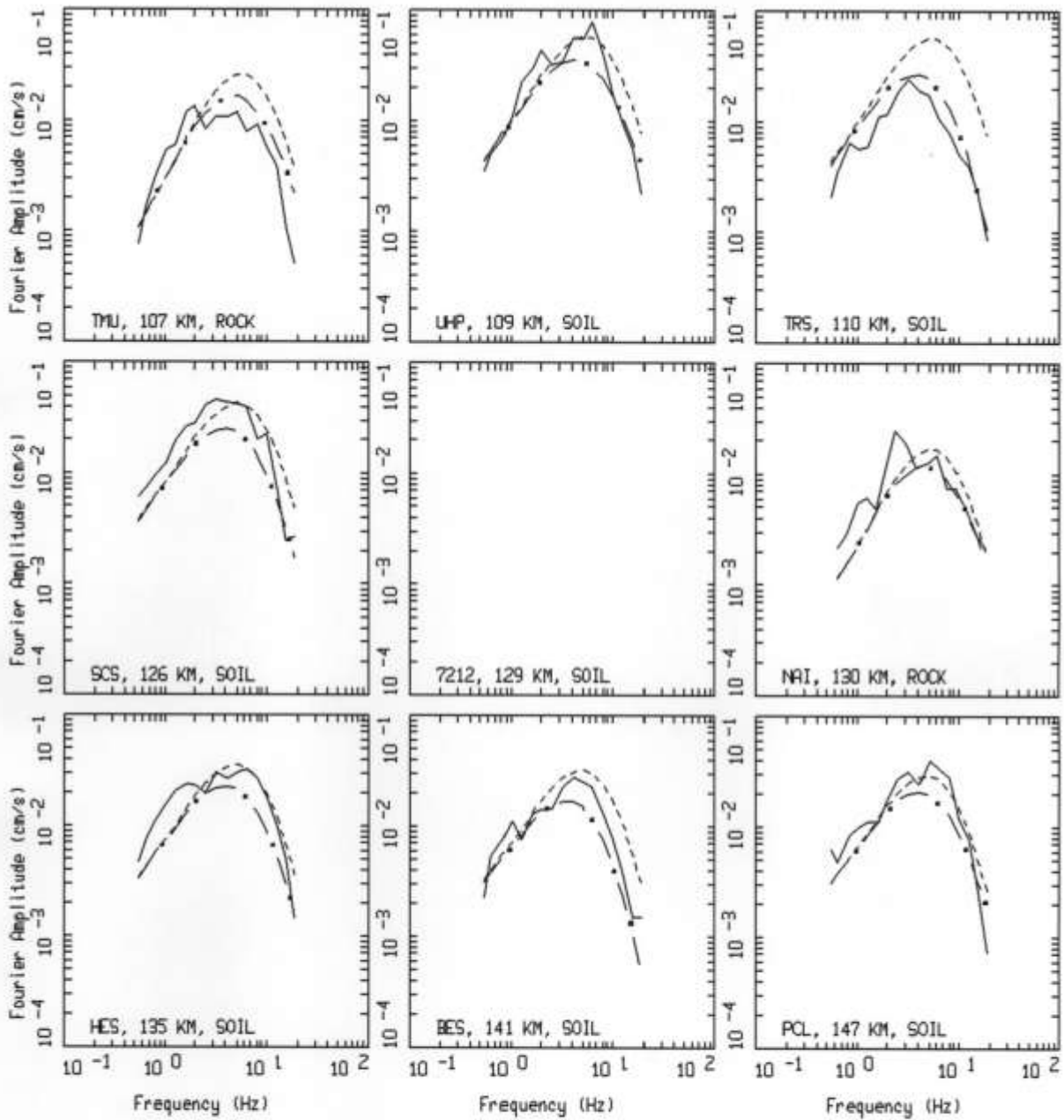
Figure 17. Spectral inversion results for Event #14.



WASATCH EARTHQUAKES, EARTHQUAKE 14, PAGE 2 OF 4.
 M = 3.41, 30 SITES (12 ROCK, 18 SOIL)

LEGEND
 — DATA
 - - - INITIAL MODEL
 · · · FINAL MODEL

Figure 17 (continued). Spectral inversion results for Event #14.



WASATCH EARTHQUAKES, EARTHQUAKE 14, PAGE 3 OF 4.
M = 3.41, 30 SITES (12 ROCK, 18 SOIL)

LEGEND
— DATA
--- INITIAL MODEL
- . - FINAL MODEL

Figure 17 (continued). Spectral inversion results for Event #14.

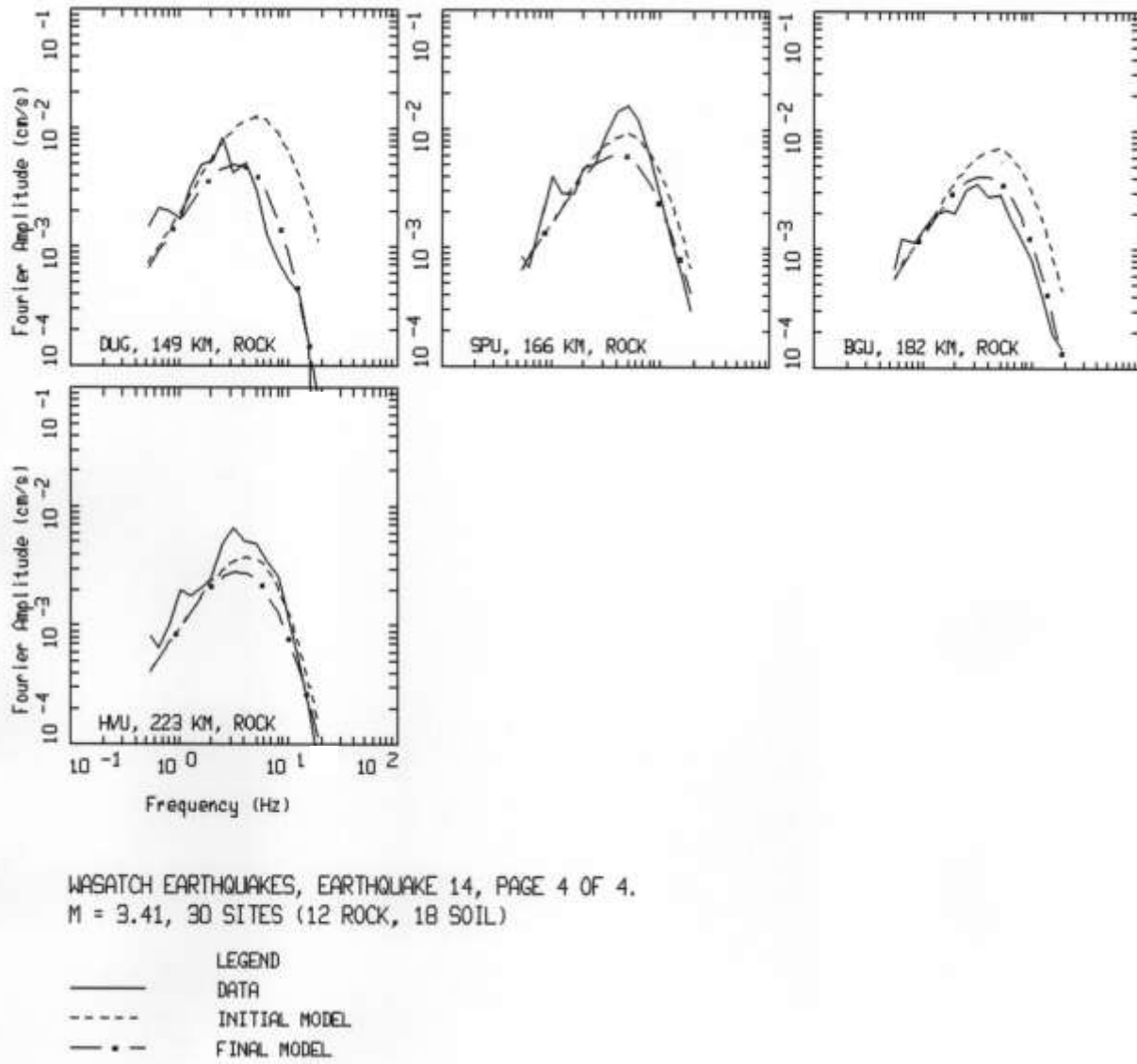


Figure 17 (continued). Spectral inversion results for Event #14.

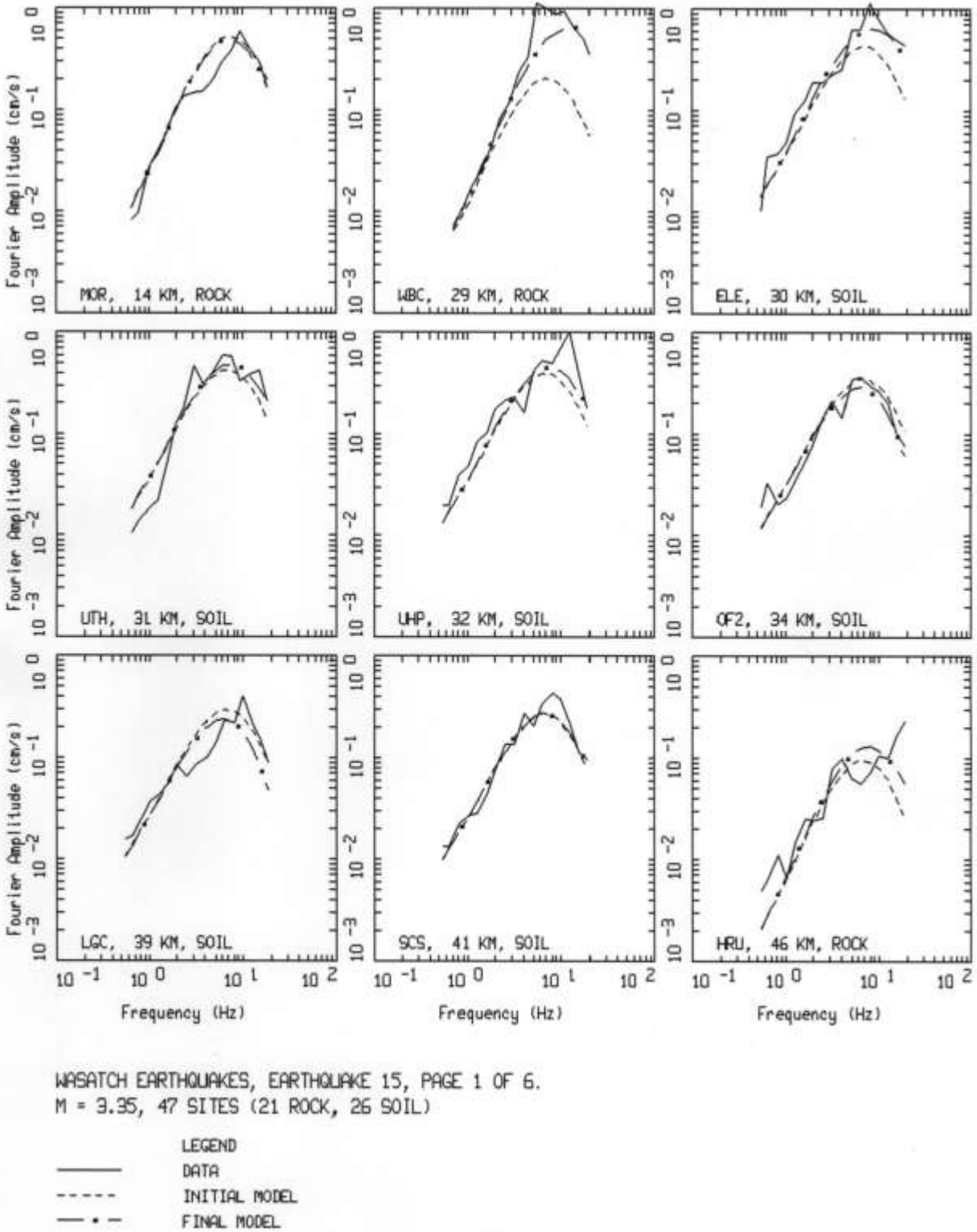


Figure 18. Spectral inversion results for Event #15.

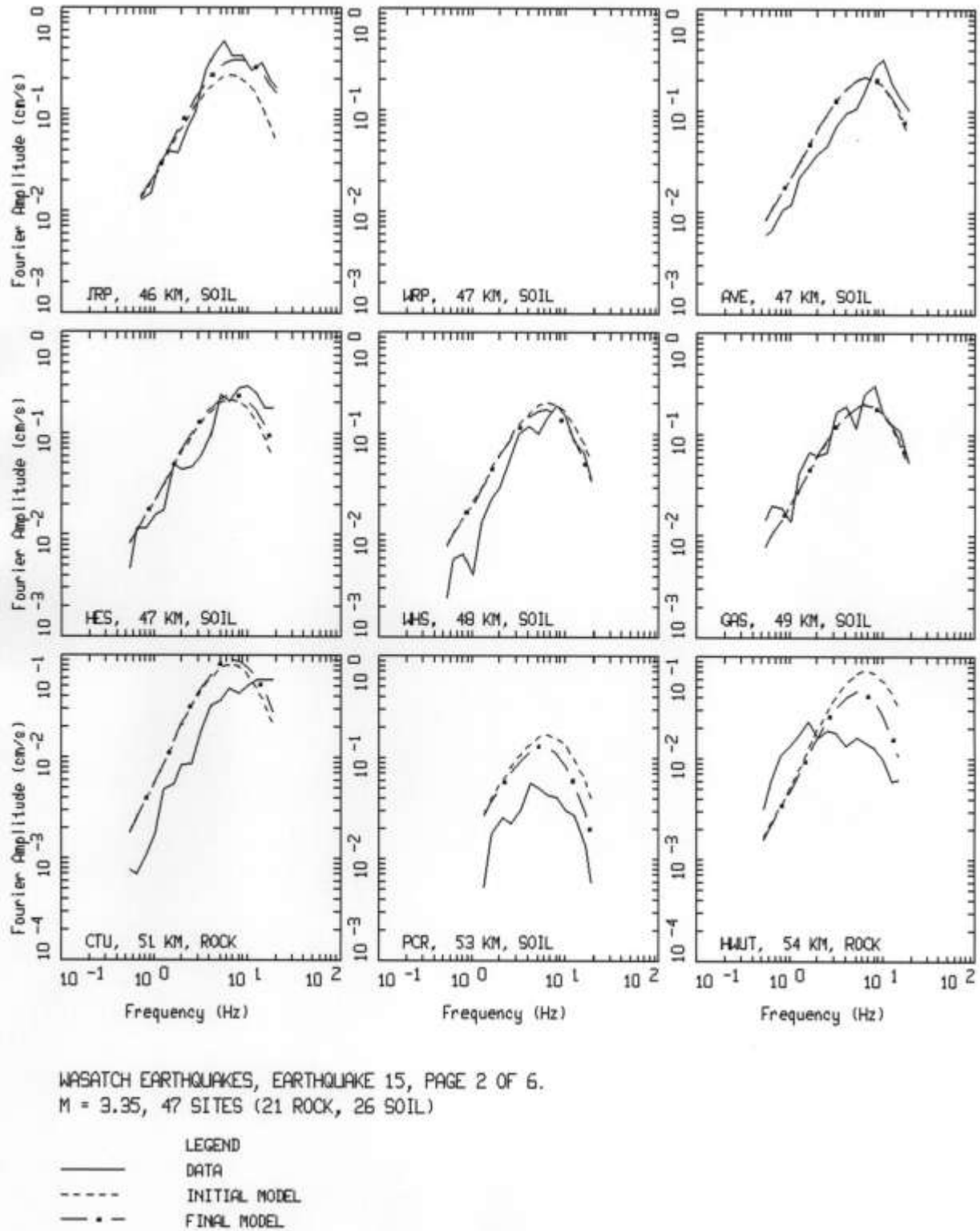


Figure 18 (continued). Spectral inversion results for Event #15.

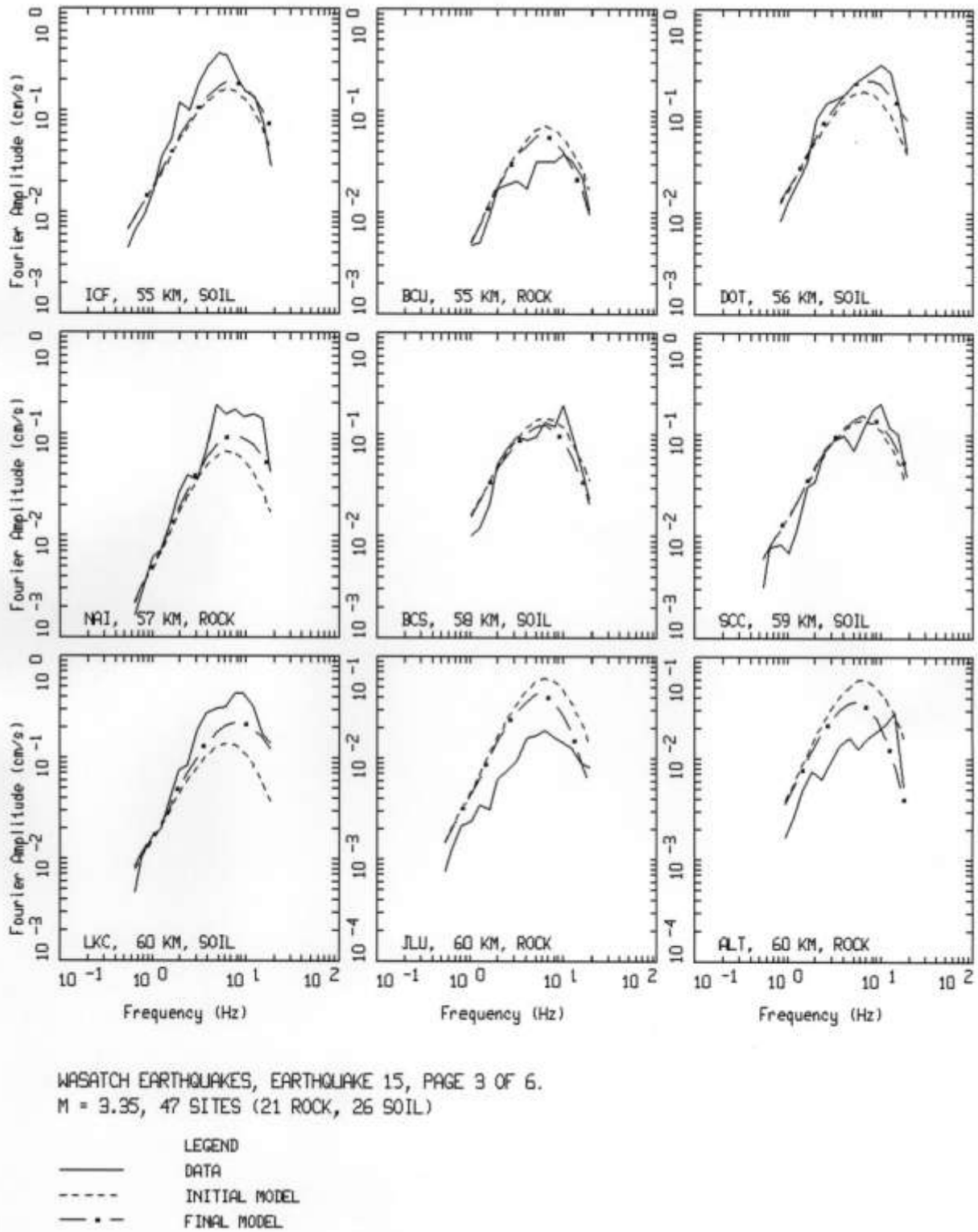
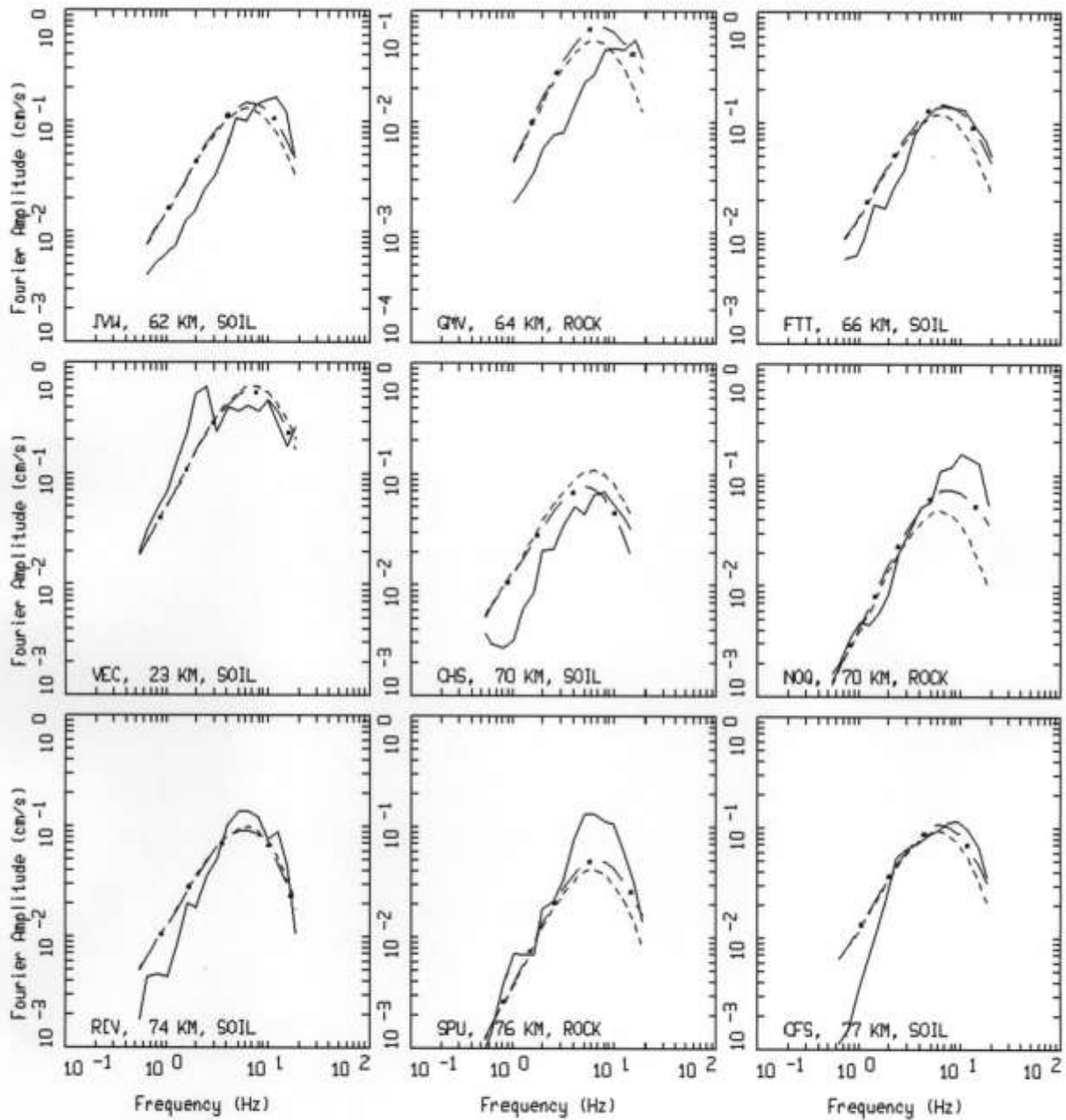


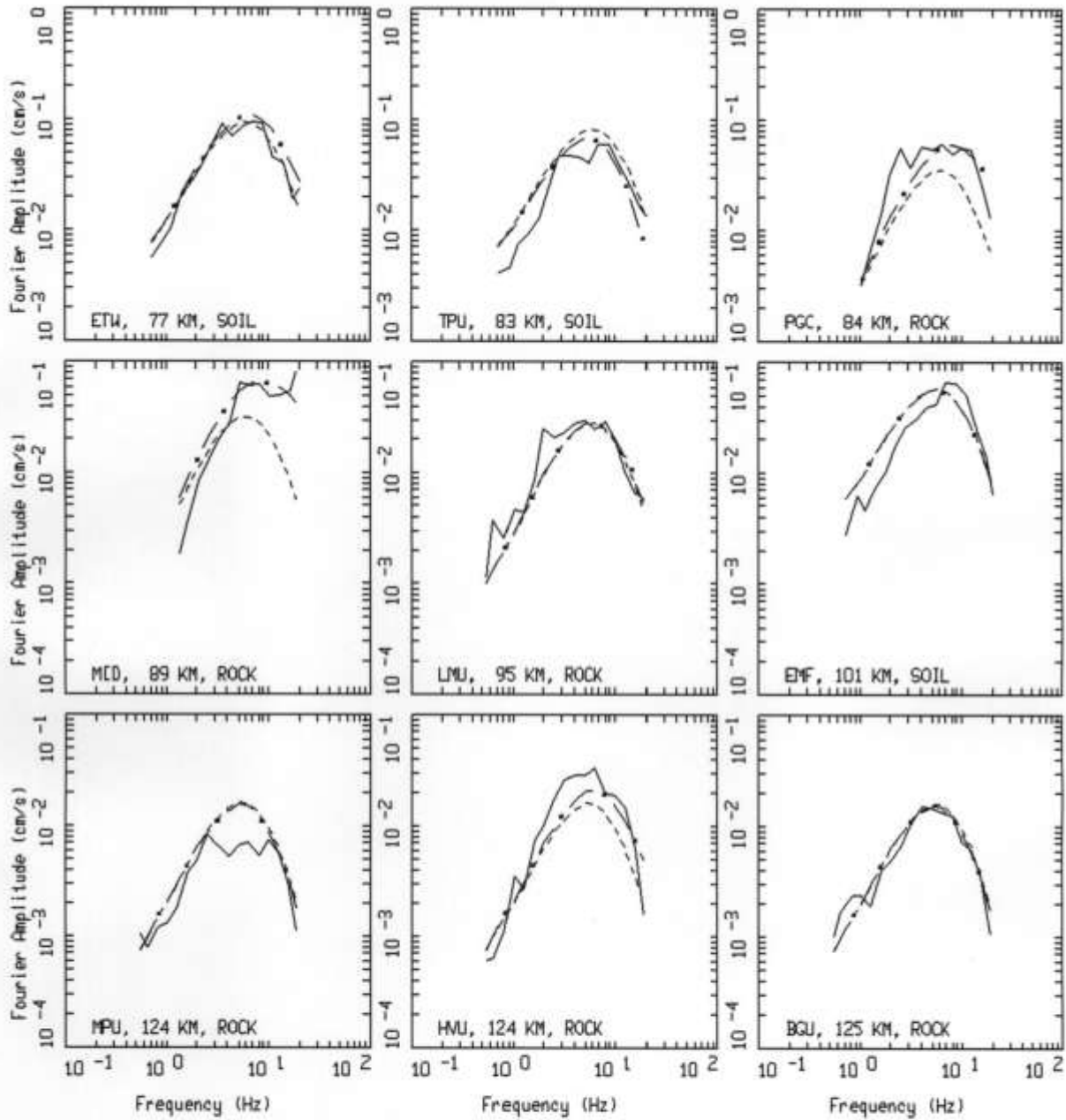
Figure 18 (continued). Spectral inversion results for Event #15.



WASATCH EARTHQUAKES, EARTHQUAKE 15, PAGE 4 OF 6.
 M = 3.35, 47 SITES (21 ROCK, 26 SOIL)

LEGEND
 — DATA
 - - - INITIAL MODEL
 - . - FINAL MODEL

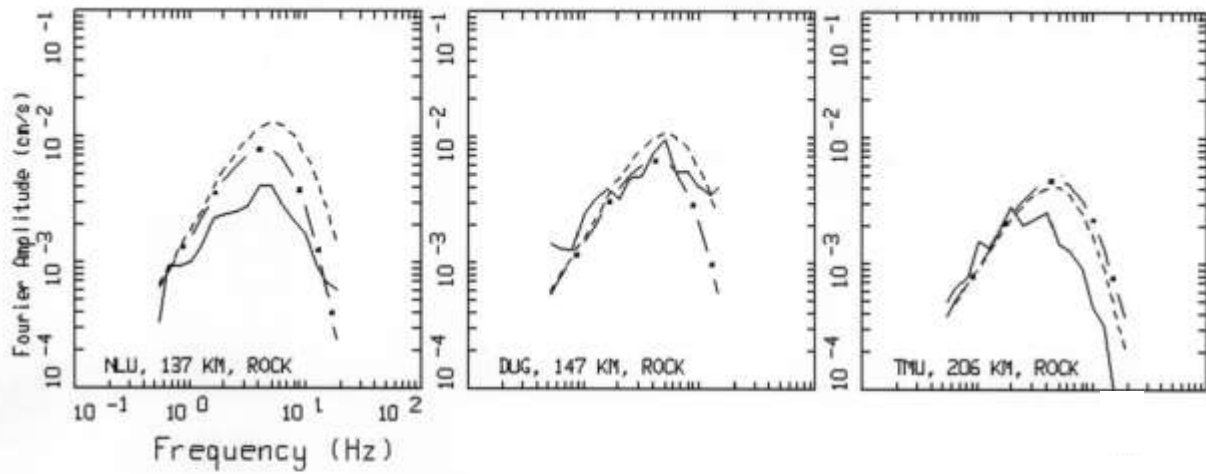
Figure 18 (continued). Spectral inversion results for Event #15.



WASATCH EARTHQUAKES, EARTHQUAKE 15, PAGE 5 OF 6.
M = 3.35, 47 SITES (21 ROCK, 26 SOIL)

LEGEND
— DATA
--- INITIAL MODEL
-•- FINAL MODEL

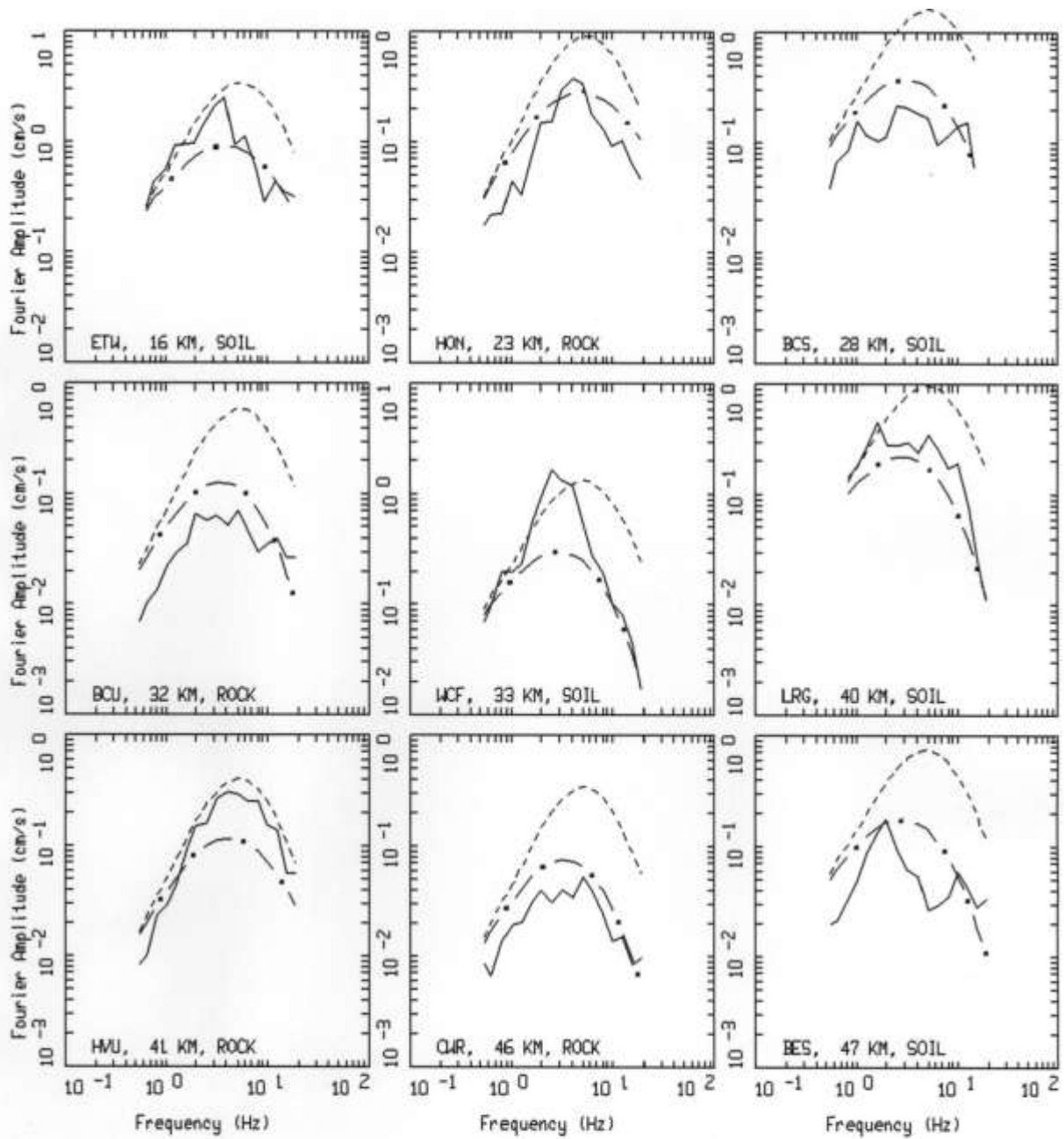
Figure 18 (continued). Spectral inversion results for Event #15.



WASATCH EARTHQUAKES, EARTHQUAKE 15, PAGE 6 OF 6.
 M = 3.35, 47 SITES (21 ROCK, 26 SOIL)

LEGEND
 — DATA
 - - - INITIAL MODEL
 - · - FINAL MODEL

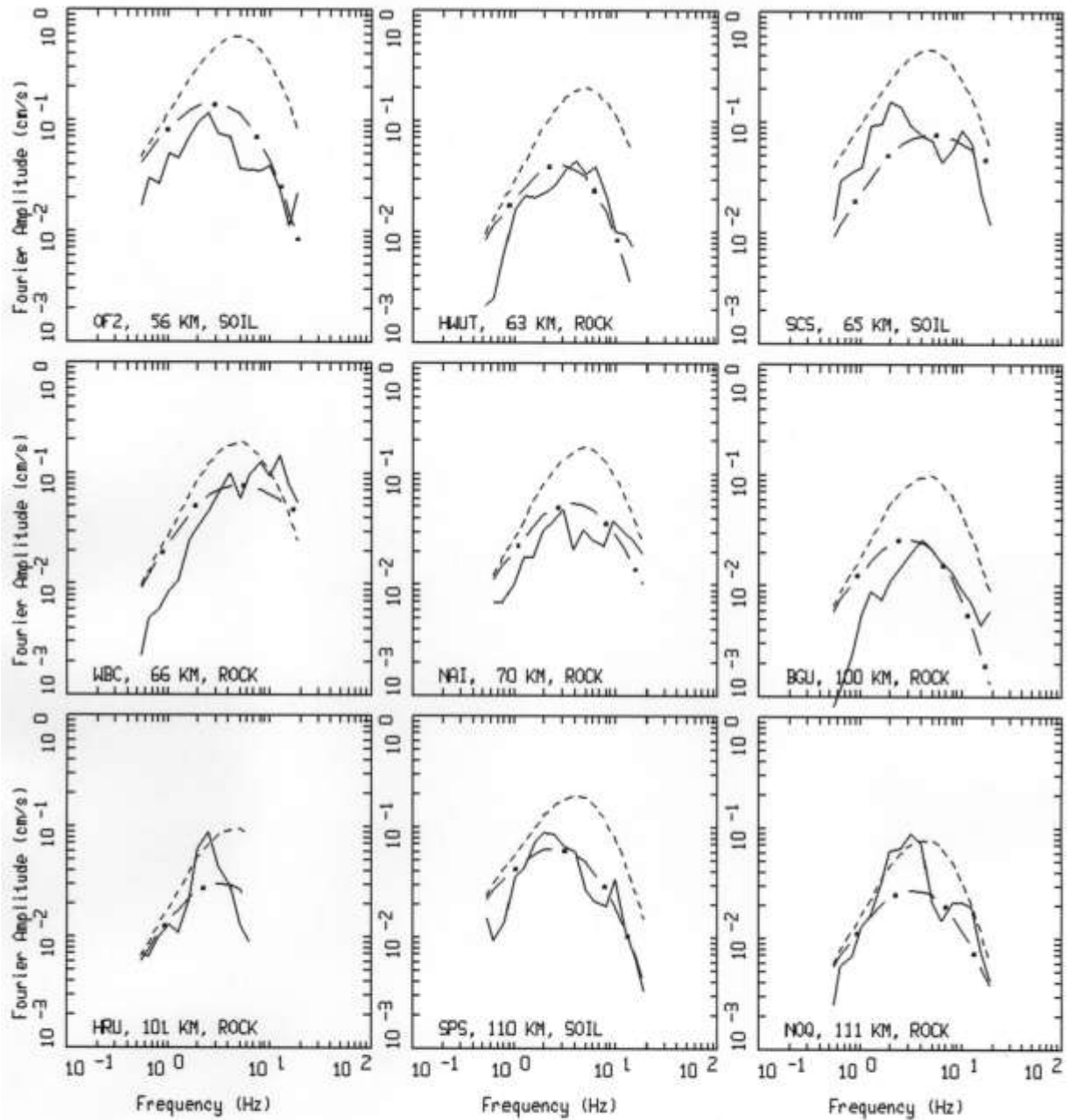
Figure 18 (continued). Spectral inversion results for Event #15.



WASATCH EARTHQUAKES, EARTHQUAKE 16, PAGE 1 OF 3.
M = 3.92, 26 SITES (16 ROCK, 10 SOIL)

LEGEND
— DATA
--- INITIAL MODEL
- · - FINAL MODEL

Figure 19. Spectral inversion results for Event #16.



WASATCH EARTHQUAKES, EARTHQUAKE 16, PAGE 2 OF 3.
 M = 3.92, 26 SITES (16 ROCK, 10 SOIL)

LEGEND
 — DATA
 - - - INITIAL MODEL
 - . - FINAL MODEL

Figure 19 (continued). Spectral inversion results for Event #16.

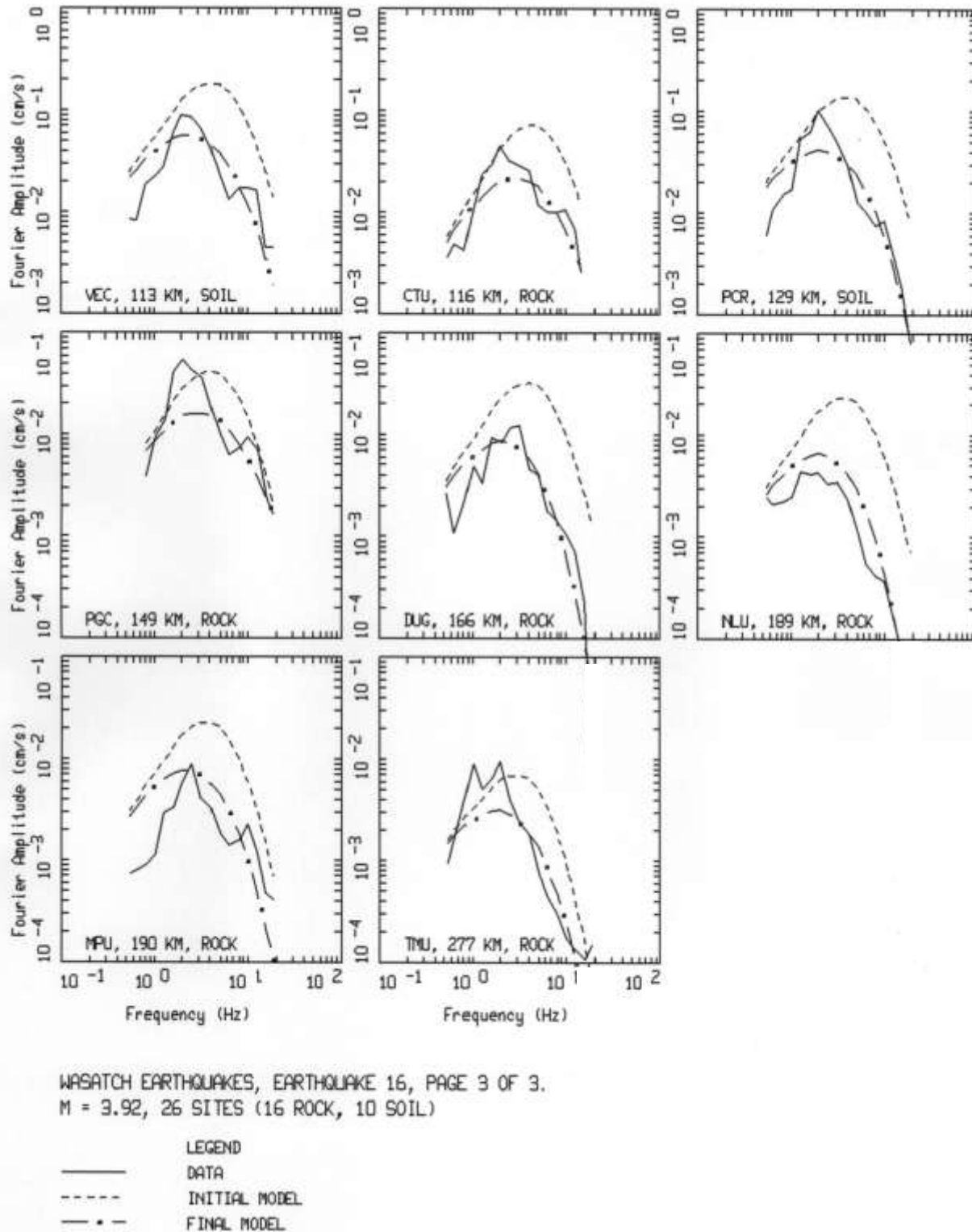
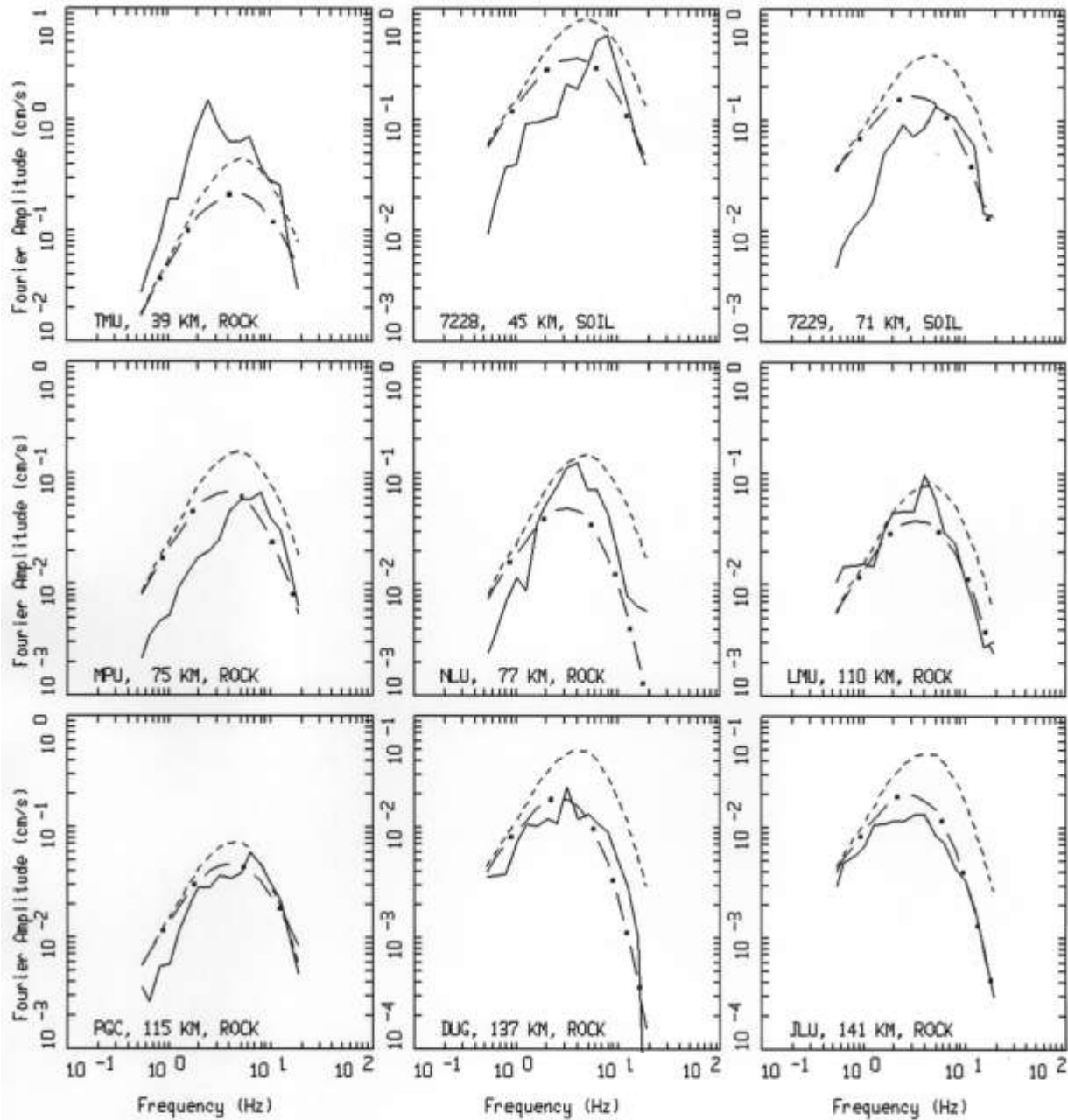


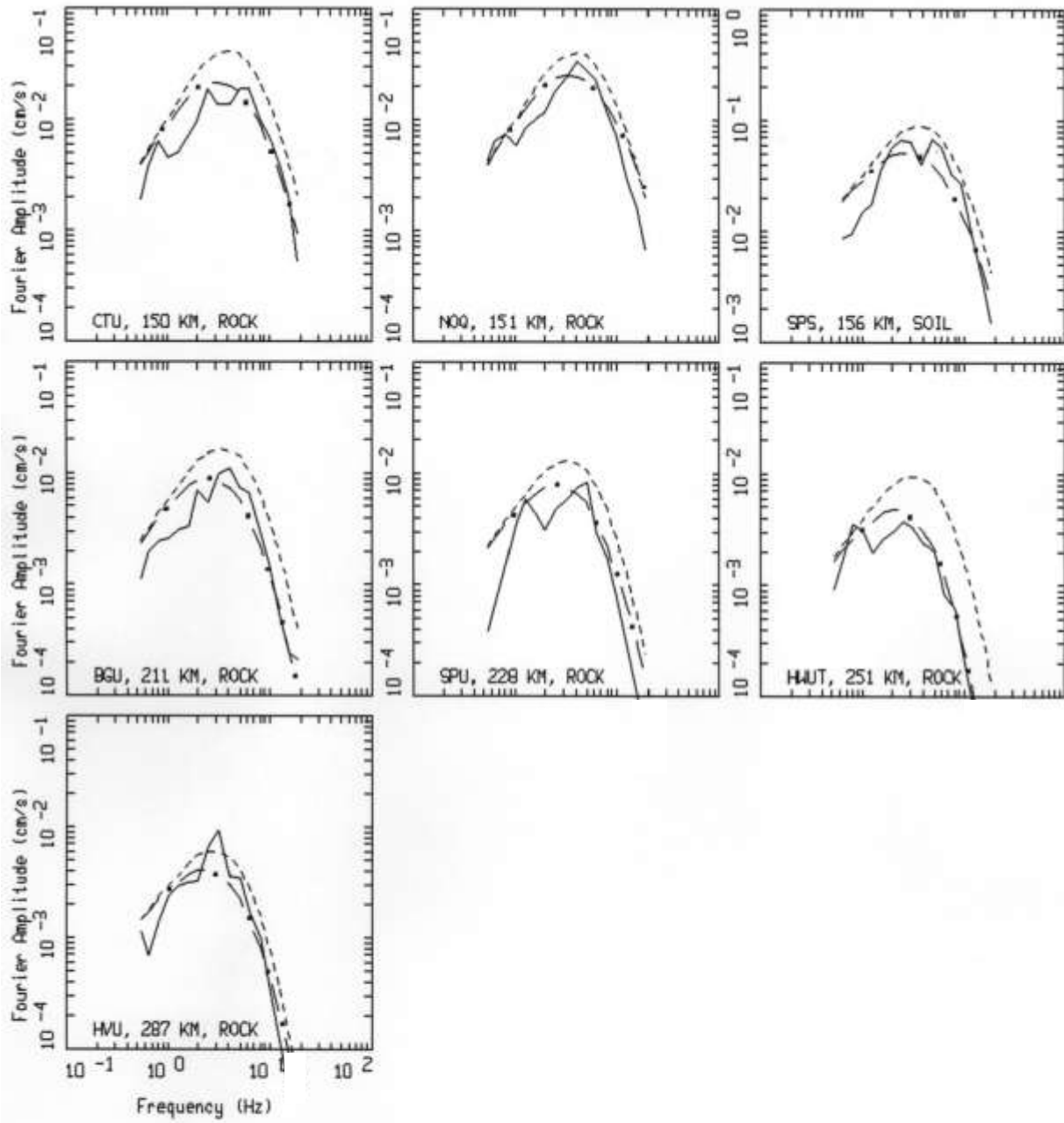
Figure 19 (continued). Spectral inversion results for Event #16.



WASATCH EARTHQUAKES, EARTHQUAKE 17, PAGE 1 OF 2.
M = 3.91, 16 SITES (13 ROCK, 3 SOIL)

LEGEND
— DATA
--- INITIAL MODEL
- · - FINAL MODEL

Figure 20. Spectral inversion results for Event #17.



WASATCH EARTHQUAKES, EARTHQUAKE 17, PAGE 2 OF 2.
M = 3.91, 16 SITES (13 ROCK, 3 SOIL)

LEGEND
— DATA
--- INITIAL MODEL
- · - FINAL MODEL

Figure 20 (continued). Spectral inversion results for Event #17.

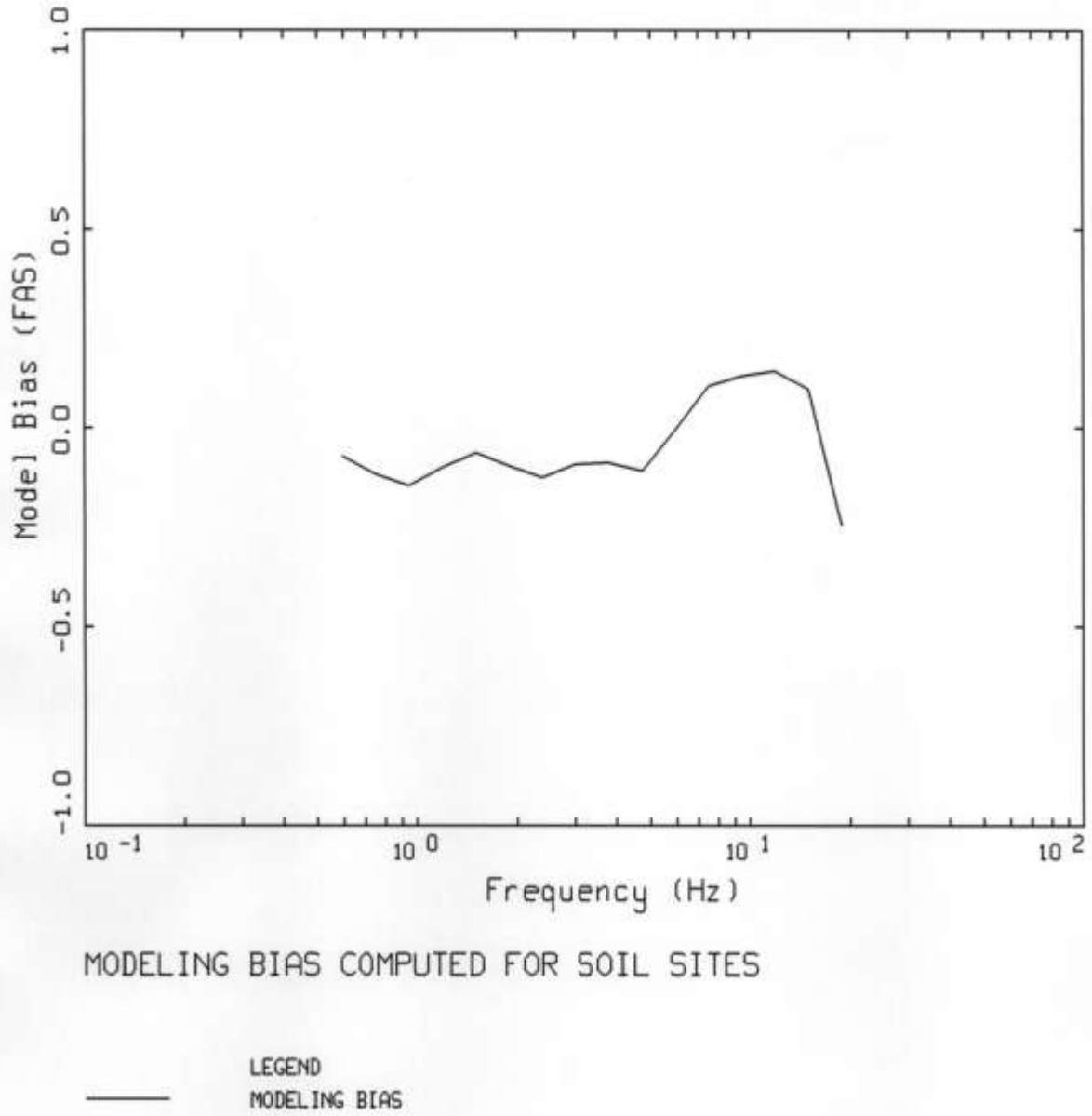


Figure 21. Model bias from Step 4 for soil sites.

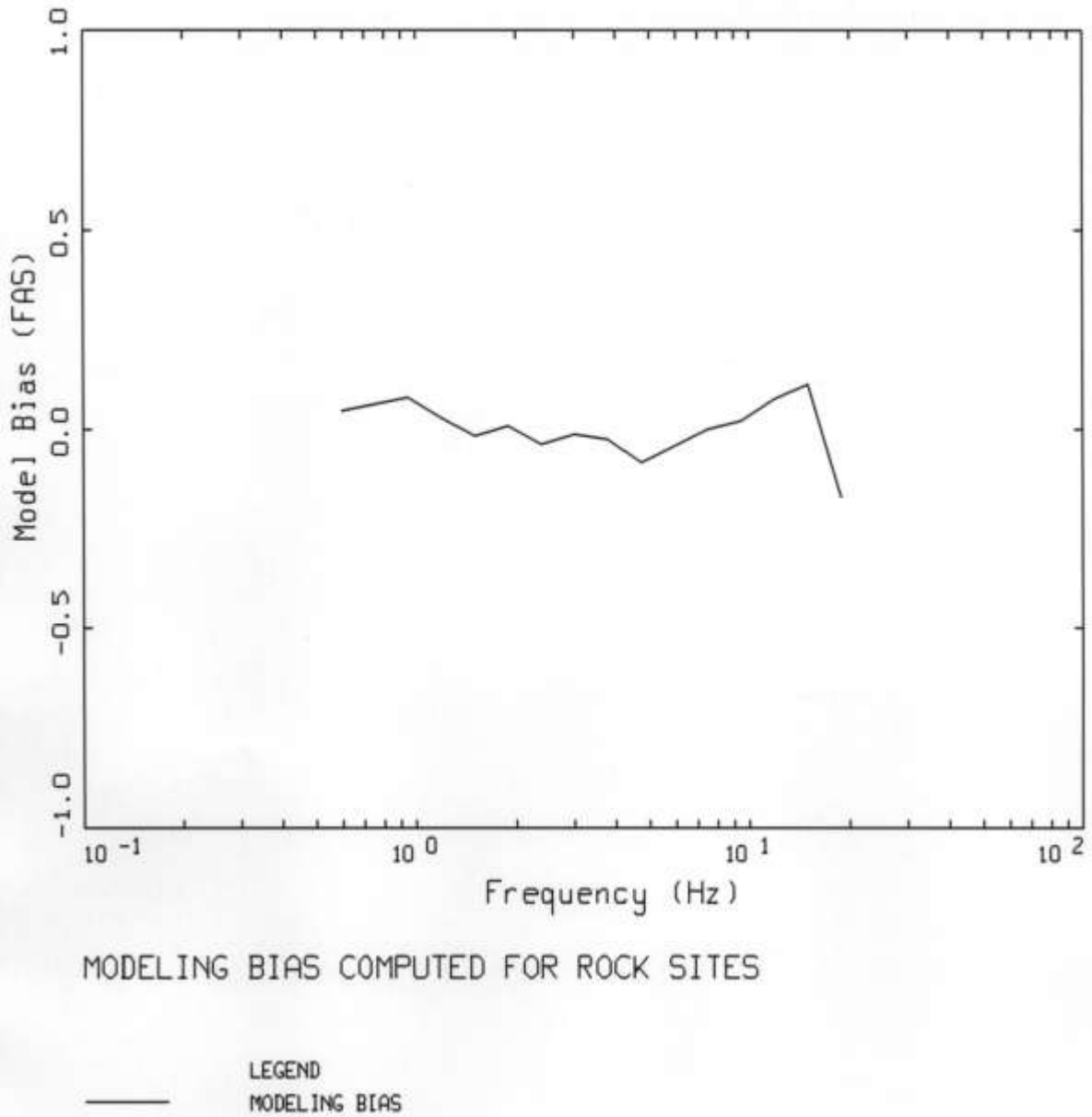
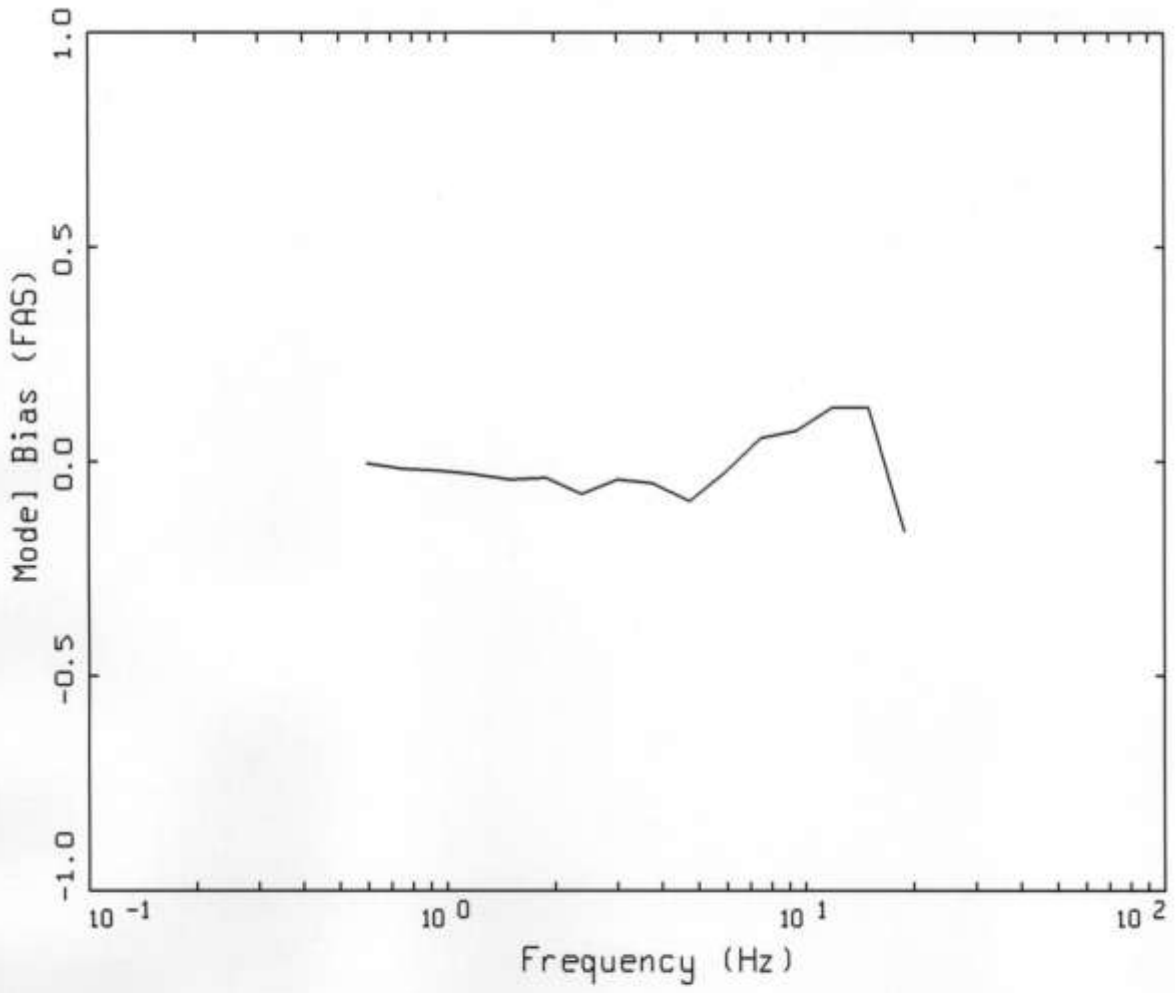


Figure 22. Model bias from Step 4 for rock sites.



MODELING BIAS COMPUTED FOR ROCK AND SOIL SITES

— LEGEND
MODELING BIAS

Figure 23. Model bias from Step 4 for all sites (rock and soil).